

©2016

Yao Ge

ALL RIGHTS RESERVED

WAVELET-BASED SOFTWARE-DEFINED RADIO RECEIVER DESIGN

by

YAO GE

A Dissertation submitted to the
Graduate School-New Brunswick
Rutgers, The State University of New Jersey
in partial fulfillment of the requirements

for the degree of

Doctor of Philosophy

Graduate Program in Electrical and Computer Engineering

Written under the direction of

David G. Daut and Zoran Gajic

and Approved by

New Brunswick, New Jersey

October, 2016

ABSTRACT OF THE DISSERTATION

Wavelet-Based Software-Defined Radio Receiver Design

By YAO GE

Dissertation Directors:
David G. Daut and Zoran Gajic

Abstract – Software-defined radios (SDRs), have become very important in both commercial as well as military applications that demand high Quality of Service (QoS) in hostile physical and spectral conditions. Simultaneously, interoperability with legacy communications equipment is also a critical requirement for widespread adoption. An ideal SDR supports multi-standard, multimode and multiband wireless communications. Such a system is reconfigurable in the sense that transmitted signals at different carrier frequencies and/or different modulation schemes can be reliably identified and appropriately demodulated in real-time. In this dissertation, such a radio system is developed using a wavelet transform-based transceiver platform, composed of four main wavelet-domain processors: Channel Estimator, Channel Equalizer, Automatic Modulation Recognition (AMR) and Demodulator.

The AMR method is blind identification of the modulation scheme used to format digital data embedded in a signal. It is investigated using the Discrete Wavelet Transform (DWT) in conjunction with techniques typically used in signal processing field of pattern recognition. In particular, the concept of wavelet-domain template matching is used to achieve modulation identification prior to signal demodulation. The digital modulation

schemes considered in this work include families of ASK, FSK, PSK and QAM. The test signals used in this study have been subjected to Additive White Gaussian Noise (AWGN) resulting in Signal-to-Noise Ratios (SNRs) in the range of -5 dB to 10 dB. Monte Carlo simulations using the wavelet-based AMR algorithms show correct classification rates that are better than most of existing methods that use other techniques

For wavelet-based demodulation original signal information can be directly obtained in the wavelet-domain without an inverse transform of a signal to its original time-domain form, and that has been proven analytically herein. Extensive Monte Carlo simulations have shown that the Bit Error Rates (BERs) obtained from wavelet-based demodulation are very comparable with the optimal case of matched filter-based demodulation.

The results of this work show the ability of wavelet transforms to enable the automatic recognition and subsequent demodulation of communications signals in a single processing sequence by solely using the computationally-friendly mathematics of the Discrete Wavelet Transform.

Acknowledgement

I would like to express my deepest appreciation to Dr. David G. Daut, who not only served as my research supervisor, providing valuable and countless resources, insight, and intuition, but also constantly gave me support, encouragement, and reassurance.

Special thanks are given to Dr. Zoran Gajic, Dr. Ken Vaz and Dr. Vivian Ho, for their constant guidance and help.

I would also like to thank Dr. Shantenu Jha, Dr. Ivan Marsic, Dr. Sophocles Orfanidis for actively participating in my committee and providing valuable inputs from their own areas of expertise.

My appreciation goes out to all my professors, laboratory staff, and the secretaries in the Department of Electrical Computer Engineering for their caring and teaching.

All my fellow graduate students are deserving of recognition for their support. I've cherished their friendship through these past years, and this will go on and be an asset in my life forever.

Finally, I would like to thank my parents and my wife for their encouragement, love and friendship. They have made many sacrifices so as to provide me with the best education in the United States.

Dedication

To my parents and my wife

Table of Contents

ABSTRACT OF THE DISSERTATION.....	ii
Acknowledgement.....	iv
Chapter 1 Introduction.....	1
1.1 Background and Motivation.....	1
1.1.1 Background.....	1
1.1.2 Motivation.....	3
1.2 Objective	4
1.2.1 System Level View	6
1.2.2 Block Diagram View.....	7
1.3 Deliverables.....	10
1.4 Organizations.....	10
Chapter 2 Literature Review	13
2.1 Survey of Automatic Modulation Recognition Methods	13
2.1.1 The Likelihood-Base (LB) Algorithm	14
2.1.2 The Feature-Based (FB) Method	19
2.1.3 Fourier Transform-Based (FD) Algorithms	25
2.1.4 Wavelet Transform-Based (WD) Algorithms	25
Chapter 3 Theoretical Preliminaries	28
3.1 Digital Communication Signals Model.....	28
3.2 An Overview of the Wavelet Transform.....	30
3.3 Review of the Continuous Wavelet Transform.....	32
3.4 Discrete Wavelet Transform	36

Chapter 4 DWT-AMR Based On Instantaneous Features	43
4.1 DWT-based AMR Preparation	43
4.2 WD-based AMR Algorithms Step by Step Illustration	50
4.3 Simulation Experiments and Results.....	56
4.4 Results Comparison.....	57
Chapter 5 DWT-AMR Based On Statistical Features	61
5.1 Preparations of the Automatic Modulation Recognition Process Using Statistical Features Templates	63
5.2 Development of the Statistical Feature AMR Algorithm:	67
5.2.1 Algorithm Development.....	68
5.3 Algorithm for the Automatic Modulation Recognition Process	79
5.3.1 Procedure for Decision Block 1	81_Toc448267766
5.3.2 Procedure for Decision Block 2.....	85
5.3.3 Procedure for Decision Block 3.....	86
5.3.4 Procedures for Other Decision Blocks.....	88
5.4 Simulation Experiment and Results Comparison.....	92
5.5 Conclusions	96
Chapter 6 Development of the Wavelet Domain-Based (WD) Demodulation Technology	97
6.1 Development of the WD-based Demodulation	100
6.2 The Architecture Design of the WD-Receiver System.....	104
6.3 Simulation Experiments and Results.....	107
6.4 Discussion of Results	114
Chapter 7 Summary and Conclusions	115
7.1 Summary	115
7.2 Contributions of the Dissertation	117

7.3 Suggestions for Future Work.....	118
7.4 Conclusions	119
References:.....	121

Lists of Tables

Table 4.1 Rates of correct classification for SNR = 10dB.....	56
Table 4.2 RATES OF CORRECT CLASSIFICATION FOR SNR = 5 dB.....	57
Table 4.3 RATES OF CORRECT CLASSIFICATION FOR SNR = 0 dB.....	57
Table 4.4 RATES OF CORRECT CLASSIFICATION FOR SNR = -5 dB	57
Table 4.5 SURVEY OF BASK CLASSIFICATION IN THE NON-DWT BASED LITERATURE ..	59
Table 4.6 SURVEY OF BPSK CLASSIFICATION IN THE NON-DWT BASED LITERATURE...	59
Table 4.7 SURVEY OF BFSK CLASSIFICATION IN THE NON-DWT BASED LITERATURE...	59
Table 4.8 SURVEY OF BASK CLASSIFICATION IN THE DWT-BASED LITERATURE	60
Table 4.9 SURVEY OF BPSK CLASSIFICATION IN THE DWT-BASED LITERATURE.....	60
Table 4.10 SURVEY OF BFSK CLASSIFICATION IN THE DWT-BASED LITERATURE.....	60
Table 5.1 Number of unique feature templates needed for different modulation schemes	61
Table 5.2 Identification of signal space quadrant using the correlation results with templates	65
Table 5.3 WD-Correlation with Template 1	70
Table 5.4 WD-correlation with Template 2.....	74
Table 5.5 WD-correlation with Template 3.....	75
Table 5.6 WD-correlation with the template 2 and the template 3.....	76
Table 5.7 Attributes of WD correlation values from test cases with Template 1	78
Table 5.8 Attributes of WD correlation values from test cases with Template 2.....	78
Table 5.9 Attributes of WD correlation values from test cases with Template 3.....	79
Table 5.10 Two groups of data identified from Template 1 using dynamic range....	82

Table 5.11 Two groups of data identified from Template 1 using multi-level.....	82
Table 5.12 Criteria used in Decision Block 1	82
Table 5.13 Dynamic range of the correlation data using Template 2.....	85
Table 5.14 AMR classification rates obtained in this research work	93
Table 5.15 Non-wavelet transform-based AMR methods	94
Table 5.16 Wavelet transform-based AMR methods	95

List of Illustrations

Fig. 1.1. Overall system-level description of a reconfigurable radio receiver.....	6
Fig. 1.2. Typical contemporary radio transceiver system.....	7
Fig. 1.3. System-level block diagram of an agile radio transceiver based on the Wavelet	9
Fig. 3.1. Different time-frequency tile allocation of the three transforms	32
Fig. 3.2. (Top) A time-domain sinusoidal signal, (bottom) The corresponding WD scalogram of the sinusoidal signal	33
Fig. 3.3. (Top) A time-domain noisy sinusoidal signal, (bottom) The corresponding WD scalogram using Haar through DWT.....	39
Fig. 3.4. Analysis and synthesis filter bank	41
Fig. 4.1. (a): (top) BASK signal without noise, 10-level WD decomposition using the Haar wavelet; (b): (bottom) BASK signal at 10 dB SNR, 10-level WD decomposition using the Haar wavelet.	46
Fig. 4.2. (a): (top) BFSK signal without noise, 10-level WD decomposition using the Haar wavelet; (b): (bottom) BFSK signal at 10 dB SNR, 10-level WD decomposition using the Haar wavelet	47
Fig. 4.3. (a): (top) BPSK signal without noise, 10-level WD decomposition using the Haar wavelet; (b): (bottom) BPSK signal at 10 dB SNR, 10-level WD decomposition using the Haar wavelet	48
Fig. 4.4. Illustration of time-domain instantaneous features templates	49
Fig. 4.5. Graphical representation of the correlation operation using different template lengths	51

Fig. 4.6. Example of a "transition period" correlation operation in the WD AMR process.....	51
Fig. 4.7. Example of WD AMR process using the instantaneous features templates	54
Fig. 4.8. Overall system-level block diagram of a radio receiver employing an AMR function	55
Fig. 4.9. System-level processing flow of the wavelet-based AMR processor	55
Fig. 5.1. Signal space representation of the three common features templates	66
Fig. 5.2. WD-AMR using statistical feature template system level view.....	68
Fig. 5.3. Block Diagram of WD AMR Process using Statistical Featured Templates	81
Fig. 5.4. Flowchart of the procedure for Decision Block 1	84
Fig. 5.5. Flowchart of the procedure for Decision Block 2	86
Fig. 5.6. Flowchart of the procedure for Decision Block 3	87
Fig. 5.7. System block diagram implementing the ASK and FSK Classifier Procedure for Group 1 signals	90
Fig. 5.8. System Block Diagram for the PSK/QAM Classifier	91
Fig. 6.1. Baseband processor using wavelet transform-based signal identification and classical demodulation	97
Fig. 6.2. Baseband processor using wavelet transform-based signal identification and demodulation.....	99
Fig. 6.3. The Contemporary Correlator based Demodulation	100
Fig. 6.4. Wavelet based-Demodulation System.....	105
Fig. 6.5. Wavelet-based Receiver Platform	106

Fig. 6.6. BPSK BER Curve Comparison	110
Fig. 6.7. QPSK BER Curve Comparison.....	110
Fig. 6.8. 8-PSK BER Curve Comparison	111
Fig. 6.9. 4-QAM SER Curve Comparison.....	111
Fig. 6.10. 4-PAM SER Curve Comparison	112
Fig. 6.11. 16-QAM BER Curve Comparison	112
Fig. 6.12. BFSK BER Curve Comparison	113
Fig. 6.13. 64-QAM SER Curve Comparison.....	113

Chapter 1 Introduction

1.1 Background and Motivation

1.1.1 Background

In typical contemporary communications systems, the transmitter and receiver can each be viewed as two-port systems that are linked via a transmission channel. One port is the antenna used to transmit/receive RF signals and the other port is the baseband data interface between the system and the user. However, the use of two-port devices place restrictions on the overall data throughput that can be achieved by the system. To overcome this drawback new lines of thinking involve the use of multi-port communication systems for consumer use. One example of such a multi-port system is provided by the use of Multi-input Multi-output (MIMO) architectures. MIMO-based systems transmit and receive multiple digitally-modulated signals on multiple antennas. The underlying principle behind such a scheme is spatial multiplexing [3, 4]. Analogous to the technique of Time-Division Multiplexing (TDM), wherein multiple data streams are separately transmitted in successive temporal windows, using spatial multiplexing multiple data streams are transmitted via different antennas thereby sharing physical space. Such a scheme allows for communications systems with higher spectral efficiency and wireless link reliability without compromising either the transmission bandwidth or power [5]. Another popular system methodology is based on the concept of Orthogonal Frequency Division Multiplexing (OFDM) [6-8]. In this technique a high-speed data stream is demultiplexed into a number of slower-speed data streams and each stream is used to modulate a carrier signal. Multiple orthogonal sub-carrier signals can be used for the various data streams, and thus the orthogonal modulated signals can be then

combined for transmission via a single antenna. The major advantage of using an OFDM-based scheme is the ability to handle severe channel fading conditions [9-11]. Naturally, the MIMO and OFDM techniques have been combined into a hybridized MIMO-OFDM scheme [12-15]. Such systems that are capable of high spectral efficiency and high channel fading and interference immunity certainly hold promise to solve problems that have existed in the area of wireless, as well as wire line communications.

Moreover, more typical contemporary communications systems are developed based on a wide range of wireless protocols and standards. For example, there are two common cellular phone systems options may be employed are Code Division Multiple Access (CDMA) and Global System for Mobile communications (GSM). With regard to personal wireless networks, the IEEE 802.11 family of standards or the newly developed technology of Worldwide Interoperability for Microwave Access (WiMAX) may be employed. Even the fundamental modulation schemes are still used for some important applications. For example, the PSK is mainly implemented by the Bluetooth, IEEE 802.11a&b and other wireless communications systems. The QAM plays important roles in cable modems for high speed internet access, digital video transmission standard for cable television and digital terrestrial television applications. Transmissions through the optical fibers utilizes ASK as one of the fundamental technologies. The FSK is predominantly used in applications such as caller ID, fax services, and transmission of telemetry data.

1.1.2 Motivation

Through observing variety of standards currently in use, there exist entire families of communications systems that are tailored specifically to each standard. However, there are some inherent limitations of them:

1. Lack of interoperability between standards;
2. Circuit complexity increased comparing to traditional two-port systems, which are also known as Single-Input Single-Output (SISO);
3. To recover the signal at the receiver for demodulation, the receiver end has to know a lot a prior signal information from the transmitter end;
4. In the last step of the contemporary demodulation processor, signals always have to be transferred back into the time-domain;
5. Each modulation scheme has to be demodulated by its unique carrier signal and corresponding specific circuit.

To overcome the drawbacks mentioned above, one reconfigurable communication system expected to be developed in this work, should be embedded with following desired capabilities:

1. Support multi-standard, multimode, and multiband wireless communications.
2. The receivers are able to recognize multiple modulation schemes of the acquired signal, and to demodulate the identified signal.
3. The identification and detection accuracy should be promising over a huge range of SNR.
4. The system should be able to learn the channel impact at the receiver end even know little *a priori* knowledge.
5. The radio receiver should be comprised largely of digital circuitry.

In summary, given the wide variety of communications standards and protocols currently in use, and with newer technologies being continually added, especially those most new systems sacrifice their design simplicity as the tradeoff for higher data throughput. Hence, a new platform for communications systems that are capable of interoperability between standards is required and designed in this work, which should be able to better balance the design cost and the performance. This new platform for efficient future communications receivers has been identified as that of reconfigurable radios and its development of communications systems is necessary for both military and commercial applications. The term of reconfigurable is in the sense that transmitted signals at different carrier frequencies, and which use different modulation schemes, when acquired by the radio, can be reliably identified and appropriately demodulated in real-time. The proposed research should advance this new design paradigm by enabling the digital baseband processing stage that is required to identify and demodulate received information-bearing signals. The availability of flexible and versatile baseband processing sub-systems is critical to the implementation of reconfigurable radios.

1.2 Objective

This work aims at building a reconfigurable radio receiver that has maximal flexibility of its functions while simultaneously minimizing the use of prescribed analog signal processing sub-systems. There are four main functional processors to enable such an agile radio system, which are AMR, channel estimation, equalization, and demodulation. Among them, the main keys to enabling such a technology are firstly the identification of modulated signal types (AMR), and secondly the demodulation of the received

communications signals. Such a radio transceiver can be realized by using the Wavelet-based platform Processors which is capable to identify modulated communications signals without a priori knowledge of the modulation scheme, and to demodulate signals by merely utilizing their wavelet transformed information. Specifically, such an identifier and demodulator are carried out by using the discrete wavelet transform.

The Wavelet transform technology has been chosen for this reconfigurable radio receiver's development since discontinuous signals can be readily analyzed after being transformed. By decomposing communications signals with different wavelet basis functions, instantaneous wavelet-domain features of each signal can be identified. Furthermore, there are many strings existing between the signal information contained in the time domain and in the wavelet domain, which can be utilized to demodulate signal efficiently and accurately while staying with the wavelet domain. Thus no extra computing effort is needed to transfer a signal back to the time domain. Briefly saying, WT is mainly useful here because it is good at characterization (analysis) of signals. Also, using the discrete wavelet transform (DWT) is more efficient than using the continuous wavelet transform (CWT). Because of that although both technologies extract around same amount information from signals, but the DWT cost much lower computational complexity than the CWT. Besides, the other two core functions mentioned earlier Channel estimation and Channel Equalization were previously-developed [80] in the discrete wavelet domain as well. By embedding these four processors into one system, a discrete wavelet-based agile transceiver is presented completely.

1.2.1 System Level View

The following paragraphs illustrate the system shown in the block diagram in Fig. 1.1 and compare the classic and wavelet-based communication platform structures. The structure of the proposed new transceiver is developed based on the typical contemporary communication receiver architecture, which is implemented with three major systems: RF front-end, digital front-end, i.e., mixed-signal system including Analog-to-Digital Converters (ADCs), and baseband demodulation and processing system, as shown in Fig. 1.1. The research effort proposed herein is focused on the development of the baseband system.

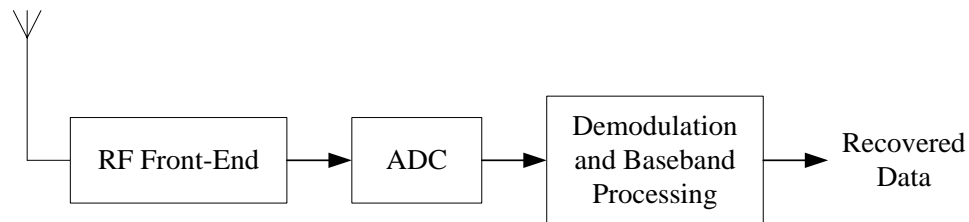


Fig. 1.1. Overall system-level description of a reconfigurable radio receiver [81].

1. Radio Frequency (RF) front-end: The RF front-end processor is performed here for the ease of subsequent processing. Its function is to down-conversion of the passband signal to an intermediate frequency. The components of RF include analog electronic sub-systems, such as mixer, local oscillators, band-pass filters, variable gain amplifiers and antennas.
2. Mixed-signal stage: The intermediate frequency signal output by the RF front-end is converted to a digitized form in this stage. The Analog-to-Digital Converter (ADC), in Fig. 1.1, converts the analog received signal into digitized form.
3. Demodulation and baseband processing units: A signal-specific demodulator can

recover modulated signal to desired baseband data, and a baseband processor can handle any following decoding of the recovered data.

1.2.2 Block Diagram View

A more detailed depiction of a modern radio transceiver system is provided in Fig. 1.2. It shows that radio transmitters also use similar signal processing strategies as those in the receiver. First, baseband data are encoded, if needed, and the data are then used to modulate a carrier signal at an intermediate frequency. The modulated signal is then up-converted to the RF passband and transmitted.

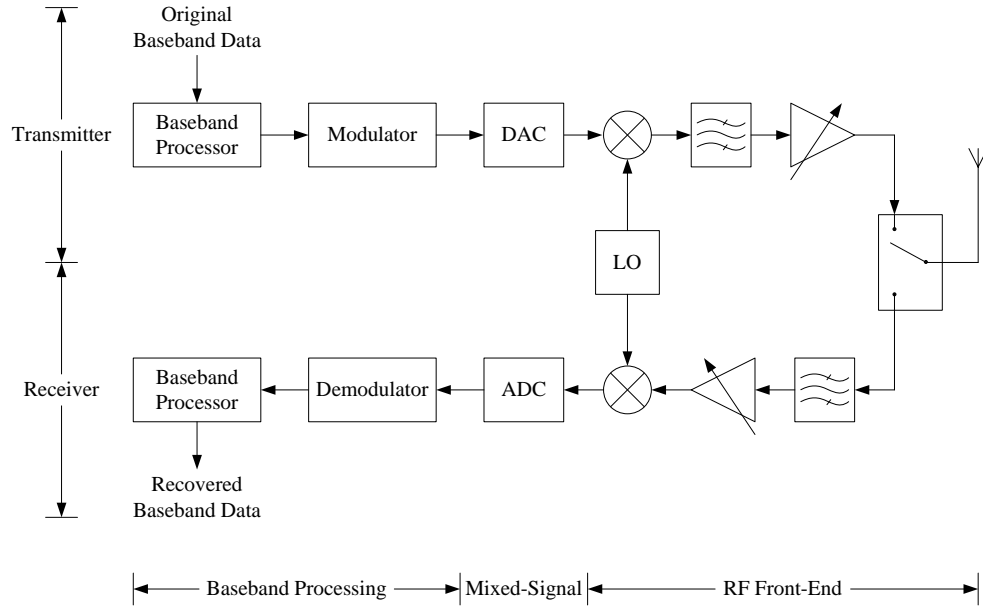


Fig. 1.2 Typical contemporary radio transceiver system [81].

As the system shown in Fig. 1.2, the lack of interoperability between radios that implement different communications standards, is the major limitation of communications systems. One specific difficulty to interoperate between standards is that various standards must utilize their unique corresponding modulation schemes.

In order to rectify the problem, an agile radio system is designed automatically

classifying the modulation scheme, which can be utilized in a received signal, and with the capacity of automatically demodulating the signal. To specify this agile radio transceiver system, a detailed block diagram will demonstrate core features of the that is composed of its core features as shown in the Fig. 1.3, which is a wavelet-based platform composed of four major components:

1. Channel Estimation: This process enables Electrical characterization of the medium through which a signal is transmitting. Besides, in order to improve the performance, channel estimation also performs to restore signal features prior to the WT-based AMR and demodulation processes.
2. Channel Equalization: This step is to eliminate unwanted channel effects carried by received signals. The reduction of unwanted channel effects present in received signals is a desirable signal conditioning step before invoking the AMR process.
3. AMR: This is a key component of this Wavelet-based transceiver Platform, which automatically identifies the modulation scheme of the received signal.
4. Demodulation: Second to AMR in importance is the automation demodulation of this Wavelet Platform.

After the modulation scheme of the unknown received signal is recognized, the signal is then jointly and automatically demodulated to recover the transmitted information.

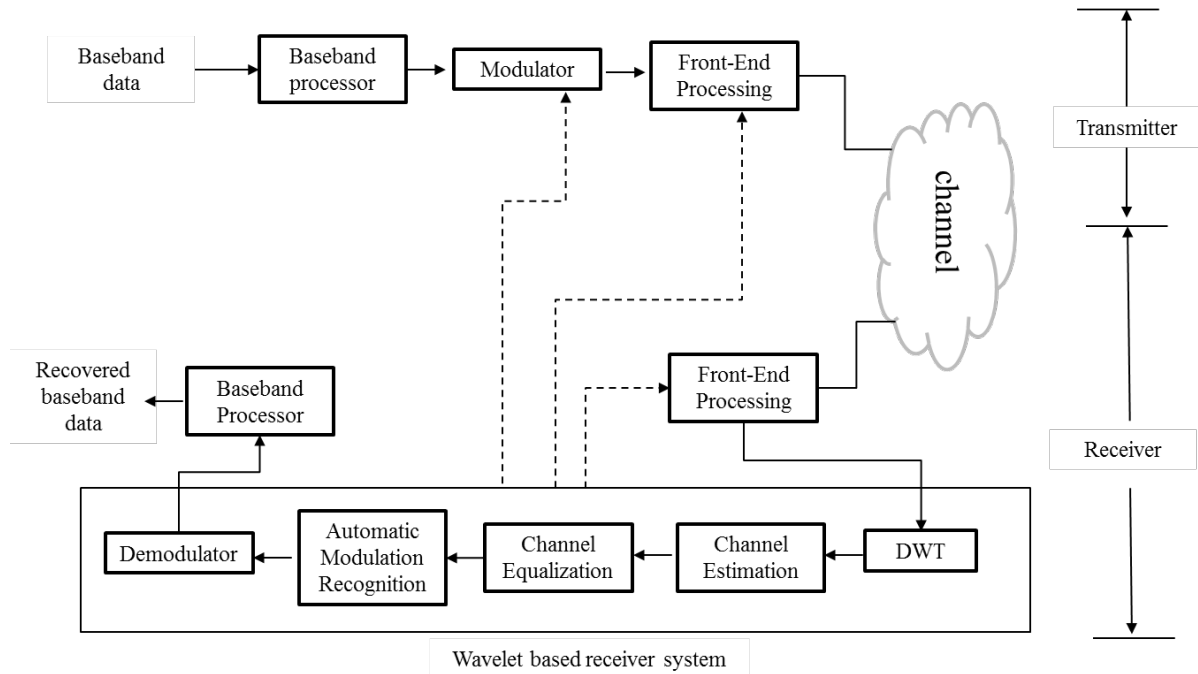


Fig. 1.3. System-level block diagram of an agile radio transceiver based on the Wavelet Platform.

Fig. 1.3 shows that a wavelet-based transceiver is consisted of a transmitter and a receiver as majority parts of the receiver which is implemented in the context of the Wavelet Domain. In this transceiver, the transmitter operation is partially controlled by the Wavelet Platform. The dashed lines indicate that sub-systems in the transmitter take feedback provided by the Wavelet Receiver, which could carry information to alter transmission characteristics such as the modulation scheme, carrier frequency, etc., as needed. This function also enables the feature of agility of the wavelet-based transceiver. The WT-based AMR and Demodulation processes both use the Discrete Wavelet Transform (DWT).

1.3 Deliverables

In brief, the intention of developing the wavelet-based AMR and wavelet-based Modulation techniques is to advance the state of the art of communication systems by providing a fundamental step towards interoperability between communication standards through the use of wavelet transforms. Summarizing from above sections, the primary objectives of this research work are:

1. Invention of a technique for choosing wavelet-domain signature templates that are needed for the AMR processes.
2. Invention of wavelet-based AMR algorithms using the templates matching methodology.
3. Invention of a technique for the wavelet-based Demodulation processes.
4. Evaluation of performances of the proposed AMR and Demodulation technologies.
5. Comparison the performance of the WT-based AMR and Demodulation methodologies with results obtained using other methodologies that have been reported in the literature.

1.4 Organizations

The dissertation is composed of six chapters. The focus of Chapter 2 is on the literature review. In this chapter, existing AMR methodologies are categorized into two main research trends, which are the likelihood function-based (LB) method and the feature-based (FB) function. The LB method is also called the theoretical method because its performance usually could be derived analytically (asymptotically) and is considered

optimal by the byes sense. The FB function provides the suboptimal results with lower computational complexity. Each trends is further grouped into varies subclass by utilizing different characters, which are very helpful for designing the proposed AMR algorithm.

Chapter 3 covers the mathematical foundation and theoretical background needed for this work. Besides of the modulation schemes introductions, the discrete wavelet transform is also illustrated from the space geometric instruction view and in the form of filter banks analyze.

Two wavelet-based AMR algorithms are developed in Chapter 4 and Chapter 5 based on two wavelet-based features as follows:

1. WD-Instantaneous features templates:

As the symbol transition that occur in the modulated waveform structure, templates that contain instantaneous features of specific type of digitally modulated signals will emerge.

2. WD-Statistics features templates:

As variations of the sinusoidal feature are contained within a symbol period of different modulation schemes, after statistical operations, some features are collected for analyzing and then being used for a modulation classification.

For each algorithm, the detailed design procedures for the AMR algorithm, results of computer simulation experiments, comparisons of the results with the existing literature and computational complexity estimation are provided in each chapter.

In Chapter 6, the techniques used for automatic signal demodulation in the wavelet domain are presented. The BER performances of the WT-based demodulation of the various modulation schemes are compared with the relevant matched filter-based BER

performances.

Finally, in Chapter 7, the important features of the AMR and Demodulation processes invented in this dissertation are summarized; extensions of the work are identified for possible future investigation. Finally, conclusions of this research work are provided.

Chapter 2 Literature Review

2.1 Survey of Automatic Modulation Recognition Methods

Before introducing this research, it is necessary and meaningful to firstly review existing technologies regarding the AMR and Demodulation technologies. The design of a modulation classifier (AMR) essentially involves two steps: signal preprocessing and proper selection of the classification algorithm. Preprocessing tasks may include, but not limited to perform some or all of, noise reduction, estimation of carrier frequency, symbol period, and signal power, equalization etc. Depending on the classification algorithm chosen in the second step, preprocessing tasks with different levels of accuracy are required; some classification methods require precise estimates, whereas others are less sensitive to the unknown parameters. Over the years, to simplify the design process of a multimode communication system, many studies have been conducted regarding these subjects. The evolution of signal processors and analog-to-digital converters allow the development and improvement of algorithms in order to support real-time recognition with less and less of *a priori* signal information.

Regarding the second step, the existing classification algorithms could be generally categorized into two main trends: likelihood-based (LB) and feature-based (FB) methods, respectively. The former is based on the likelihood function of the received signal and the decision is made comparing the likelihood ratio against a threshold. A solution offered by the LB algorithms is optimal in the Bayesian sense, by minimizing the probability of false classification. The optimal solution suffers from computational complexity, which in many cases of interest naturally gives rise to suboptimal classifiers. On the other hand, the FB algorithm's core idea is composed by the statistical pattern recognition approach

which is based on extracting some basic characteristics of the signal features. These features are normally chosen in an *ad hoc* way. Although an FB-based method may not be optimal, it is usually simple to implement, and can have near-optimal performance when designed properly. Once the modulation format is correctly identified, other operations, such as signal demodulation and information extraction, can be subsequently performed. In general, AMR is a challenging task, especially in a non-cooperative environment, where in addition to multipath propagation, frequency-selectivity and time-varying nature of the channel, no prior knowledge of the incoming signal is available. In the following, some AMR papers are reviewed with these two main methodologies.

2.1.1 The Likelihood-Base (LB) Algorithm

The LB algorithm [16] is a utilization of the decision-theoretic approach, which indicates to a probabilistic solution based on *a priori* knowledge of probability functions and certain hypotheses. In this methodology, the modulation schemes classification could be viewed as a composite hypothesis-testing problem. Composite hypothesis contains more than one unknown quantity which characterizes the hypothesis ranges over a set of values. Depending on the model chosen for the unknown quantities, there are usually three LB-AMR methodologies being used as the solution of this multiple-hypothesis testing problem: (a) the Average Likelihood Ratio Test (ALRT), where the unknown signal and channel parameters are treated as random variables with known probability density functions (PDFs), and the likelihood functional is averaged over this PDF. It results in an optimal classifier in the Bayesian sense; (b) the Generalized Likelihood Ratio Test (GLRT), where the unknown parameters are treated as deterministic but unknown

variables and the likelihood functional is maximized with respect to them; (c) a hybrid of the two tests is named as the Hybrid Likelihood Ratio Test (HLRT), where some of the parameters are treated as in (a) and the rest as in (b).

ALRT: The first work reviewed on this topic [17] addresses AMR for PSK (BPSK, QPSK) and QAM (16-QAM, 32-QAM and 64-QAM) signals under coherent and non-coherent conditions. For coherent case, it firstly assumes all parameters are known. The signal could be classified by forming likelihood ratios from the demodulated matched-filter output. Because the conditional PDF of output is obtainable given a certain modulation type, the coherent maximum likelihood (ML) classifier is simply a rule for choosing among the candidate modulation types by selecting which one provides the maximum conditional output PDF. Non-coherent ML classification is evaluated by assuming all signal parameters are known except the carrier phase. However, the conditional joint PDF of amplitude and phase difference of received signal given certain modulation schemes is available. Thus, by selecting the modulation type that corresponds to the largest of this conditional PDF value, Non-coherent ML classifier is implemented successfully.

In [18] the research developed in an ideal situation where all signal parameters as well as the noise power are known, the data symbols are independent and the pulse shape is rectangular. A theoretical performance analysis of the generic ML classifier that is applicable to any digital amplitude-phase (PSK, PAM and QAM) modulation by assuming all modulation types are equal likely. In details, the conditional joint PDF of the in-phase and quadrature portion of the received signal given a modulation hypothesis is available, thus the likelihood function could be obtained by multiplying all symbols

together since they are assumed independent. The ML classifier will claim the decision which one leads likelihood function to the maximum value.

Study in [19] utilizes the ML classifier to recognize M-ary PSK signals. Setting the ALRT threshold value as 1 turns it into the ML classifier. In details of the classifier construction, the conditional joint PDF of the in-phase and quadrature component of the signal was firstly derived upon the independence of these two parameters. Then the classification performance is analytically derived with the help of an extension of the n^{th} moment.

In [20] and [21], a promising approach for BPSK and QPSK modulation type identification is developed. The resulting classifier is optimum in the sense that it minimizes the average cost function of misclassification probability. In this approach, modulation classification is considered as a composite binary hypothesis testing problem, and ALRT is applied with the signal level as the random parameter for which PDS is known. This method works well at low SNR in [20], by assuming the signal level is constant and known to a receiver. However, in practice, wireless communication environment suffers from noise interference, fading, and multipath. Thus [21] extended this work by considering the signal level as a Rayleigh-distributed random variable. The maximum *a posteriori* classifier is derived by averaging over the signal level with the prior knowledge of the probability distribution of the signal level. This work is not appropriate to extend to higher-order modulation scheme since its computation complexity increases exponentially as modulation order increases.

From ALRT transit to GLRT and HLRT: To summarize, the ALRT is basically a Bayesian based approach, and it provides the optimal performance in the Bayesian sense

by assuming that unknown parameters are random variables with certain known PDF and averages the conditional LFs over these quantities. However, the need for the PDF of all unknown parameters that are usually unavailable, and multidimensional integrals involved in the derivation of this average likelihood ratio test make the computational cost impractical. Hence, developing alternative algorithms are necessary.

In another classical theory of statistical decisions, unknown parameters are usually treated as unknown deterministic values. The uniformly most powerful (UMP) test is optimal in the sense that it finds the most powerful test independent of the unknown parameters; however, because of the complicated unknown parameter space, usually met in practice, the UMP test rarely exists. Instead, we may substitute the maximum likelihood (ML) estimates of the unknown parameters in the LFs and then develop the generalized likelihood ratio tests (GLRT) using the estimated values.

Despite the fact that the GLRT is widely used in the signal activity detection problems, it is not applicable for the modulation classification, as the different constellation sets are mostly nested. We can average the conditional Likelihood functions (LFs) over the symbols and substitute the ML estimates of other unknown parameters in the LFs. The last approach, namely hybrid likelihood ratio test (HLRT) removes the nested constellation difficulty of GLRT and is of more interest in recent research on AMR.

GLRT and HLRT: The work of [21] is first re-studied in research of [22] by utilizing the GLRT approach. The signal level is treated as an unknown parameter and is estimated using the maximum likelihood method. The estimated value is used in the average likelihood ratio test for classification. The paper proposed and studied a HLRT based classifier to distinguish BPSK signal and QPSK signal without a priori knowledge of the

received signal level. The unknown signal level is first estimated using the maximum likelihood method and is then used in the average likelihood ratio test over the signal phase for classification. Simulation shows that the proposed classifier has high classification accuracy and is superior to the classifier assuming a known and constant signal level. The classification accuracy increases when the number of observed symbols or the variance of the signal level increases. Similarly, [23] is another research regarding BPSK and QPSK recognition using the HLRT method. It treats the carrier phase as the random variable with known PDF, and estimates unknown signal power that is used in the average likelihood ratio test over the carrier phase to form the test statistics for classification.

Paper [24] presents both the GLRT and HLRT based decision theoretic approaches to the solution of the ARM problem, It compared their performances with two ALRT-based algorithms that have appeared in the literatures [17, 20]. The simulation results indicate that these two algorithms can achieve significant performance gains over the ALRT-based ones for the classification of non-constant envelope modulations. In details, the GLRT algorithm treats the carrier phase and data symbols as unknown, which are estimated through the ML estimation. However, for constellation nested signals, the GLRT is easier to detect falsely. To alleviate the problems associated with nested constellations, HLRT is utilized by modeling the data symbols as discrete random variables uniformly distributed over the alphabet set and the carrier phase as a deterministic variable. By averaging over the data symbols and maximizing the resulting function with respect to the carrier phase, it led to the desired likelihood function.

Research in [25] and [26] investigated a classifier using two to multiple element antenna

array receivers to distinguish BPSK signal and QPSK signal embedded in AWGN. The classifiers applied the HLRT to determine the modulation type of an intercepted signal. The unknown phase shift of a signal received at the spatially separated antenna elements is first estimated. It is then used in the average likelihood ratio over the carrier phase to form the test statistic for classification. Two estimation techniques for the phase shift are examined. One utilizes the maximum likelihood technique by assuming the signal is deterministic, but unknown. The other one applies linear least squares technique by minimizing the squared difference between the received data and the assumed signal. Simulation shows that the proposed classifier has high classification accuracy. Estimating phase shift by MLE and constellation projection gives a higher classification accuracy than using a linear least squares estimation. Furthermore, the proposed method is much superior to the classifier that has only one received antenna.

Summary of LB leads to FB: In total, all the (A/G/H) LRT solutions resolve the AMR problem with a promising performance. However, they suffer from the computational complexity. Hence, in many other cases it gives rise to another main research trend to provide a suboptimal AMR performance, but carries an appropriate computational workload, which is the so called Feature-based method.

2.1.2. The Feature-Based (FB) Method

FB Methods: The FB approach is generally divided into two subsystems: (a) a features extraction subsystem, which is used to extract several key features from the received signal in order to reduce the dimension of the pattern representation, and (b) a pattern

recognition subsystem, which decides about the modulation format of the signal. The latter is usually trained beforehand by a pre-processor aside, so that a decision can take place when the actual observed data arrives. This preprocessor usually runs operations like normalization; centralization; noise reduction and so on to make features tend to be more significant or easier to be extracted later. A side processor studies the original signals' information or features and stores them as the templates in its buffer, which will be used to compare with received signals' information obtained from the features extraction subsystem, and then claims detections based on the pattern match results.

Specifically, FB approaches could be further categorized according to different methods for subsystem (a) features extraction, such as: instantaneous amplitude; phase and frequency based algorithms; statistical feature based; Fourier/wavelet transform based and so on. The corresponding literature reviews are presented below. Most FB classifiers are designed with a hierarchical structure. The hierarchical approach attempts to first identify the signal modulation class by utilizing the Macro characteristics. It then refines the exact orders of certain modulation scheme through the use of the Micro features.

Instantaneous amplitude, phase and frequency based algorithms: The most intuitive way to identify the modulation class of the incoming signal is to use the information contained in its instantaneous amplitude, phase and frequency. To extract such information, different methods were applied in the literature [27–35].

The following differences between signal classes (**ASK/PSK/FSK**) were employed for classification in [27–31]: FSK signals are characterized by constant instantaneous amplitude, whereas ASK signals have amplitude fluctuations, and PSK signals have

information of the phase. The maximum of the discrete Fourier transform (DFT) of centred (the term ‘centred’ specifies that the average is removed from the data set) normalized instantaneous amplitude was used as a feature to distinguish between **FSK and ASK/ PSK classes**.

ASK and BPSK signals have no information in the absolute phase, whereas M-PSK ($M > 2$) has. The variance of the absolute centred normalized phase was used to distinguish between M-PSK and real-valued constellation, BPSK and ASK.

ASK signals have no phase information by their nature, whereas BPSK has. The variance of the direct (not absolute) centred normalized phase was used to distinguish between BPSK and ASK classes. A binary decision tree structure was employed to discriminate between classes, and furthermore, within each class, as we will briefly mention later. At each node of the tree, the decision was made by comparing against a threshold.

The specific orders are also estimated based on the instantaneous amplitude and phase-based algorithms. After categorizing the modulation class, the next step is to classify modulation type accurately to different orders. Information extracted from the instantaneous amplitude and phase of the received signal was again exploited for modulation orders recognition, as follows. The variance of the absolute value of the normalized centred instantaneous amplitude was used to distinguish between 2-ASK and 4-ASK, as for the former the amplitude changes between two levels, equal in magnitude and opposite in sign, so, it has no information in the absolute amplitude, whereas it has for the latter [27–31]. The statistics was compared against a threshold for decision making at a tree node, as a part of the binary decision tree classifier. Similarly to using

the information contained in the instantaneous phase to identify the order of the PSK modulation, the information extracted from the instantaneous frequency is exploited to recognize the order of the FSK modulation. In [27–31], the variance of the absolute value of the normalized centred instantaneous frequency was used to distinguish between 2-FSK and 4-FSK. The feature was compared against a threshold for decision.

FSK, PSK and UW class separation: In [32] and [33], the variance of the zero-crossing interval was used as a feature to distinguish FSK from PSK and the unmodulated waveform (UW). The zero-crossing interval is a measure of the instantaneous frequency, and it is a staircase function for FSK signals, whereas a constant for UW and PSK signals. Thus, the AMR is treated as a two hypothesis testing problem: H1 for FSK, H2 for UW and PSK. The variance of the instantaneous frequency was also employed in [34, 35] to discriminate FSK from UW and PSK. In fact, the autoregressive spectrum modeling was used to extract the instantaneous frequency. The decision was made by comparing the feature against a threshold.

FSK, PSK order recognition: The histogram of the phase difference between two adjacent symbols was used in [32, 33] for PSK order identification, with the decision based on the comparison of the histogram against particular patterns. As for FSK order identification, the number of modes in the instantaneous frequency histogram was employed to determine the order of the FSK modulation in [32, 33]. In [34], the instantaneous frequency derivative was used to distinguish between 2-FSK and 4-FSK, under the assumption of the same bandwidths of the signals. The height of the peaks which occur in the differentiated instantaneous frequency is proportional to the frequency

deviation, and thus, for 4-FSK this is expected to be two times lower than for 2-FSK. If the peak average falls below a certain threshold, 4-FSK is chosen, otherwise 2-FSK.

Signal statistical-based (Moment and Cumulants) algorithm

Moment based Approach for PSK/QAM class separation: The moment-based feature used in [36], which is the nt^h -order/ q -conjugate moment of the matched filter output. The joint power estimation and classification method was performed, where the key point to develop the relationships between the second- and higher moments of received signal and signal and noise power, which means moments could be represented in terms of signal and noise power. The goal was to recognize the PSK and QAM.

Moment based Approach for PSK/QAM orders recognition: this is also considered in [36]. The signal-moment feature was employed to identify the order of QAM signal, with the decision made based on the minimum absolute value of the difference between the sample estimate and the prescribed values of the feature.

Signal moments were applied to distinguish between QPSK and 16-QAM in [37]. Specifically, a linear combination of the fourth-order/two-conjugate moment and the squared second-order/one-conjugate moment were employed, with the coefficients and the delay vector optimized to maximize the probability of correct classification. A set of features was chosen and classification was made based on the correlation between the sample estimate and theoretical feature vectors.

Cyclic Cumulant (CC) based approach: In [38, 39] the focus is on single-signal problems involving digital QAM signals. A feature based on fourth-order/two-conjugate

and second-order/one-conjugate CCs at the CF (cycle frequency) equals to the symbol rate, to identify the order of QAM modulations. The similar decision criterion as the one used in [37] was employed here. To be specific, a (normalized [39]) linear combination of the symbol-rate CCs is selected as the features vector. Parameters/coefficients of the combination are estimated by numerical optimization. The final identification is claimed based on correlation between estimated features and theoretical feature vectors, which actually follows with the classical match filters identically.

Cumulants Based Approach: In the work of Swami, Sadler, et al [40, 41], the classification feature consists of the magnitude of a single fourth-order cumulant. The idea is to use the lowest-order cumulant that provides discrimination for digital QAM/PSK signals. The focus is on two, four and eight classes. These statistics are natural as they characterize the shape of the distribution of the noisy baseband samples. It is shown that cumulant-based classification is particularly effective when used in a hierarchical scheme, enabling separation into subclasses at low signal-to-noise ratio with a small sample size. The research of [42] could be viewed as the extension of work in [40] as it implements a hierarchical classifier by combining several normalized moments and cumulants as extracted features for training a neural network to identify MPSK, MFSK and MQAM. It considers also multipath propagation channel and noise distortion environments.

The PDF [43-45] and its statistical moments [46-48] features extraction based method: The phase PDF is multimodal, and the number of modes provides information for the PSK order identification. In the high-SNR region, M-PSK exhibits M distinct

modes, while the SNR decreases or M increases, the peaks smear off and finally the PDF converges to a uniform PDF [47]. Specifically, an approximation using the Tikhonov PDF and a Fourier series expansion of the phase PDF were employed in [43–45] for PSK signal classification, combining with a log-likelihood ratio test for decision. [45] provides a suboptimal performance by the means of using the Tikhonov function as the approximated expression of the signal phase PDF, instead of the exact expressions derived in [43, 44].

By defining the moment of phase as the feature, signals could also be recognized using similar methodology as mentioned above. The moment could either be expressed using the exact phase PDF [46, 48], or can be derived from the approximation to the PDF [47].

2.1.3 Fourier Transform-Based (FD) Algorithms

In [49], the empirical characteristic function of the phase was exploited for classification. Specifically, the periodic components of the phase PDF were analyzed for PSK order identification in [49], using the DFT of the phase histogram. Furthermore, in [50] the algorithm was extended to QAM signal classification, by exploiting the additional information provided by the magnitude of the received signal.

2.1.4 Wavelet Transform-Based (WD) Algorithms

WD class categorization: The utility of the wavelet transform to localize the changes in the instantaneous frequency, amplitude and phase of the received signal was also studied for AMC. The distinct behavior of the Haar WT (HWT) magnitude for PSK, QAM and FSK signals was employed for class identification in [51–53]. For a PSK signal this is a

constant, with peaks occurring at phase changes. On the other hand, because of the frequency and amplitude variations in FSK and QAM, respectively, the HWT magnitude is a staircase function with peaks at phase changes. These peaks do not provide useful information for non-continuous phase FSK signals. If only the phase is retained for a QAM signal, it behaves like a PSK signal and thus, the HWT magnitude is constant. On the other hand, as PSK and FSK signals are of constant amplitude, amplitude normalization has no effect on their HWT magnitude. After peak removal, the variance of the HWT magnitude with amplitude normalization was used to discriminate FSK from PSK and QAM. Furthermore, the variance of the HWT magnitude without amplitude normalization was employed to distinguish between QAM and PSK. The decisions were made by comparing the features against some thresholds, chosen based on the statistical analysis of the features, to minimize the probability of error for PSK signals [51–53].

WD modulation orders recognition: Different PSK signals give rise to different sets of peak values in the magnitude of the Haar wavelet transform. The histogram of the peak magnitudes was employed to identify the order of a PSK signal in [52], with the decision made by comparing the histogram with the theoretical PDFs corresponding to different orders. The number of modes in the histogram of the Haar wavelet transform magnitude was investigated for the FSK order identification in [51, 52]. If $M/2+1$ to M modes appear in the histogram, the input is identified as M-FSK.

Some previous WD-based AMR studies that have been reported in the literature have used both the Continuous Wavelet Transform (CWT) and the Discrete Wavelet Transform (DWT) [54]–[56]. Most of these studies have involved computing histograms of the CWT and/or DWT wavelet coefficients of the received signals. Based on the

characteristic number of peaks contained in the histograms, different types of digitally modulated signals can be identified [54], [57], [58]. The communications signals considered in those studies are M-ary PSK and M-ary FSK [54]; Quadrature Phase Shift Keying (QPSK) and Gaussian Minimum Shift Keying (GMSK) signals [59]; as well as M-ary QAM and M-ary ASK signals [60]. The wavelets used in these studies have been largely focused on the Haar, although the Daubechies wavelet family has also been used in some cases.

After reviewing various successful AMR algorithm utilizing different methodologies and providing promising performances, it is inspired to develop a new AMR approach in this work by combining those approved advance methods together. In Chapter 3 and Chapter 4, a wavelet-based instantaneous AMR method and a wavelet-based statistics method will be designed and illustrated in detail.

Chapter 3 Theoretical Preliminaries

3.1 Digital Communication Signals Model

Several different families of digital modulation schemes are studied in this dissertation. Specifically, binary and quaternary ASK and FSK signals, M-ary PSK signals for $M = 2, 4$, and 8 , and multiple-level QAM signals for $M = 4, 16$ and 64 are investigated in conjunction with developing wavelet based recognition and demodulation strategies.

1. M-ary Phase Shift Keying (M-ary PSK)

- (a) BPSK IEEE 802.11a and ZigBEE standards.
- (b) QPSK IEEE 802.11b systems and Bluetooth
- (c) 8-PSK Wireless communications systems applications.

2. M-ary Quadrature Amplitude Modulation (M-ary QAM)

The QAM plays important roles in cable modems for high speed internet access, digital video transmission standard for cable television, and digital terrestrial television applications.

3. M-ary Amplitude Shift Keying (ASK)

- (a) BASK LED Transmitters
- (b) 4ASK Transmission of digital data over an optical fiber.

4. Frequency Shift Keying (FSK)

- (a) BFSK North America Caller ID, two-tone Morse code transmitting, Fax services,
- (b) 4FSK Most early telephone-line modems, Transmission of telemetry data,
(amateur, shortwave) radio.

The time-domain ASK signals are defined as [74]

$$s_i(t) = \begin{cases} A_i \sqrt{\frac{2E_b}{T_b}} \cos(2\pi f_c t), & 0 \leq t \leq T_b \\ 0, & \text{otherwise} \end{cases}$$

where $i = 1, 2, 3, 4, \dots$. The variable A_i represents the different levels of amplitude in ASK signals. In the case of BASK, two amplitudes, A_1 and A_2 , denote data symbols '0' and '1', respectively. In the case of 4-ASK signals, the four amplitudes, A_1 , A_2 , A_3 , and A_4 , correspond to the data symbols '00', '01', '10', and '11.' The parameter E_b denotes the energy per symbol, T_b denotes the temporal duration of the symbol, and the carrier frequency is denoted by f_c .

The time-domain FSK signals used are defined as [74]

$$s_i(t) = \begin{cases} \sqrt{\frac{2E_b}{T_b}} \cos(2\pi f_i t), & 0 \leq t \leq T_b \\ 0, & \text{otherwise} \end{cases}$$

Where $i = 1, 2, 3, 4, \dots$. The parameter f_i denotes the different carrier frequencies that are required for different orders of FSK signals. For example, f_1 and f_2 denote the carrier frequencies used to represent the data symbols '0' and '1' in a BFSK signal, respectively, etc.

Time-domain M-ary PSK signals are defined as [74]

$$s_i(t) = \begin{cases} \sqrt{\frac{2E_b}{T_b}} \cos\left[2\pi f_c t + \frac{2\pi}{M}(i-1)\right], & 0 \leq t \leq T_b \\ 0, & \text{otherwise} \end{cases}$$

Where $i = 1, \dots, M$. The parameter M represents the order of the PSK signals, e.g.,

$M = 2$ for BPSK signals, $M = 4$ for QPSK signals, etc. In the case for $i = 1$ and 2, the corresponding data symbols are '0' and '1' in a BPSK signal. In the case when $i = 1, 2, 3$, and 4, the data symbols are denoted as '00,' '01,' '10' and '11' in a QPSK signal, respectively.

The M-QAM signals are defined as [74]

$$s_k = \sqrt{\frac{2E_b}{T_b}} a_k \cos(2\pi f_c t) - \sqrt{\frac{2E_b}{T_b}} b_k \sin(2\pi f_c t), \quad 0 \leq t \leq T_b$$

where $k = 0, \pm 1, \pm 2, \dots$, and the quantities a_k and b_k represent the discrete amplitudes for the in-phase and quadrature carriers, respectively.

3.2 An Overview of the Wavelet Transform

This section introduces the mathematical theorem of the WT [61], [62]-[65] is presented in this section. WTs can be further categorized as the CWT or the DWT [66]-[70], which are excel at characterizing (analysis) digital communication signals, and processing signal or image for reconstruction and synthesis [69].

Wavelets can be generally viewed as basis functions representing signals utilizing rapidly decaying oscillatory functions. They are especially useful in representing all types of signals that are aperiodic and/or have jump discontinuities which appear in practice and realistic a lot. Following paragraph will show how the wavelet transforms differ or being complement to the Fourier transform.

In the Fourier transform theory, a time-domain signal is expressed in terms of sinusoidal functions (a continuous-time basis set) in the spectral domain. By definition, the Fourier transform use the entire time signal to produce the frequency-domain description of the

signal. However, in another word, only frequency information is preserved but all the temporal detail of the signal is lost in this process.

For the preservation of the temporal information of the signal, the Short-Time Fourier Transform (STFT) [71] is designed base on the regular Fourier Transformation by adding windowing functions on it. In the STFT, signals firstly multiply with a user-defined window function before go into the Fourier transform. By translating the window along the signal function in time, the Fourier transform of each “windowed signal” is computed. In this way, both the spectral content and the temporal content of the signal could be the captured in the STFT domain.

Unfortunately, even the STFT has its drawback caused by the fact that the window can only be in a fixed size. leads to an inherent problem of resolution: a function with narrow, highly-localized, time-domain window waveform of fixed size, provides poorly localized spectral-domain resolution. Conversely, a broad, or non-localized, temporal window function provides highly localized spectral resolution. This drawback, associated with fixed window sizes, is especially problematic in the analysis of digitally modulated communications signals. An improvement solution would be when the size of the window function can be altered to accommodate variations of phase and frequency that are characteristic of a digitally modulated communications signal.

WTs may be used instead in order to overcome this problem. In the WT, a window function, i.e., a wavelet can be translated and dilated in time. The dilation of wavelets allows for the variation in the size of window function so as to achieve a specific temporal resolution. The translated and dilated wavelets at different level of resolution are correlated with the signal, resulting in the desired wavelet coefficients. These wavelet

coefficients implicitly contain the frequency information of the original signal, and also explicitly preserve the temporal information of the signal. Figure 3.1 [73] shows how signal is differently reconstructed in the time-frequency by these three transforms:

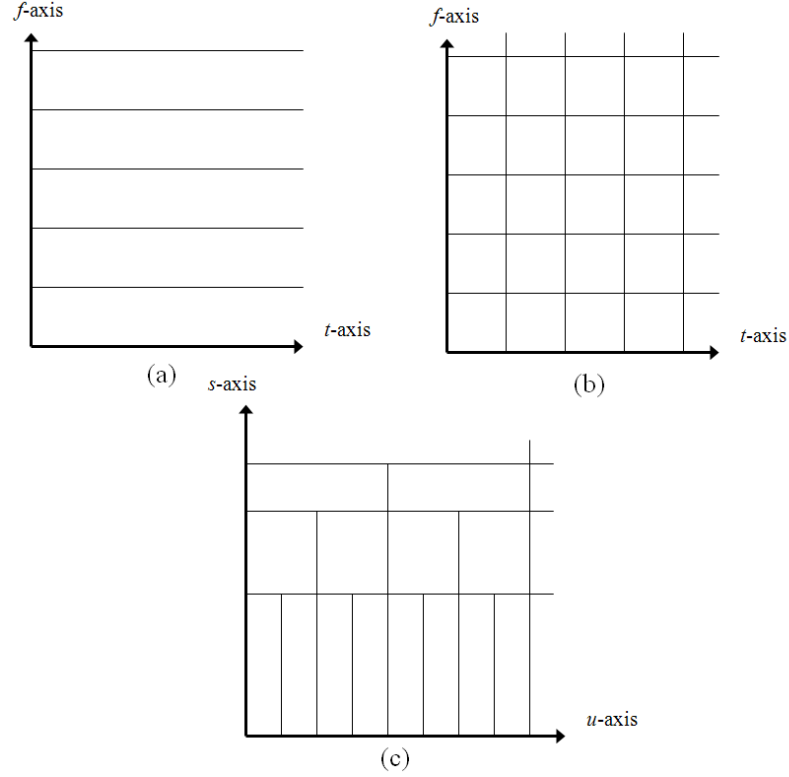


Fig. 3.1. Different time-frequency tile allocation of the three transforms: (a) Fourier Transform, (b) STFT and (c) wavelet transform

3.3 Review of the Continuous Wavelet Transform

The window function of the wavelet transforms had properties that the function $\psi(t)$

averages to zero over all time and has finite energy [67], i.e., $\int_{-\infty}^{\infty} \psi(t) dt = 0$ and

$\int_{-\infty}^{\infty} |\psi(t)|^2 dt < \infty$, respectively. It follows that the window function so described, allow for

not only temporal translation but also for time dilation. In other words, the width of the

windows can be varied to achieve a required resolution in either the temporal or spectral domains. Such window functions are called wavelets. Transforming, that is comparing translated and scaled (dilated) wavelets with the original signal yields correlation coefficients. In this way, at different scales, correlation coefficients contain the frequency content of the original signal while automatically preserving the temporal information of the signal. The CWT, for a given wavelet $\psi(t)$, is formally defined as

$$W(a,b) = \int_{-\infty}^{\infty} f(t) \psi_{a,b}^*(t) dt \quad (3.1)$$

where $\psi_{a,b}(t) \equiv \frac{1}{\sqrt{|a|}} \psi\left(\frac{t-b}{a}\right)$, $f(t)$ is the function to be transformed, a is the scale, or dilation, variable and b is the translation variable.

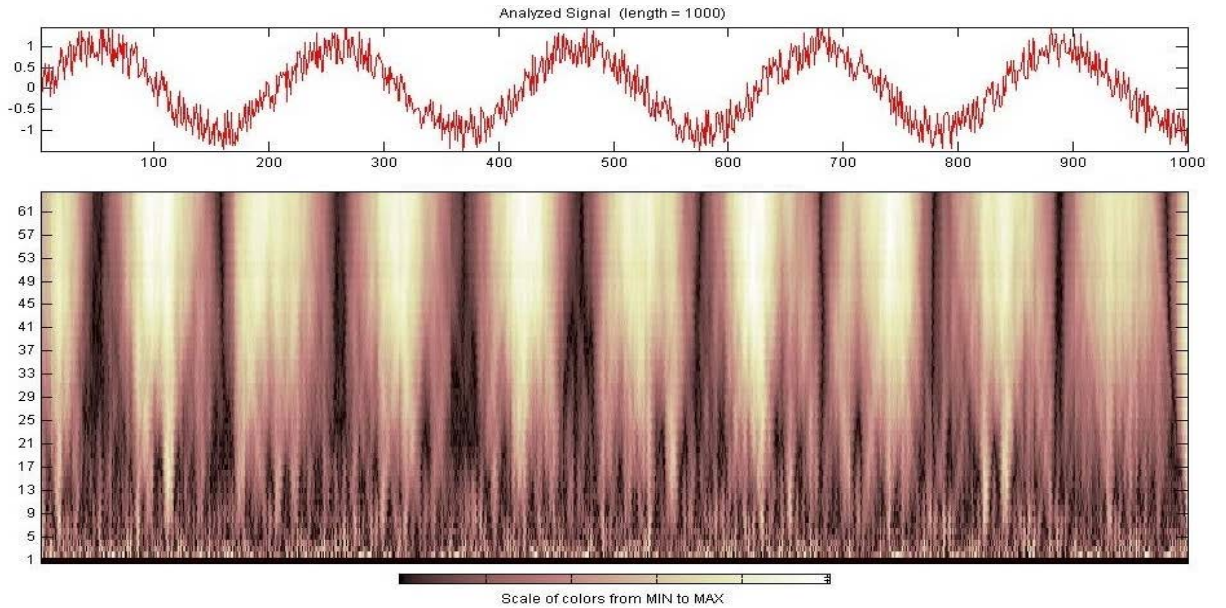


Fig. 3.2. (Top) A time-domain noisy sinusoidal signal,(bottom) The corresponding WD scalogram using Haar through CWT.

An example of a sinusoidal signal in both the time-domain and the wavelet-domain is shown in Fig. 3.2. The abscissa represents the time axis of the signal for both time- and wavelet-domains. The amplitude of the signal is represented by the ordinate of the time-domain plot. And in the wavelet-domain, the correlation outputs between the wavelets and the time-domain signal at different scales, or dilations of the wavelet function is represented at the ordinate of the wavelet-domain scalogram. The different scales are defined as the levels of resolution.

Through observing the fractal patterns of the segments appearing in the scalograms, it is clear to see that, when one-dimensional time-domain modulated signals are transformed into the WD, structural details are present in two-dimensions (translation and scale). Signals are represented richly at some levels of resolution in the WD. On the other hand, at other resolution levels, the representation of the signal energy content is very weak. In the WD scalogram shown in Fig. 3.2 (bottom), the darker areas represent smaller correlation values obtained when the windowed time-domain signal is compared with a wavelet of choice. The lighter areas in the scalogram represent larger magnitude wavelet coefficients obtained with the windowed signal and the choice of wavelet. This particular characteristic of the scalogram data is utilized advantageously in the WD AMR process.

Wavelets that are used for the CWT are typically required to satisfy the following properties [71]:

- i. **Admissibility:** Wavelets are required to be square integral functions and must not have a non-zero component at zero frequency. It is important that this

property be satisfied in order for the inverse CWT.

Mathematically, this condition is described as

$$c_\psi = \int_{-\infty}^{\infty} \frac{|\Psi(\omega)|^2}{|\omega|} d\omega < +\infty \quad (3.2)$$

Where $\Psi(\omega)$ is the Fourier transform of the wavelet $\psi(t)$, and c_ψ is the admissibility constant.

- ii. **Regularity:** This condition ensures that the wavelet transform coefficients, obtained using (3.1), decrease quickly in magnitude as the dilation changes. By doing this, the wavelets can be very highly localized in time without causing an unbounded time-bandwidth product.

Therefore, if a wavelet satisfies the condition that

$$M_p = \int_{-\infty}^{\infty} t^p \psi(t) dt = 0 \quad \text{for } p = 0, 1, 2, \dots, n \quad (3.3)$$

where M_p is the p^{th} moment of the wavelet, then the wavelet is said to be of order n .

- iii. **Linear Transformations:** The wavelet transform, $W_f(a, b)$, must satisfy the following conditions:

$$\text{a) Superposition: } W_{f_1+f_2}(a, b) = W_{f_1}(a, b) + W_{f_2}(a, b) \quad (3.4a)$$

$$\text{b) Translation: } W_{f(t-t_0)}(a, b) = W_{f(t)}(a, b-t_0) \quad (3.4b)$$

$$\text{c) Rescaling: } W_{m^{1/2}f(mt)}(a, b) = W_{f(t)}(ma, mb). \quad (3.4c)$$

Variety of communications signals could be expressed in terms of wavelets by using the CWT technology. The resulted wavelet coefficients are specifically corresponding to combinations of signals and different being used. Furthermore precisely, the wavelet coefficients could be obtained for different scales and translations of the wavelet. Identification of the changes and the statistical attributions from their wavelet coefficients of communication signals can reveal the amplitude, phase and frequency fluctuations inherent in a communications signal, which are keys for modulation type identification.

However, on studying the CWT further, it is found that information it provides is highly redundant as far as the reconstruction of the signal is concerned, which is beneficial for processing communications signals. But this redundancy requires a significant amount of computational effort. The discrete wavelet transform (DWT), on the other hand, provides sufficient information both for analysis and synthesis of the original signal, with a significant reduction in the computation time.

3.4. Discrete Wavelet Transform

It should be emphasized that, the discrete wavelet transform is not simply the discretized continuous wavelet transform. It is inspired by multi-resolution analysis. The introduction could be either starting from the space geometrical point of view or the filter bank format.

Geometrical Interpretation of the DWT:

Defining the direct sum, $L^2(\mathbb{R}) = V_j \oplus V_j^\perp$. Hence, for an arbitrary function $f(t)$, it results in the decomposition of $f(t)$ into two orthogonal parts:

$$f(t) = f_j(t) + w_j(t), \quad f_j(t) \in V_j, w_j(t) \in V_j^\perp, f_j(t) \perp w_j(t) \quad (3.5)$$

Besides, a featured structure called wavelet multi-resolution analysis expands a time signal into components representing different scales (from a coarser to a finer resolution).

The sets of scale are defined in terms of a sequence of nested subspaces V_j of the space

$$L^2(\mathbb{R}), \text{ i.e., } \dots \subset V_{-2} \subset V_{-1} \subset V_0 \subset V_1 \subset V_2 \subset \dots \subset L^2(\mathbb{R}).$$

The spaces V_j have a special structure, being defined as linear spans of the scaled and translated replicas of a single function, called the scaling function, or the father wavelet.

Its scaled/translated replicas are defined for any integer of j, n by: $\phi_{jn}(t) = 2^{j/2} \phi(2^j t - n)$.

The functions $\phi_{jn}(t)$ are orthonormal for each fixed j , and form a basis of space

$$V_j. (\phi_{jn}, \phi_{jm}) = \delta_{nm}$$

Now the projection of an arbitrary signal $f(t) \in L^2(\mathbb{R})$ onto the subspace V_j is defined by

the following expansion in the ϕ_{jn} basis:

$$f_j(t) = \sum_n c_{jn} \phi_{jn}(t) = \sum_n c_{jn} 2^{j/2} \phi(2^j t - n) \quad (3.6)$$

The projection $f_j(t)$ can be thought of as an approximation of $f(t)$ at scale j with time resolution of 2^{-j} . Because $V_i \subset V_j$ for $i \leq j$, so $f_j(t)$ incorporates information about $f(t)$ from all coarser resolution.

Another wavelet function $\psi(t)$ and its scaled and translated replicas are actually spanning the orthogonal complement V_j^\perp of V_j with respect to $L^2(\mathbb{R})$. Note that

$\psi_{in}(t) = 2^{i/2} \psi(2^i t - n)$, $i \geq j$, which are orthogonal to $\phi_{jn}(t)$, and are also mutually

orthonormal, $(\psi_{in}, \psi_{i'n'}) = \delta_{ii'} \delta_{nn'}$, $(\phi_{jn}, \psi_{in}) = 0, i \geq j$.

The component $w_j(t)$ from equation (3.5) is referred to as the “detail” and incorporates

the details of $f(t)$ at all the higher resolution levels $i \geq j$, or finer time scales $2^{-i} \leq 2^{-j}$.

It is spanned by the ψ -basis expansion:

$$w_j(t) = \sum_{i \geq j} \sum_n d_{in} \psi_{in}(t) = \sum_{i \geq j} \sum_n d_{in} 2^{1/2} \psi(2^i t - n) \quad (3.7)$$

Hence, taking (3.6) and (3.7) into (3.5) to complete form of the multiresolution decomposition analysis of $f(t)$,

$$f(t) = f_j(t) + w_j(t) = \sum_n c_{jn} \phi_{jn}(t) + \sum_{i \geq j} \sum_n d_{in} \psi_{in}(t) \quad (3.8)$$

Now if we set J and J_0 to the highest and lowest resolutions of interest, we have

$$f(t) = \sum_n c_{Jn} \phi_{Jn}(t) = \sum_k c_{J_0 k} \phi_{J_0 k}(t) + \sum_{j=J_0}^{J-1} \sum_k d_{jk} \psi_{jk}(t), \quad (3.9)$$

Until now, the discrete wavelet transform (DWT) is essentially implemented by mapping of the expansion coefficients from level J to the levels j through $J-1$, $c_{Jn} \rightarrow \{c_{jn}; d_{in}, j \leq i \leq J-1\}$.

The DWT of the sinusoidal signal from Fig. 3.2 is plotted in Fig. 3.3. The DWT-based scalogram presents similar patterns structure with CWT-base scalogram at different time and frequency location.

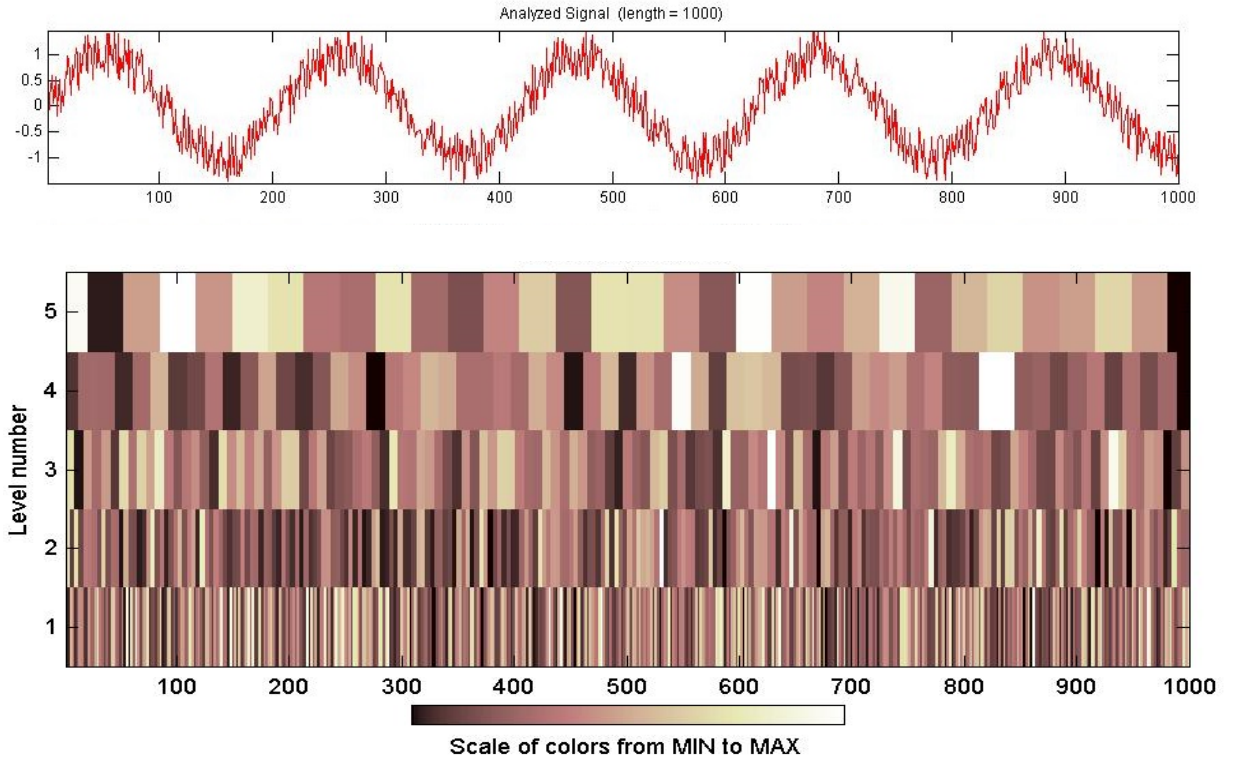


Fig. 3.3 (Top) A time-domain noisy sinusoidal signal,(bottom) The corresponding WD scalogram using Haar through DWT.

Multiresolution and Filter Bank Analysis of DWT:

An alternative classical way to study DWT is called filter bank analysis, and this form could be derived from the wavelet geometric structure analysis.

The whole real space was defined as: $L^2(\mathbb{R}) = V_j \oplus V_j^\perp$. Now for the subspace V_1 , there is another direct sum states: $V_1 = V_0 \oplus W_0$, where the W_0 is the orthogonal complement of V_0 relative to V_1 . Since $V_0 \subset V_1$, then the scaling function $\phi(t) \in V_0$ can be expanded in the basis $\phi_{1n}(t)$ that spans V_1 . Thus, there must exist coefficients h_n such that

$$\phi(t) = \sum_n h_n \phi_{1n}(t) = \sum_n h_n 2^{1/2} \phi(2t - n) \quad (3.10)$$

Besides, because $\psi(t) \in W_0 \subset V_1$, it can be also expanded in the $\phi_{1n}(t)$ basis, as in the following equation:

$$\psi(t) = \sum_n g_n \phi_{1n}(t) = \sum_n g_n 2^{1/2} \phi(2t - n) \quad (3.11)$$

We can have more general equations of $\phi_{jn}(t)$ and $\psi_{jk}(t)$ through simply iterations of (3.10) and (3.11),

$$\begin{aligned} \phi_{jk}(t) &= 2^{j/2} \phi(2^j t - k) = 2^{j/2} \sum_m h_m 2^{1/2} \phi[2(2^j t - k) - m] \\ &= \sum_m h_m 2^{(j+1)/2} \phi(2^{j+1} t - 2k - m) = \sum_m h_m \phi_{j+1, m+2k}(t) = \sum_n h_{n-2k} \phi_{j+1, n}(t) \end{aligned}$$

$$\text{Similarly, } \psi_{jk}(t) = \sum_n g_{n-2k} \phi_{j+1, n}(t)$$

Using the orthogonality property $(\phi_{j+1, n}, \phi_{j+1, m}) = \delta_{nm}$, coefficients h and g could be obtained: $h_{n-2k} = (\phi_{jk}, \phi_{j+1, n})$, $g_{n-2k} = (\psi_{jk}, \phi_{j+1, n})$.

Also, according to space direct sum equation: $V_{j+1} = V_j \oplus W_j$, an arbitrary function

$$f(t) = \sum_n c_{j+1, n} \phi_{j+1, n}(t) = \sum_k c_{jk} \phi_{jk}(t) + \sum_k d_{jk} \psi_{jk}(t) \quad (3.12)$$

The right-hand coefficients in (3.12) are:

$$c_{jk} = (f, \phi_{jk}) = \left(\sum_n c_{j+1, n} \phi_{j+1, n}, \phi_{jk} \right) = \sum_n c_{j+1, n} (\phi_{j+1, n}, \phi_{jk}) = \sum_n h_{n-2k} c_{j+1, n} \quad (3.13)$$

$$d_{jk} = (f, \psi_{jk}) = \left(\sum_n c_{j+1, n} \phi_{j+1, n}, \psi_{jk} \right) = \sum_n c_{j+1, n} (\phi_{j+1, n}, \psi_{jk}) = \sum_n g_{n-2k} c_{j+1, n} \quad (3.14)$$

Equations (3.13) and (3.14) are the analysis equations since the higher scale level coefficients are decomposed into two parts in the next lower scale level.

Conversely, the coefficients $c_{j+1, n}$ can be reconstructed from c_{jk} , d_{jk} to format the

synthesis:

$$\begin{aligned}
 c_{j+1,n} &= (f, \phi_{j+1,n}) = \left(\sum_k c_{jk} \phi_{jk} + \sum_k d_{jk} \psi_{jk}, \phi_{j+1,n} \right) \\
 &= \sum_k c_{jk} (\phi_{jk}, \phi_{j+1,n}) + \sum_k d_{jk} (\psi_{jk}, \phi_{j+1,n}) \\
 &= \sum_k h_{n-2k} c_{jk} + \sum_k g_{n-2k} d_{jk}
 \end{aligned} \tag{3.15}$$

The analysis and synthesis procedure could be design as the filter bank format by defining $\bar{h}_n = h_{-n}$ and $\bar{g}_n = g_{-n}$. Now we can turn equations (3.13)-(3.15) into systems composed by convolution with filters and down/up samplers.

$$\begin{aligned}
 c_{jk} &= \sum_n h_{n-2k} c_{j+1,n} = \sum_n \bar{h}_{2k-n} c_{j+1,n} = (\bar{h} * c_{j+1})(2k) = (\bar{h} * c_{j+1})_{down} \\
 d_{jk} &= \sum_n g_{n-2k} c_{j+1,n} = \sum_n \bar{g}_{2k-n} c_{j+1,n} = (\bar{g} * c_{j+1})(2k) = (\bar{g} * c_{j+1})_{down}
 \end{aligned} \tag{3.16}$$

$$c_{j+1,n} = \sum_k h_{n-2k} c_{jk} + \sum_k g_{n-2k} d_{jk} = \sum_m h_{n-m} c_{jm}^{up} + \sum_m g_{n-m} d_{jm}^{up} = h * c_j^{up} + g * d_j^{up} \tag{3.17}$$

Corresponding filter banks to equation (3.16) and (3.17) is drawn as below:

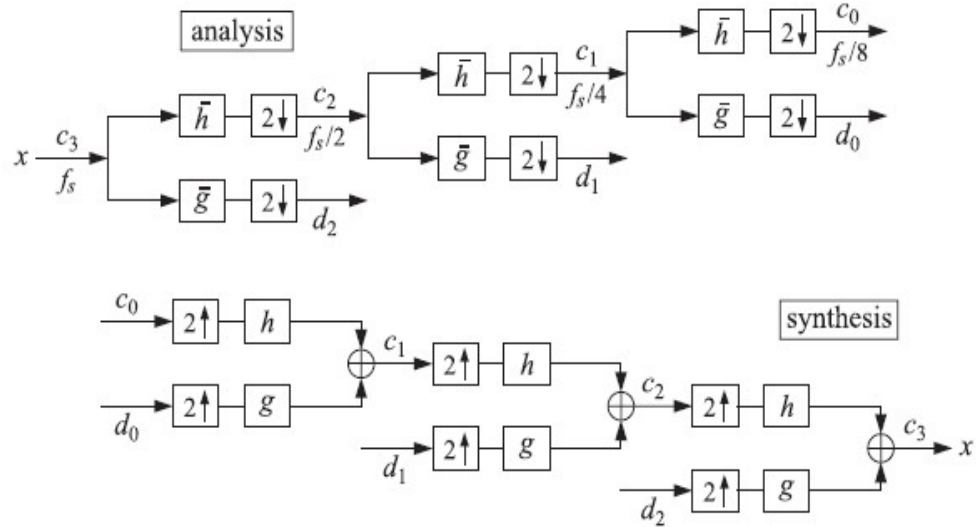


Fig 3.4 Analysis and synthesis filter bank [83]

Besides, the subspace direct sum $V_{j+1} = V_j \oplus W_j$ leads to the complete spaces direct-sum decomposition: $V_J = V_{J_0} \oplus (W_{J_0} \oplus W_{J_0+1} \oplus \dots \oplus W_{J-1})$

Hence, deriving from equation (3.12), the corresponding multi-resolution expansion equation is, (if J and J_0 are the highest and lowest resolutions of interest) identical with the geometrical interpretation equation (3.9):

$$f(t) = \sum_n c_{Jn} \phi_{Jn}(t) = \sum_k c_{J_0 k} \phi_{J_0 k}(t) + \sum_{j=J_0}^{J-1} \sum_k d_{jk} \psi_{jk}(t)$$

Chapter 4 DWT-AMR Based On Instantaneous Features

DWT-AMR means that the received signal is transformed into the wavelet-domain using the DWT. Then DWT-based signatures, or feature templates extracted from DWT modulated signal, which contain characteristic features of a particular modulation scheme expressed in the wavelet-domain. The correlations between the transformed received signal and the WD signatures are computed as the decision variables to show the similarity. The decision variables are used in decision-making operations comprising the AMR algorithm. Decision-making operation heralds the last step of completing the AMR algorithm. The efficacy of the AMR algorithm is validated using computer simulations. The simulations are Monte Carlo experiments conducted in a manner so as to provide statistically significant results.

4.1 DWT-based AMR Preparation

The proposed DWT-based AMR algorithms introduced are classified as the feature-based pattern recognition approach follow categories from literatures' methodologies, two approaches will be introduced in Chapters 4 and 5. The first algorithm mainly relies on signals' instantaneous changes in the wavelet domain to extract features for pattern comparisons. And the second method utilizes the statistical features extracted from wavelet transformed signals to implement the AMR function. This chapter mainly focuses on the AMR development utilizing the former algorithm of pattern recognition. Specifically, extracting instantaneous changes which are able to represent digital communication signal features well. It is natural to look at symbol transitions where changes in the amplitude, frequency, and/or phase of a digitally modulated signal take

place. It will be shown that after the discrete wavelet transform those inherent signatures do not disappear, but become more distinctive when analyzed at different resolution levels. Such wavelet based outputs are shown suitable to be set as templates for the blind identification of digitally modulated communications signals acquired by a communications receiver. This work is inspired by some previous instantaneous feature based AMR work [27-35, 84].

Let us first start with the binary modulations cases, which are BASK, BPSK and BFSK. The AMR process consists of two steps. First, a received signal that has been corrupted with AWGN is transformed into the wavelet-domain via the DWT. The resulting wavelet-domain signal is then correlated with the pre-defined templates corresponding to all three types of binary modulation schemes. The modulation type that is declared to be operative at the receiver input is determined on the basis of decision logic that employs a majority vote strategy. Following diagrams show this idea from both the system view and the logical flow view. In details, it needs to be introduced completely from four parts: 1. Wavelet type selection; 2. WD template setup; 3. Simulation algorithms illustration; 4. Simulation results and analysis.

Wavelet type selection: The family of sixty-five commonly used wavelets has been summarized from existing literatures for the BASK, BFSK and BPSK modulation families. The different wavelets, and wavelet families, that were used in this study include the following:

- i. Haar wavelet[51-54,60]
- ii. Mexican Hat wavelet[85]
- iii. Morlet wavelet[86, 87]

- iv. Meyer wavelet [87]
- v. Daubechies wavelet family (ten distinct wavelets) [87]
- vi. Family of symlets (seven distinct wavelets) [87]
- vii. Family of Coiflets (five distinct wavelets) [87]
- viii. Rseverse biorthogonal spline wavelets (fifteen distinct wavelets) [55]
- ix. Biorthogonal spline wavelets (fifteen distinct wavelets) [84]

Among above different wavelets, the Haar is the one which has been most utilized.

WD Templates Setup:

The aim of these computer simulation experiments is to decompose three modulated signals in the wavelet-domain using the Haar wavelets and then identify the wavelet that provides the most distinct decomposition for each of the modulation schemes. The graphical results shown in Figs.4.1-4.3 are meant to serve as visual and intuitive guides to demonstrate the signal identification capabilities of the wavelet transform, particularly employing the DWT.

In Figs.4.1-4.3 the DWT decompositions of test signals are shown. The computer simulation results were obtained using MATLAB. In all cases the input signal was decomposed to ten levels of resolution. Each level corresponds to dilating the wavelet by a power of two. It has been observed that by increasing the scaling factor in powers of two dramatically reduces the computational time involved in the signal decomposition process, and simultaneously provides a level of accuracy very well-suited to the methodology proposed in this study. In the wavelet-domain decomposition plots of Figs.4.1-4.3 the DWT detailed coefficients are plotted to produce the fractal patterns. Note that the ordinate corresponds to the dilation parameter a , and the abscissa

corresponds to the translation parameter b .

It should be noted that the fractal patterns shown in Figs.4.1-4.3 are effectively visual representations of the magnitudes of the wavelet coefficient matrix elements, graded from black to white in sixty-four grayscale levels, with black being the lowest magnitude and white the highest. It was found that of the data symbol transition portions of the signals, the similarity between the noise-free scalograms and the noisy scalograms is obvious, especially at the higher levels of resolution. This similarity is the most important feature that is exploited in the AMR algorithm developed in this work. Later, simulations will be conducted to test the similarity using the correlation function. It will be shown that the information contained in the DWT detailed coefficients at the lower levels of resolution is actually sufficient to achieve reliable AMR results.

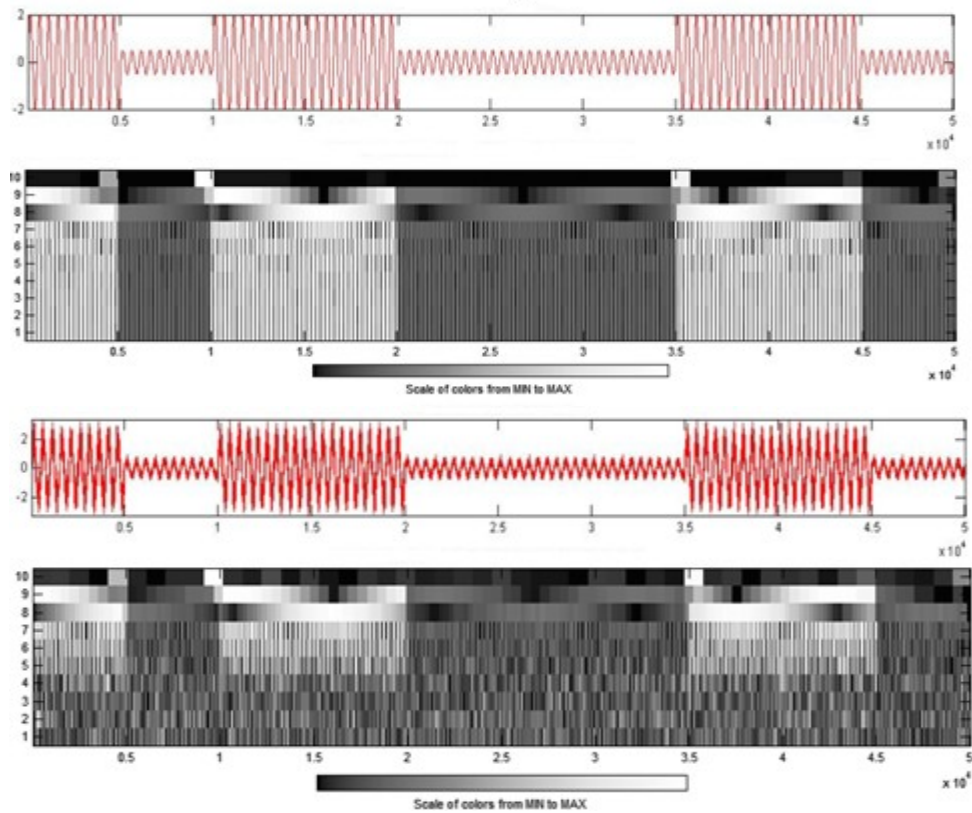


Fig.4.1 (a): (top) BASK signal without noise, 10-level WD decomposition using the Haar wavelet; (b): (bottom) BASK signal at 10 dB SNR, 10-level WD decomposition using the

Haar wavelet.

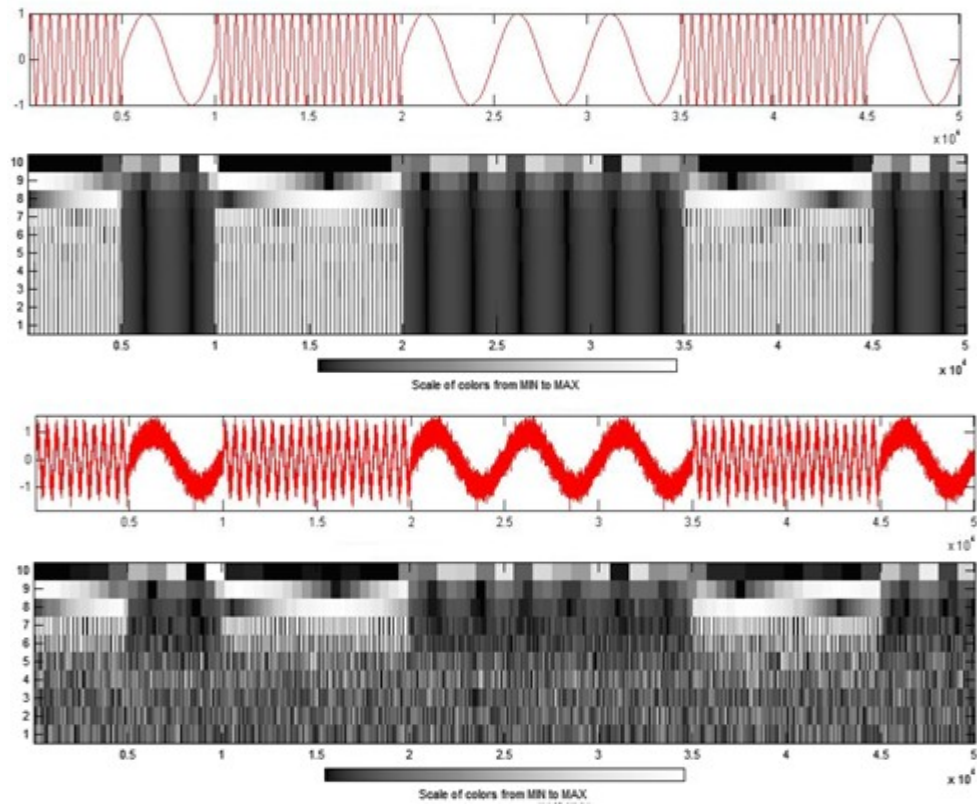


Fig.4.2 (a): (top) BFSK signal without noise, 10-level WD decomposition using the Haar wavelet; (b): (bottom) BFSK signal at 10 dB SNR, 10-level WD decomposition using the Haar wavelet

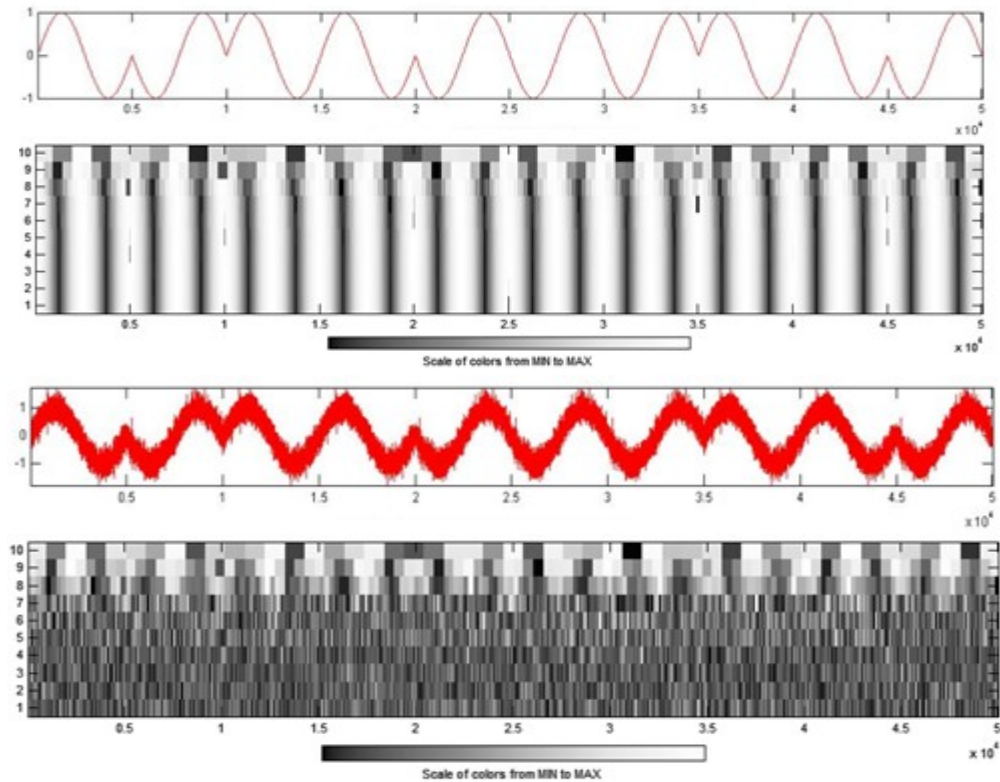


Fig.4.3 (a): (top) BPSK signal without noise, 10-level WD decomposition using the Haar wavelet; (b): (bottom) BPSK signal at 10 dB SNR, 10-level WD decomposition using the Haar wavelet.

The DWT-based Instantaneous templates represent the unique features of the modulated signals in the wavelet-domain, which reflect amplitude variations, frequency alternations, or phase changes of the signals in the time domain. Hence for binary modulated noise free signal, the WD Instantaneous templates are extracted from the symbols transition period (binary symbol 0 to binary symbol 1, and 1 to 0). The templates are constructed in the WD using the DWT detailed coefficients of test signals that correspond to each of the three digital modulation schemes considered herein; the Daubechies 1 (Haar) wavelet is used. Therefore, for each of the binary modulation schemes, two templates are required in order to completely characterize the two possible data state transitions. The templates are stored for later use in the AMR process. As seen in Fig.4.4, a communications signal

having a frame length of 3 symbols is shown with each of the two possible symbol transitions present, i.e., “0” to “1” and “1” to “0.” The two instantaneous features templates, T_1 and T_2 , can be described based on the mathematical models presented in (4.1)-(4.3).

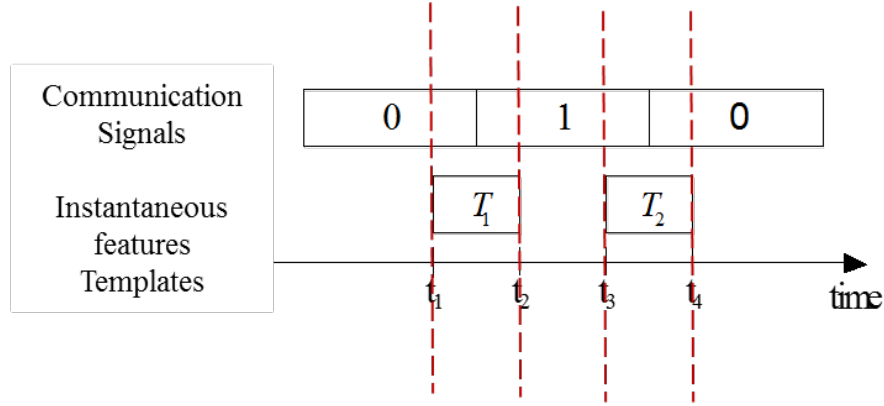


Fig.4.4 Illustration of time-domain instantaneous features templates.

The WD templates are described based on symbol transitions that occur within a digitally modulated communications signal. Two instantaneous features templates can be extracted from each of the 3 binary digitally modulated signals. The models in time domain of these templates are defined according to the following:

$$p_{BASK,1}(t) = \begin{cases} A_1 \cos(2\pi f_c t), & t_1 < t \leq t_2 \\ A_2 \cos(2\pi f_c t), & t_3 < t \leq t_4 \end{cases} \quad (4.1a)$$

$$p_{BASK,2}(t) = \begin{cases} A_2 \cos(2\pi f_c t), & t_1 < t \leq t_2 \\ A_1 \cos(2\pi f_c t), & t_3 < t \leq t_4 \end{cases} \quad (4.1b)$$

$$p_{BFSK,1}(t) = \begin{cases} \cos(2\pi f_1 t), & t_1 < t \leq t_2 \\ \cos(2\pi f_2 t), & t_3 < t \leq t_4 \end{cases} \quad (4.2a)$$

$$p_{BFSK,2}(t) = \begin{cases} \cos(2\pi f_2 t), & t_1 < t \leq t_2 \\ \cos(2\pi f_1 t), & t_3 < t \leq t_4 \end{cases} \quad (4.2b)$$

$$P_{BPSK,1}(t) = \begin{cases} \cos(2\pi f_c t), & t_1 < t \leq t_2 \\ \cos(2\pi f_c t + \pi), & t_3 < t \leq t_4 \end{cases} \quad (4.3a)$$

$$P_{BPSK,2}(t) = \begin{cases} \cos(2\pi f_c t + \pi), & t_1 < t \leq t_2 \\ \cos(2\pi f_c t), & t_3 < t \leq t_4 \end{cases} \quad (4.3b)$$

In (4.1)-(4.3), A_i represents the amplitudes, f_i represents the symbol frequencies and f_c denotes the carrier frequency of the modulated signals. The time instant t_i represents the locations of the template boundaries within the communications signal under consideration.

4.2 WD-based AMR Algorithms Step by Step Illustration

Once the pre-defined templates are generated, the AMR process is implemented according to the following algorithm:

Step 1.) Compute the DWT of the received signal and extract the detailed WD coefficients, up to 10 levels of resolution using the Haar wavelet.

Step 2.) Correlate the extracted detailed WD signal information obtained in Step 1 with all six of the pre-defined WD templates. This step is illustrated more clearly in Fig.4.5, wherein the process of the sliding correlation operation between a template and a communications signal is illustrated. A signal segment is shown in Fig.4.5 representing a data symbol period within the received signal. The template is then slid so as to be aligned with the next signal segment, and the two are correlated. The process is continued until the template has been correlated with all segments of the signal. All simulations have been performed using MATLAB. The carrier in each signal segment, representing a baseband data symbol, is composed of 1024 samples per symbol. Hence the maximum

template length is also 1024 samples, and other possible lengths of templates are 512, 256, 128, 64, 32, 16, 8, 4, and 2 samples. The length of the templates representing the WD templates, however, cannot be too short due to the loss of resolution in the WD scalogram which would directly affects the performance of the WD AMR process. For the sake of illustration, only templates of size 128, 64 and 32 samples are presented here.

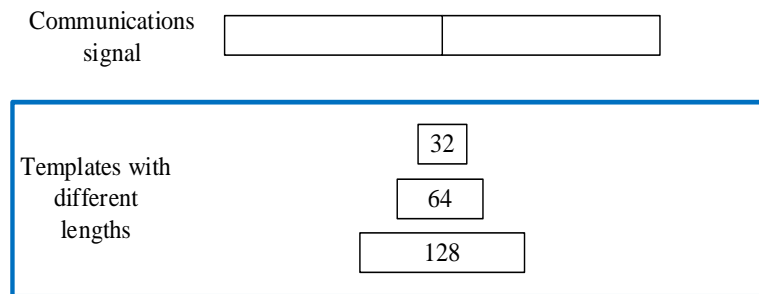


Fig.4.5 Graphical representation of the correlation operation using different template lengths.

Step 3.) Compare the resulting correlation values of the two BASK templates with the signal specifically at multiples of each baseband symbol period. Select the larger one of two values in each comparison, and in this manner generate a set of “transition period” correlation results for the two BASK templates. This operation is depicted in Fig. 4.6.

BASK Test Signal bit sequence	1	1	0	1	1	0	0	1
Correlation values with BASK Template 1	L	H	L	L	H	L	L	
Correlation values with BASK Template 2	L	L	H	L	L	L	H	
BASK “time-and-merged” correlation results	L	H	H	L	H	L	H	

Fig.4.6 Example of a “transition period” correlation operation in the WD AMR process.

Step 4.) Repeat Step 3 using the BPSK templates, and then repeat it again for the BPSK templates.

Step 5.) Compare each data element in the three sets of "transition period" correlation values. Select the largest value and record the template type to which the value belongs, i.e., whether it corresponds to BASK, BFSK or BPSK.

Step 6.) Declare the specific modulation type of the received signal to be that of the same type as the template that was selected most often in Step 5, i.e., by a majority vote.

In Fig. 4.7, it illustrates Steps 1 through 6 of the algorithm for the BASK signal AMR process in details. The top row blocks represent of symbol of noisy BASK signal is transformed into the discrete wavelet-domain using the Haar wavelet, which is the output of the AWGN channel with unknown modulation type. Then this WD received signal is correlated with 6 pre-defined featured templates (2 templates for each of the 3 binary modulation schemes). Consequently, the correlations generate 3 sets of "transition period" correlation results. In Fig. 4.7, the following notations are used:

- H The overall Highest correlation output
- L The overall Lowest correlation output
- HA The highest correlation with BASK templates
- LA The lowest correlation with BASK templates
- HF The highest correlation with BFSK templates
- LF The lowest correlation with BFSK templates
- HP The highest correlation with BPSK templates
- LP The lowest correlation with BPSK templates

The "transition period" correlation results for this example are highlighted in the bottom box of Fig.4.7. They are then input to the decision processor. For each symbol transition period, three corresponding correlation results are compared and the largest "transition period" correlation value is selected. The template generating the largest correlations means it is the best candidate modulation type as it has the best match to it. After deciding modulation type of each "transition period", a majority vote is then ran for all "transition period" template identifications. The final recognition of the unknown modulation scheme to a signal sequence is the most voted candidate modulation type. Until now, the final AMR is accomplished. In the example of Fig.4.7, BASK templates are identified as the most voted candidate modulation recognition. Therefore, the BASK is claimed as the final modulation scheme employed by the received test signal.

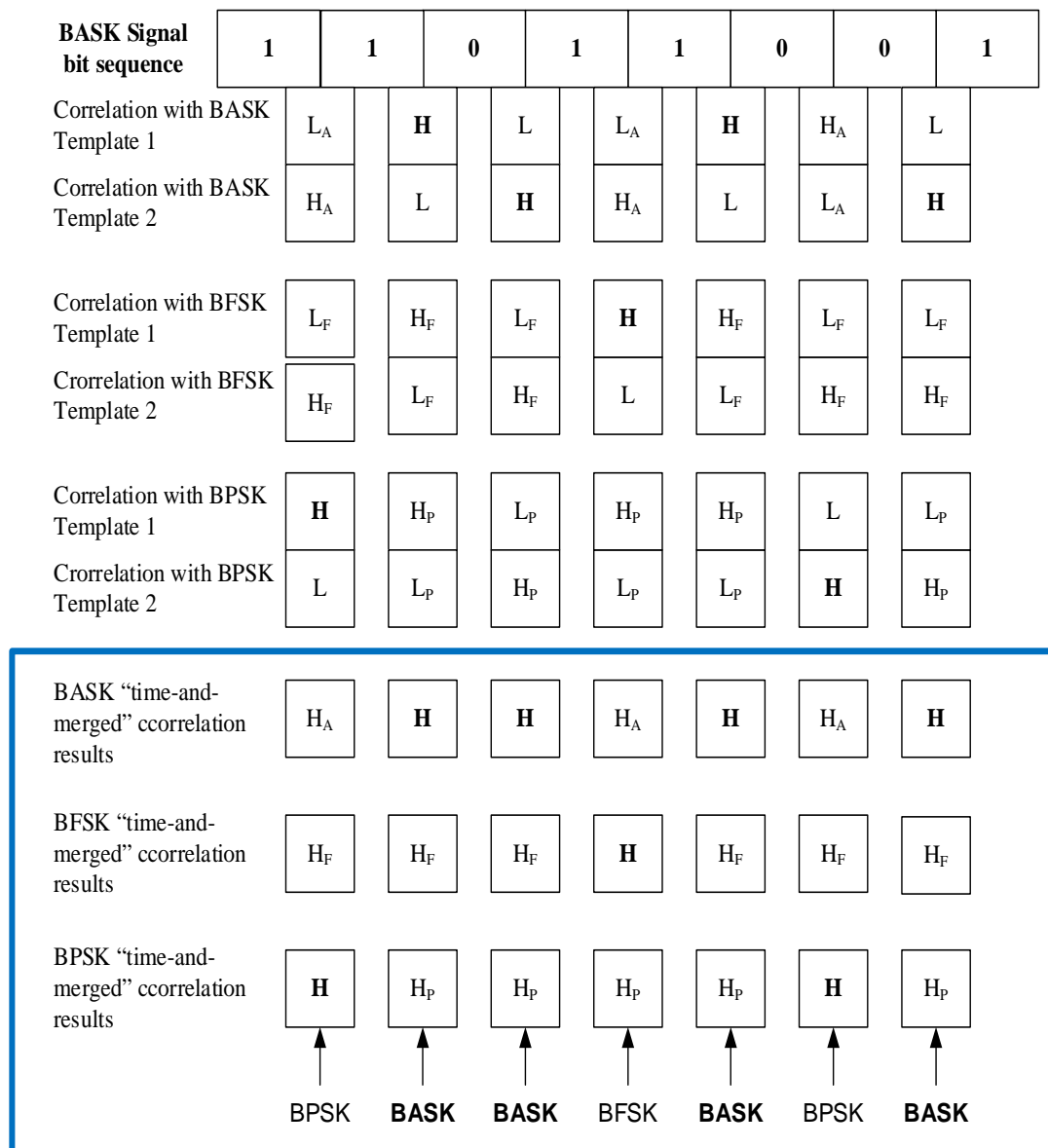


Fig.4.7 Example of WD AMR process using the instantaneous features templates.

In summary, the algorithm process could be expressed as the following diagram block system and its processing flow in Fig.4.8 & 4.9.

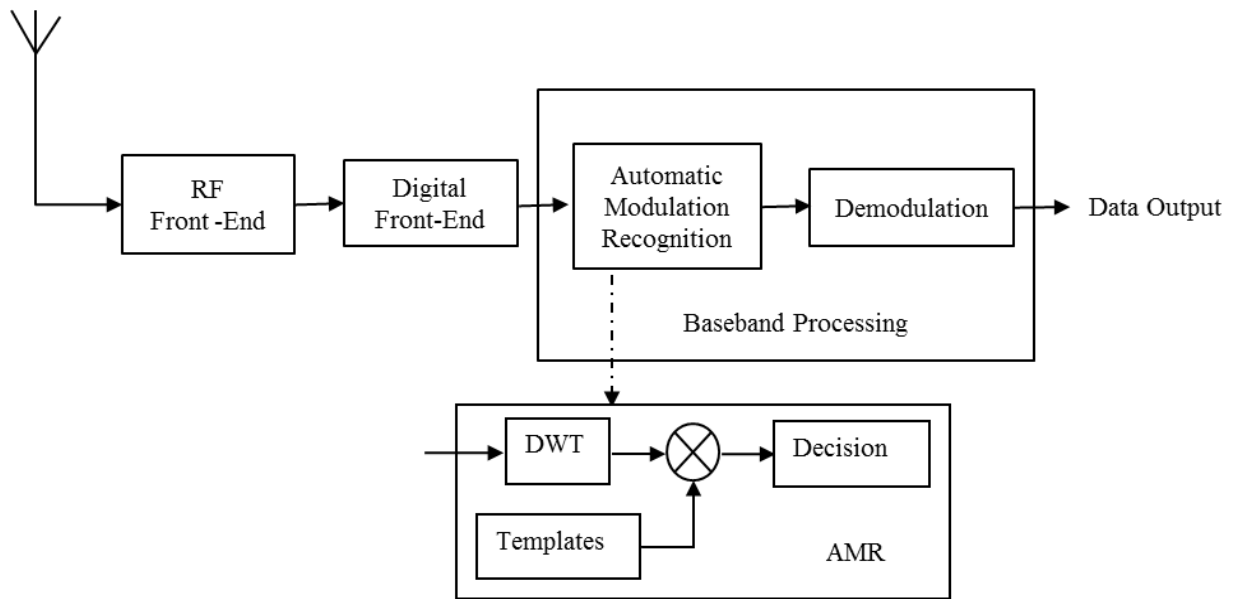


Fig.4.8 Overall system-level block diagram of a radio receiver employing an AMR function.[82]

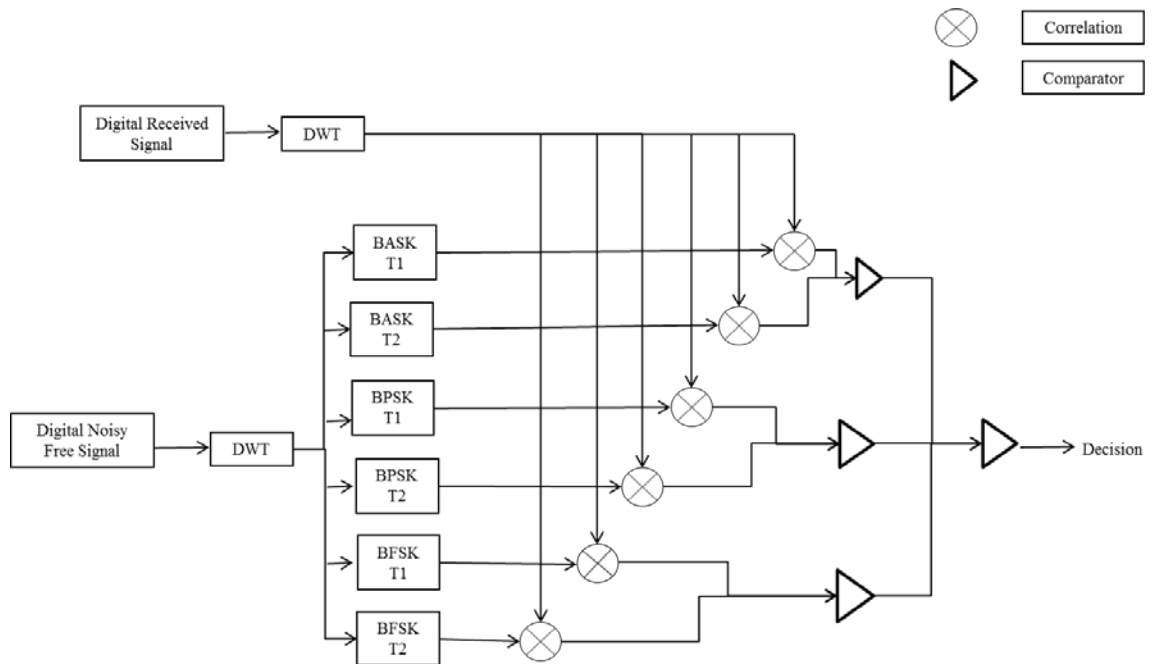


Fig.4.9 System-level processing flow of the wavelet-based AMR processor [82]

4.3 Simulation Experiments and Results

In this simulation, all binary digitally modulated test signals are transmitted through the zero-mean AWGN channel with SNR values range over -5 dB to 10 dB. The correct classification rates of this WD instantaneous features templates AMR algorithm were produced by using 20,000 Monte Carlo trials, where each simulation experiment contains 50 bits per frame. Each test signal used in the 20,000 trials were randomly assigned with their modulation schemes among the BASK, BFSK or BPSK. The signals are oversampled by a factor of sixteen over the Nyquist rate corresponding to the carrier frequency. Oversampling is used because more signals content can be represented in the WD scalogram, which in turn enhances the WD AMR process. Perfect symbol timing, with no timing offset, are also prior assumed for this work.

In the simulations conducted in this study, the length of the templates is firstly tried from the maximum 1024 samples, and later is dropped down to be 64 samples so as to achieve a balance, or tradeoff, between complexity and resolution. It still provides promising simulations results as listed in Tables 4.1-4.4, which contain the rates of correct classification for signals with unknown modulation schemes corrupted by AWGN resulting in SNR values of 10 dB, 5 dB, 0 dB, and -5 dB.

TABLE 4.1 Rates of correct classification for snr = 10dB

		Signal classified as (%)		
		BASK	BFSK	BPSK
TX Signal	BASK	100	0	0
	BFSK	1.53	98.37	0
	BPSK	0	0	100

TABLE 4.2 Rates of correct classification for snr = 5 dB

		Signal classified as (%)		
		BASK	BFSK	BPSK
TX Signal	BASK	100	0	0
	BFSK	2.57	96.15	1.28
	BPSK	2.06	1.10	96.84

TABLE 4.3 Rates of correct classification for snr = 0 dB

		Signal classified as (%)		
		BASK	BFSK	BPSK
TX Signal	BASK	100	0	0
	BFSK	2.96	95	2.04
	BPSK	2.93	1.46	95.61

TABLE 4.4 Rates of correct classification for snr = -5 dB

		Signal classified as (%)		
		BASK	BFSK	BPSK
TX Signal	BASK	100	0	0
	BFSK	2.36	97.06	0.70
	BPSK	3.42	1.71	94.87

4.4 Results Comparison

In this section, some prior AMR studies available from the literature are surveyed and compared with the results obtained in this study. Both WD-based and non-WD based AMR methods comparisons are presented in Tables 4.5-4.10. Specifically, Tables 4.5-4.7 present the comparison between this work and existing non-DWT (CWT and other non-WD) based AMR methods. Tables 4.8-4.10 only focus on comparing DWT-based AMR method between this work and previous works.

The values in Tables 4.5-4.7 were obtained from existing CWT-based and non-WD based

AMR techniques. More specifically, works [51], [57], [75] employ CWT-based techniques, while works [76], [27], [77], [78] use non-WD based methods. The comparison with previous work showed that, the performance of this DWT-based AMR algorithm is generally better than those results generated from other existing non-DWT based AMR techniques. The main enhancement is that of the performance improvement at the SNR of -5 dB for BFSK and BPSK signals. The CWT-based AMR can only achieve a rate of correct classification of 54% [75], while the DWT-based AMR can identify the correct modulation with a 97% success rate.

Also, through the comparison of results obtained with existing DWT-based AMR methods [59, 79] in Tables 4.8-4.10, it is once again found that the DWT-based AMR algorithm invented in this work is favorably competitive with previous similar work. But the range of the SNR considered in this dissertation is wider and centered in a more practical range of interest for radio receivers.

It should be understood that a direct comparison of different AMR methodologies is not the only criteria of judgment because that prior works may be implemented under different test environmental, such as SNR values, symbol numbers per transmission, channel types, synchronization or time offset and so on.

TABLE 4.5
Survey of BASK classification in the non-DWT based literature

AMR method devised by	Correct classification at highest SNR (%)	Correct classification at lowest SNR (%)
Hossen, et al. [76]	97.5 at 3 dB	82.5 at -5 dB
Azzouz, et al. [27]	100 at 20 dB	98.25 at 10 dB
Lopatka, et al. [77]	100 at 30 dB	~92 at 0 dB
Yang, et al. [78]	-	97.5 at 10 dB
This work	100 at 10 dB	100 at -5 dB

TABLE 4.6
Survey of BPSK classification in the non-DWT based literature

AMR method devised by	Correct classification at highest SNR (%)	Correct classification at lowest SNR (%)
Hossen, et al. [76]	100 at 5 dB	87.5 at 3 dB
Azzouz, et al. [27]	90.75 at 20dB	96.25 at 10 dB
Ho, et al. [51]	-	98 at 13 dB
Jin, et al. [57]	100 at 13 dB	99.5 at 8 dB
Ou, et al. [75]	100 at 20 dB	~54 at -5 dB
This work	100 at 10 dB	95 at -5 dB

TABLE 4.7
Survey of BFSK classification in the non-DWT based literature

AMR method devised by	Correct classification at highest SNR (%)	Correct classification at lowest SNR (%)
Hossen, et al. [76]	100 at 5 dB	75 at 3 dB
Azzouz, et al. [27]	100 at 20 dB	91 at 10 dB
Jin, et al. [57]	100 at 13 dB	95.3 at 8 dB
Ou, et al. [75]	100 at 20 dB	~54 at -5 dB
This work	98 at 10 dB	97 at -5 dB

TABLE 4.8
Survey of BASK classification in the dwt-based literature

AMR method devised by	Correct classification at highest SNR (%)	Correct classification at lowest SNR (%)
Effrina, et al. [79]	-	-
P.Prakasam,et al. [59]	-	-
This work	100 at 10 dB	100 at -5 dB

TABLE 4.9
Survey of BPSK classification in the dwt-based literature

AMR method devised by	Correct classification at highest SNR (%)	Correct classification at lowest SNR (%)
Effrina, et al. [79]	100 at 25 dB	93at 10 dB
P.Prakasam, et al. [59]	98.6 at 3 dB	-
This work	100 at 10 dB	95 at -5 dB

TABLE 4.10
Survey of BFSK classification in the dwt-based literature

AMR method devised by	Correct classification at highest SNR (%)	Correct classification at lowest SNR (%)
Effrina, et al. [79]	99 at 25 dB	98at 10 dB
P.Prakasam, et al.[59]	100 at 3 dB	-
This work	98 at 10 dB	97 at -5 dB

Chapter 5 DWT-AMR Based On Statistical Features

Although the recognition accuracy is promising from the work proposed in Chapter 4, it is impractical to extend this instantaneous featured templates approach to higher order modulation schemes AMR work. This is due to the higher-order modulation schemes contain more possible symbol transitions parts, which means more instantaneous templates needs to be required and involved into this algorithm. Hence, the large number of templates will increase inefficiency of the process.

Table 5.1
Number of unique feature templates needed for different modulation schemes

Modulation Scheme	Number of Instantaneous Features Templates Needed
BASK	2
4-ASK	16
BFSK	2
4-FSK	16
BPSK	2
QPSK	16
8-PSK	64
4-QAM	16
16-QAM	256
64-QAM	4096

Table 5.1 illustrates that the number of templates must be extracted from different modulation schemes for the use in the DWT-based AMR process, if the instantaneous featured templates AMR methodology is still used. It is easily seen that as the order of the digital modulation scheme increases, the number of templates required for the WD AMR

process also increases rapidly, which causes the computational effort for classifying modulation schemes significantly growing. Besides, it will also enhance the system design complexity and cost. Therefore, a new DWT-based AMR algorithm only utilizing certain number of templates is demanded to classify higher order modulation schemes. Meanwhile, this new methodology should maintain reliable correct classification rate as well.

This new AMR algorithm developed in this chapter is designed upon signal statistical featured templates extracted from their wavelet domain expressions. By analyzing these features, the algorithm could be implemented with only few fixed number of templates involved in. In details, extracted wavelet templates will be used in the correlation operation with wavelet expressions of different modulation signals. Then attributes of their correlation outputs are extracted, observed, and utilized as decision variables for the modulation type recognition process. The digital modulation signals will be considered in this chapter include M-ary ASK, M-ary FSK for $M=2$ and 4 ; M-ary PSK for $M=2, 4$ and 8 ; and M-ary QAM for $M=4$ and 16 . The communication signals are corrupted with AWGN channel in the range of SNR from -5 dB to 10 dB.

The content of Chapter 5 is composed with four sections. In Section 5.1, preliminary knowledge and preparations required for the WD AMR process using the statistical features templates are described. This WD AMR algorithm is developed in Section 5.2. Then, the WD AMR process is simulated and verified. Simulation results are represented and analyzed in Section 5.3. Besides, comparisons of the rates of correct modulation classification obtained in this study are also made with performances obtained from previous literatures.

5.1 Preparations of the Automatic Modulation Recognition Process Using Statistical Features Templates

As described in Chapter 3, the candidate modulation signals being researched in this work are expressed in terms of the cosine and sine signal basis functions mathematically. Thus, the first statistical features template is intuitively constructed based on the sinusoidal feature inherent in all of the digitally modulated communications signals considered in this study. In general, the sinusoidal feature is defined as $s(t) = \cos(2\pi f_c t)$, where f_c is used to denote the carrier frequency of the signal. In the vector space, these signals are represented in terms of the I and Q basis signal functions, just as depicted as Fig. 3.1-3.2 in the work of Proakis [74], sinusoidal signals are most common component carried by all modulation signals. Thus, two common statistical features templates called as the Template 1 and Template 2, are defined as the cosine function, $p(t) = \cos(2\pi f_c t + \theta)$, $\theta=0$, and $\theta=90$, $T_1 < t < T_2$, where θ represents the different phase shifts of the sinusoidal carrier, while T_1 and T_2 represent the beginning time and ending time of the template.

Take the first template as the example, statistical features are investigated through observations of the correlation values between signals and the Template 1 in the wavelet domain:

1. When the signal is within ± 90 degree phase difference from the template signal, their correlation value is always positive. Oppositely, if two signals' phase difference is more than ± 90 degrees, then their correlation is always negative. According to the algebraic sign information of correlation outputs, the quadrant of the signal location can be

determined.

2. When two signals' phase difference is equal to ± 90 degree, then their correlation value is always zero because they are mutual orthogonal to each other. According to this orthogonality feature, the components of signals can be detected through correlation with different template signals.

3. The self-correlation of a signal always generates the maximum positive correlation value. The correlation of a signal and its "mirror" signal, which carries 180 degree phase difference from it, generates the minimum negative correlation value. The positive and negative peak contain the same absolute values.

4. Two signal's correlation value is decreasing from the maximum positive to the minimum negative while their phase difference increase from 0 degree to 180 degree.

5. Oppositely, if two signals' phase difference range from 180 to 360 degree, then their correlation is increasing from the minimum negative value up to the maximum positive, as the phase difference increment from 180 degree to 360 degree.

6. The last but not the least attribute is the feature of symmetry. The correlation values are identical if signals are symmetric about the I axis. If signals are symmetric of the Q axis, then their correlation carries the same absolute value, but opposite positive/negative sign.

Above features of signals correlation could be extracted and concluded as important modulation classifier parameters, among which include dynamic range of correlation results, the number of distinct levels contained by correlation outputs, as well as the orthogonality detection and components estimation. It is also noticed that, as showed in the term 4 and 5, signals' different quadrant space location could be detected upon algebraic signs of their correlation with template signals. This attribute is also

summarized in the Table 5.2.

Table 5.2 Identification of signal space quadrant using the correlation results with templates

Quadrant	Correlation with T1	Correlation with T2
I	+	+
II	-	+
III	-	-
IV	+	-

To recognize modulation schemes included in this work, two templates are not sufficient and more templates are required. Their statistical attributes will be collected and jointly analyzed to develop the WD AMR process and algorithm. As mentioned earlier in this chapter, the sinusoidal features can be extracted at different temporal locations within a data symbol period of a communications signal. Also, a statistical featured template can be subjected to a time-shift, which would correspond to a phase shift of the carrier signal. Therefore, in general, a common features template, $p(t)$, can be defined as $p(t) = \cos(2\pi f_c t + \theta)$, $T_1 < t < T_2$, where θ represents the different phase shifts of the sinusoidal carrier, while T_1 and T_2 represent the beginning time and ending time of the template. The various statistical features templates used in the development of the WD AMR process are described for the cases of $\theta = 0$, $\pi/2$, and $5\pi/4$, denoted as Template 1, Template 2, and Template 3, respectively in Fig. 5.1. These three featured templates are selected because they are presenting the I (cosine) signal basis functions, the Q (sine) signal basis functions and the combination of both signal basis functions, just as depicted in Fig. 6.1. Template 1 is based on a cosine carrier with no phase shift. Template 2 is

based on the sine carrier that is phase offset by $\pi/2$ radians. Template 3 is based on the cosine carrier basis function having a phase shift of $5\pi/4$ radians.

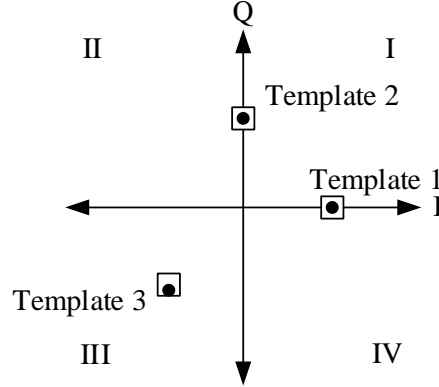


Fig. 5.1 Signal space representation of the three common features templates.

In short, templates selection procedure is mainly based on mathematical models of the communications signals components described in Chapter 3. Template 1 and Template 2 are chosen as the cosine signal and the sine signal, because most communications signals considered in this work can be described mathematically and expressed by either the I or the Q basis functions. For classification of more complex modulation schemes, a third template must be used, which is the combination of the first two templates. By extracting all these common parts of different signal sets, it is very helpful to limit the number of templates required by this algorithm. Besides, the use of wavelet transfer enabling analyze signals from various levels of resolution. Meanwhile, statistical features of signals in the time domain could be reserved in the wavelet domain because the linearity of the wavelet transform operation.

In following section, all test signals will correlate with these templates in the wavelet domain and their correlation's statistical features will be studied. After comparison and observation, the quadrant of the signal location, the components of modulation signals

and the orthogonality existence could be detected accordingly. These attributions are then analyzed jointly to finalize the modulation reorganization decision.

5.2 Development of the Statistical Feature AMR Algorithm:

After all templates were defined in Section 5.1, the following content will focus on the illustration of the WD-AMR algorithm development. The first part of this new AMR algorithm is the same as the description in Chapter 4. Communications signals are firstly discrete wavelets transformed using the Haar. The resulting DWT expression of signals is correlated with different discrete wavelet transformed Templates 1, 2 and 3, which represent WD statistical signatures of candidate modulated signals. Further details of this algorithm will be illustrated in Section 5.2.1.

The correlation results between all test signals and Template 1 must first be plotted and analyzed. Upon comparing the dynamic range and multi/single level features, all test signals are categorized into several subgroups. Each subgroup, which contains multiple members, will eventually need to be all recognized individually. So both Templates 2 and 3 are introduced to further analyze each subgroup, until each single modulation type is detected and identified. The steps of this WD AMR algorithm and its working flow chart are represented in Section 5.2.2.

5.2.1 Algorithm Development

The system-level block diagram for this statistical feature WD AMR is plotted below Figure 5.2. It is systematically different from the algorithm proposed in Chapter 4. Specifically, as showed in the bottom block, the AMR system could be viewed as a two-layer decision procedure. In the first half of the AMR, signals are expressed in the wavelet domain. Their correlating statistical features are then generated, collected, processed, and analyzed through the first layer decision procedure, which is composed by one correlator, one pre-processor, and one decision-maker. The output of the first decision processor will be used in the second part of the AMR, which runs the similar methodology and process with the first part. The main difference for the second correlator lies in the fact that more templates are inputted into it compared to the first correlator.

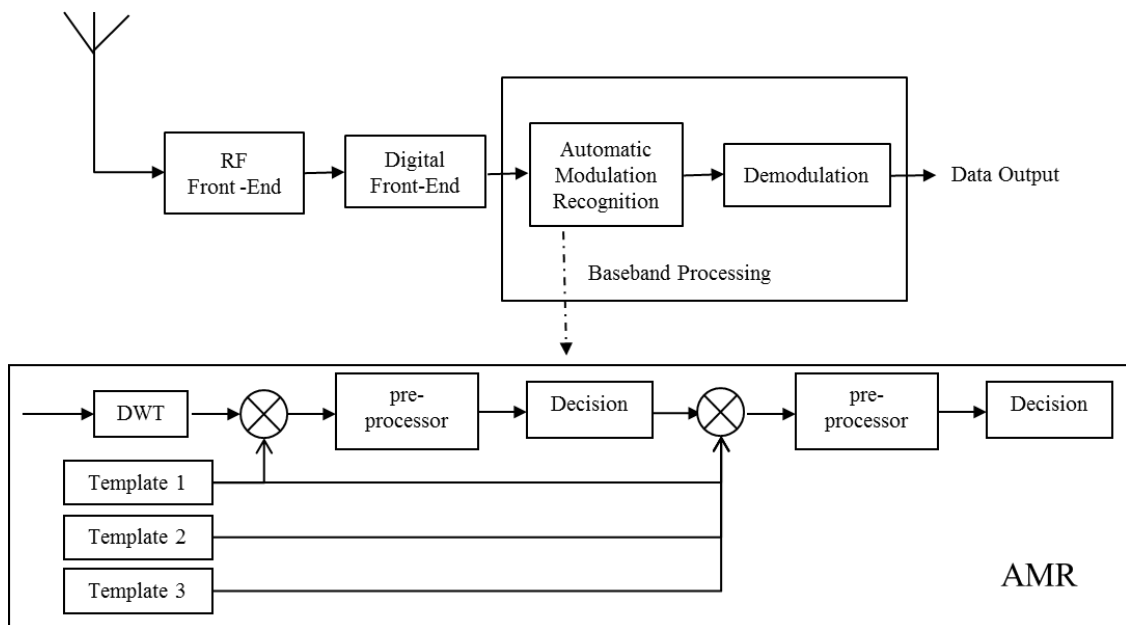


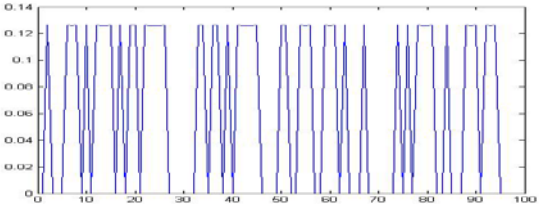
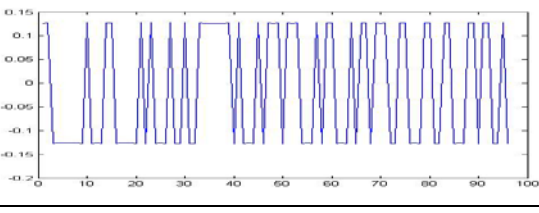
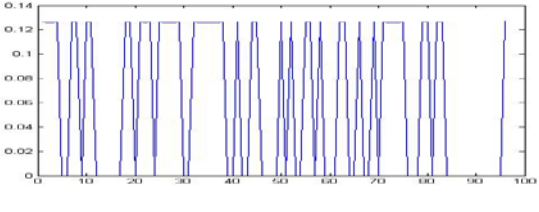
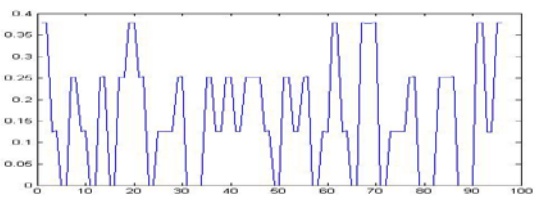
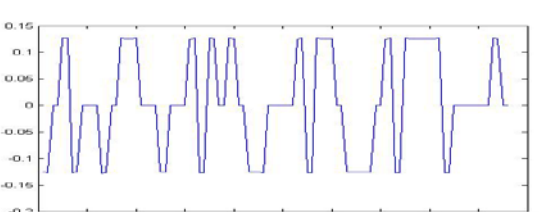
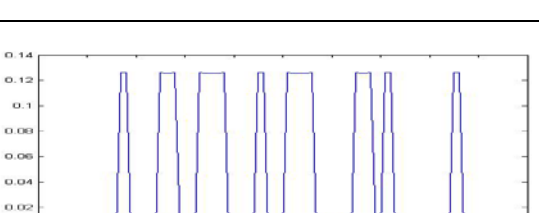
Figure 5.2 WD-AMR using statistical feature template system level view

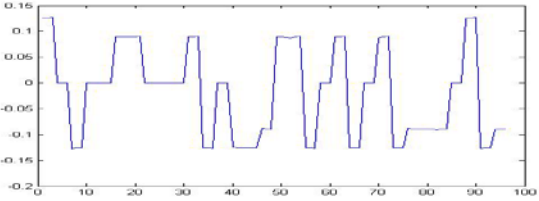
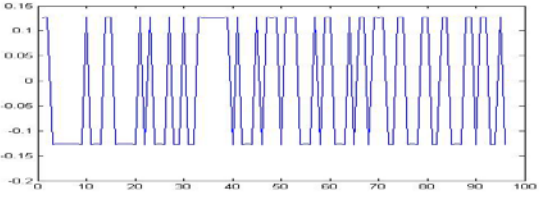
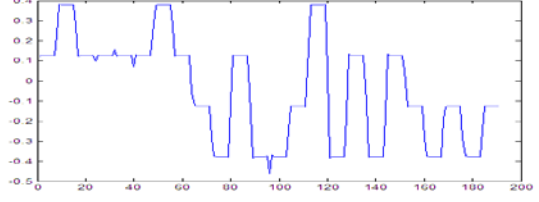
Wavelet correlation outputs are placed through a pre-processor because the original correlation of signals and templates generates different value ranges. Hence, to better investigate their statistical attributes, all correlation outputs are normalized by this pre-processor to the dynamic range of -3 to 3 before the decision procedure. So the normalized correlation outputs will be categorized as three groups with value ranges: a. no negative (0 to 3), b. no positive (-3 to 0), and c. mixed (3 to -3). This range detection acts as a part of the decision procedure to distinguish and label these three groups as "a", "b", or "c".

1. In Table 5.3, all nine tested modulation schemes are separated into two subgroups by the range detector and each subgroup contains multiple candidates. BASK, BFSK, 4FSK and 4ASK are members of group "a". BPSK, 4PSK, 8PSK, 4QAM and 16QAM are modulation signals that correlate with T1 and their correlation is identified as mixed values belonging to group "c". There are no possible options among all candidates for group "b". Next, these groups could be further divided into smaller subgroups by introducing another statistical character of T1 correlation outputs; this attribute is called the multiple/single (M/S) level value.

2. The correlation results from the figure above yields that the most important statistical attributes are range detection and multiple/single (M/S) level distinctions. In the following details, the M/S level feature detection procedure will be applied and analyzed to each subgroup defined in the previous step.

Table 5.3 WD-Correlation with Template 1

BASK*T1		a&S
BPSK*T1		c&S
BFSK*T1		a&S
4ASK*T1		a&M
4PSK*T1		c&M
4FSK*T1		a&S

8PSK*T1	 A line plot showing a signal with a period of 10 units. The signal has 8 distinct levels, ranging from approximately -0.15 to 0.15. The x-axis is labeled from 0 to 100, and the y-axis is labeled from -0.2 to 0.15.	c&M
QAM*T1	 A line plot showing a signal with a period of 10 units. The signal has 16 distinct levels, ranging from approximately -0.15 to 0.15. The x-axis is labeled from 0 to 100, and the y-axis is labeled from -0.2 to 0.15.	c&S
16QAM*T1	 A line plot showing a signal with a period of 10 units. The signal has 16 distinct levels, ranging from approximately -0.4 to 0.4. The x-axis is labeled from 0 to 200, and the y-axis is labeled from -0.5 to 0.4.	c&M

a. Among all possible members of group "a", it is clear to observe that only the 4ASK generates a multiple (4) levels correlation output, which divided the whole range from 0 to 3 into three equal subspaces, and each value's occurrence follows the uniform distribution. Hence, if the amount of data that falls into each subspace is detected to be equal, then it will be labeled as multiple levels and labeled group "M". If a majority of values are significantly concentrated in one certain (top or bottom) subspace only, then it is recognized as the single level data, and labeled as group "S". After combining both the range detection results and M/S level features, testing signals from subgroup "a" are further divided into "a&S" and "a&M" classes. The "a&S" class contains candidates of BASK, BFSK and 4FSK. The 4ASK is identified as the only member for class "a&M" after this step.

b. For subgroup "c" correlation outputs that carry mixed values, their M/S feature can also be detected based on the "central zone" values existence. The main idea behind this method is that if data is in single level format, then all values must concentrate at the top (positive peak) and the bottom (negative peak) parts. Conversely, for multiple level mixed values, the data will be equally distributed on each level of the whole data range. Hence, if a sufficient amount of data is detected to exist in the median levels, i.e. "central zone", then it could be recognized as multiple levels. Otherwise, it would be considered single level data. Applying this methodology to our study, to determine M/S feature of 4/16 QAM and 2/4/8PSK signals, the existence of "central values" needs to be proofed as the key evidence. First of all, half 4PSK signals are orthogonal to T1, thus value 0's occurrence in their correlation data should be around 50%. Similarly, the probability of 0's existence should be equal to 25% for 8PSK correlation with T1. Thus, if a certain number of 0's are detected in the central zone, it indicates that their correlation value would be multiple level data. This is different for 16QAM signals. Here, the correlation with T1 does not generate a "0" value because it lacks orthogonality. However, it does generate other values equally distributed among the whole range. The values detected in the central zone are not equal to but very close to "0", and 16QAM is also labeled as "M". The other two modulation schemes, firstly, 4QAM and BPSK have no signal orthogonal with T1 so their correlation has no "0" values. Secondly, since their signals have equal distance to T1, as shown in the constellation Fig. 3.2 [74], their correlation only generates constant positive and constant negative

envelopes, which is claimed as single level. In conclusion, a multiple levels output is recognized as long as “0” or “close to 0” values are found in the central zone, but a single level output has no value available at the central zone. This is the criterion to determine the M/S level.

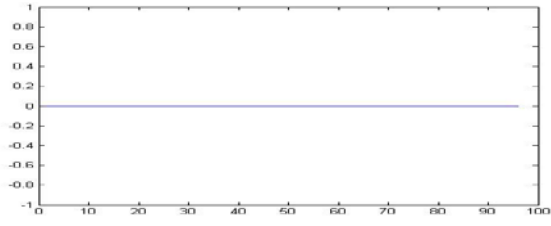
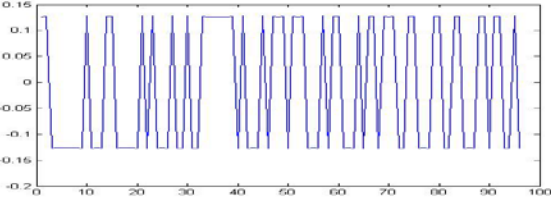
c. The study of subgroup “b” is considered null since there isn’t any matched correlation data that allows for any possible candidate modulation schemes to correspond.

Now the group “c” is classified as group “c&S” which contains 4QAM and BPSK signals, and group “c&M” includes 4PSK, 8PSK and 16QAM modulation schemes. After applying range detection and M/S identification to all test signals' correlation with T1, all data set can be sorted into four combinations: a&S, a&M, c&S, c&M. They are also the output of the first decision block in the Fig. 5.2. Respectively, group “a&S” indicates single level with no negative data, and its candidate modulation schemes are BASK, BFSK and 4FSK. Group “a&M” means multiple levels with no negative data which points to the sole model 4ASK. Group “c&S” stands for single level data with mixed values and its matched possible modulation options are 4QAM and BPSK. 16QAM, 4PSK and 8PSK produce the mixed and multiple level correlation value with Template 1, which is labeled as “c&M”. To further recognize each modulation scheme one by one, Template 2 and Template 3 are introduced into the next analysis process. This is illustrated in the second part of the AMR system shown in Fig. 5.2.

3. By correlating with the Template 2, signal members in the “c&S” class can be identified successfully. From previous steps, the “c&S” class is known as holding the BPSK and the 4QAM two possible modulation schemes. As both BPSK symbols are

completely orthogonal to the T2, their correlation produces “0” values only.

Table 5.4 WD-correlation with Template 2

BPSK*T2		All “0”
4QAM*T2		Range +3~-3

Conversely, none of the 4QAM signals is orthogonal to Template 2. Hence, “0” does not exist in the correlation of 4QAM and Template 2. This proves the following detection criteria: if the signal and Template 2 correlation's range is detected around "0" axis and is labeled as single value, then the modulation scheme is claimed as the BPSK; otherwise, it will be identified as a 4QAM signal as its correlation values range from +3 to -3 and most data only gathers at both end of the range. For reference, the correlation results of BPSK and 4QAM with Template 2 are plotted in Table 5.4.

4. There are three signal members, QPSK, 8PSK and 16QAM contained in the class “c&M”. Because each template can only distinguish two signals at most, at least two templates are required to identify the modulation members in the "c&M" class. Firstly, all possible signal members are correlated with Template 3 and the M/S level recognizer is applied on the respective correlation outputs sets of each signal member. The only single level correlation and modulated signal value that is filtered out and

detected is QPSK. To detect the two remaining modulation types, the residue signals 8PSK and 16QAM are then correlated with Template 1. Due to the partial 8PSK symbols being orthogonal to Template 1, their correlation results will partly include "0" values. At the same time, due to the lack of orthogonality, 16QAM and Template 1 can only generate non-zero correlation outputs. Since both signals' correlation with Template 1 is distributed in the same value range, 16QAM and Template 1's correlation produces a larger absolute summation than 8PSK. This process can be repeated by correlating with Template 2 and the decision strategy remains the same.

Table 5.5 WD-correlation with Template 3

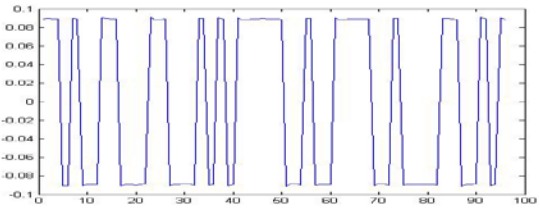
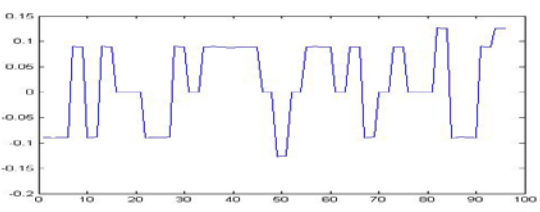
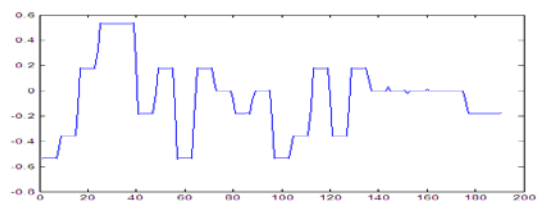
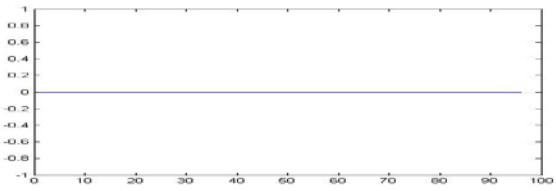
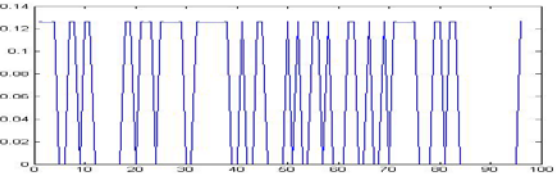
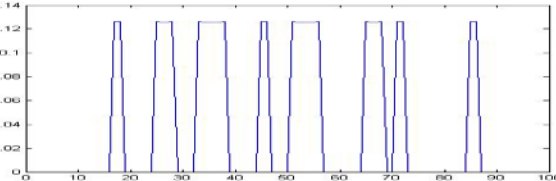
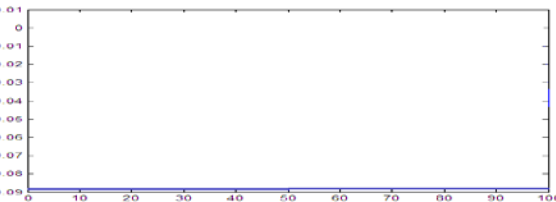
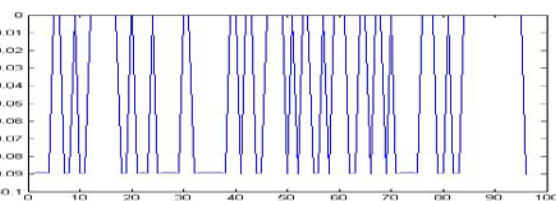
QPSK*T3		Containing no "0"
8PSK*T3		Containing "0"
16QAM*T3		Containing "0"

Table 5.6 WD-correlation with Template 2 and Template 3

BASK*T2		All "0"s
BFSK*T2		Positive single level output with around 1/2 "0" values
4FSK*T2		Positive single level output with around 3/4 "0" values
BFSK*T3		All -3
4FSK*T3		Half -3 half 0

5. The last signal class "a&S" includes BASK, BFSK, and 4FSK as its possible members and they are detected by two templates in two steps:

- a. Firstly, an ASK/FSK classifier must be designed to separate the BASK from FSK signals. Template 2 is ideal achieve this goal because it is completely orthogonal with BASK, thus their correlation will only produce "0" values every time. BFSK and

4FSK signals are partially orthogonal with Template 2, thus their correlation value dynamic range covers from 0 to 3.

b. After ASK/FSK classifier is designed, the next step is to focus on distinguishing the remaining two FSK signals, BFSK, and 4FSK. By correlating both signals with Template 3, despite both correlation data containing negative values, there is a significant difference in results. BFSK correlating with Template 3 generates a constant envelope at the negative value of -3; the 4FSK signal correlation values with Template 3 contain both 0 and -3 equally.

6. Since 4ASK is the sole candidate of the “a&M” class, this modulation type was directly filtered out in the step 2a.

In short, the WD statistical features of correlations between signals and templates enabled the reorganization of different modulation schemes. The key concepts for developing this WD-AMR algorithm using the category of statistical features templates include:

- a. Algebraic sign information of correlation results obtained with templates leads to the identification of symbol constellation quadrant locations within the signal constellation of a modulation type.
- b. By combining other statistical characteristic combinations of all three template correlation results such as dynamic range detection, single/multi-level, and zero-valued outputs, those combinations could jointly identify the signals' component and the modulation schemes. Among these, the dynamic range and S/M level attributes are the two most useful. They are summarized in Tables 5.7- 5.9.

Table 5.7 Attributes of WD correlation values from test cases with Template 1

Communications Signal	Dynamic Range	Multi-Level	Label
BASK	0 to 3	No	a&S
4-ASK	0 to 3	Yes	a&M
BFSK	0 to 3	No	a&S
4-FSK	0 to 3	No	a&S
BPSK	-3 to 3	No	c&S
QPSK	-3 to 3	Yes	c&M
8-PSK	-3 to 3	Yes	c&M
4-QAM	-3 to 3	No	c&S
16-QAM	-3 to 3	Yes	c&M

Table 5.8 Attributes of WD correlation values from test cases with Template 2

Communications Signal	Dynamic Range	Multi-Level	Label
BASK	0	No	-
4-ASK	0	No	-
BFSK	0 to 3	No	a&S
4-FSK	0 to 3	No	a&S
BPSK	0	No	-
QPSK	-3 to 3	Yes	c&M
8-PSK	-3 to 3	Yes	c&M
4-QAM	-3 to 3	No	c&S
16-QAM	-3 to 3	Yes	c&M

Table 5.9 Attributes of WD correlation values from test cases with Template 3

Communications Signal	Dynamic Range	Multi-Level	Label
BASK	0 to -3	No	a&S
4-ASK	0 to -3	Yes	a&M
BFSK	-3	No	c&S
4-FSK	0 to -3	No	a&S
BPSK	-3 to 3	No	c&S
QPSK	-3 to 3	Yes	c&M
8-PSK	-3 to 3	Yes	c&M
4-QAM	-3 to 3	Yes	c&M
16-QAM	-3 to 3	Yes	c&M

5.3 Algorithm for the Automatic Modulation Recognition Process

The general WD AMR algorithm using the statistical features templates is described as following steps:

- Step 1: Conduct the DWT with the Haar wavelet to the received signal with an unknown modulation scheme.
- Step 2: The wavelet coefficients of signals are then correlated with the statistical featured templates, which were pre-defined in the wavelet-domain representing WD signatures of signals.
- Step 3: To have a fixed dynamic correlation range for convenient following analyzing, the correlation values are extracted and normalized in the pre-processing blocks.
- Step 4: After normalization, correlation values are analyzed by decision blocks to produce recognition results of the unknown modulation schemes.

Corresponding to the overall system block diagram as shown in the Fig. 5.2, a more detailed WD-AMR system-level processor using statistical features templates is illustrated in Fig. 5.3.

The functionality of the pre-processing block operation described in Step 3 of the algorithm is to ensure that the correlation data are normalized to have an identical dynamic range from -3 to 3, which benefits to later analysis. After the data are processed, AMR decision metrics are developed for each decision block, which is illustrated in Fig. 5.3. This is to discriminate between different modulation schemes. The decision blocks are developed based on the statistical characteristic combinations of correlation results, i.e. algebraic sign, dynamic range, zero-values or multi/single-level numerical values. These statistical features combinations extracted from the correlation results with multiple templates are compared to classify various modulation schemes. The development of these decision procedures is illustrated in detail in the remainder of this section including working flow charts of each decision procedure.

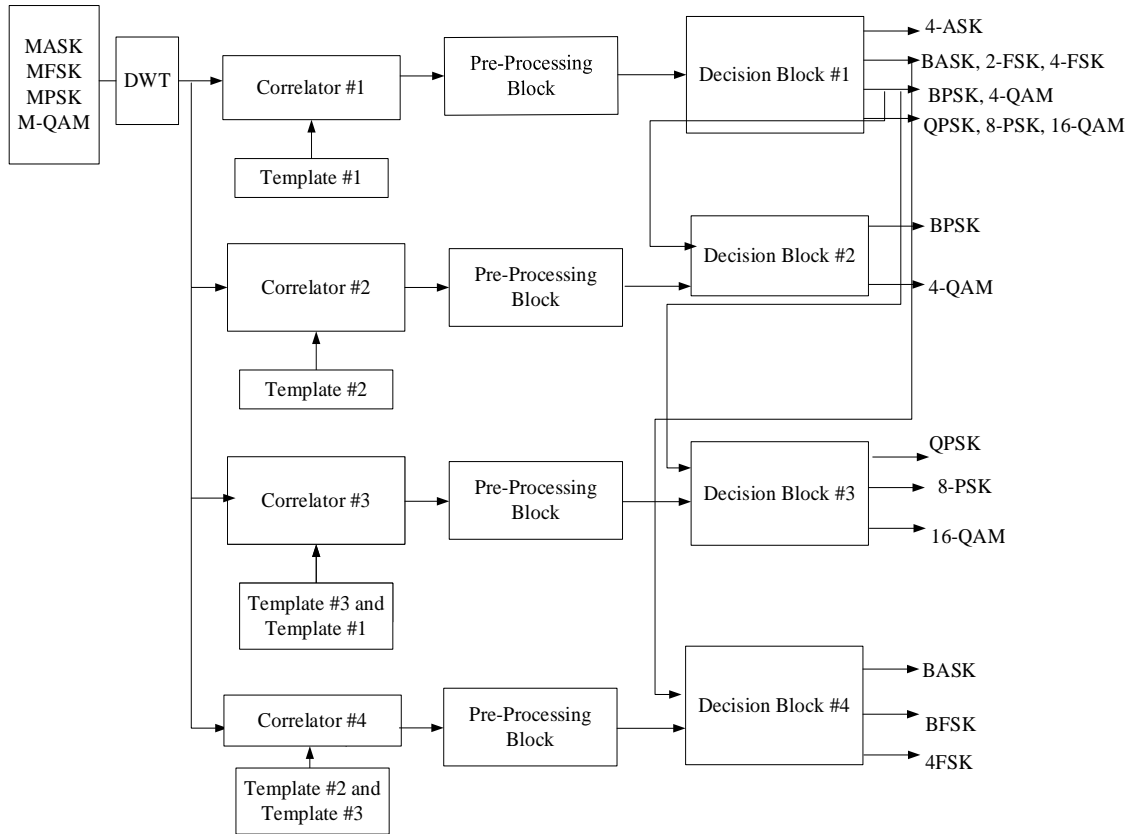


Fig. 5.3 Block diagram of the WD AMR process using statistical features templates.

5.3.1 Procedure for Decision Block 1

Based on the dynamic range and the multi/single level attributes of the correlation results listed in Table 5.7, the modulated signals can be categorized into four groups. The correlation values using Template 1 are processed in Decision Block 1, which are consisted of two processors: the dynamic range detector and the M/S level detector.

Looking at the dynamic range attribute, one subgroup signals has a dynamic range that is strictly positive from 0 to 3. The other subgroup contains correlation values ranging from -3 to 3. Modulation schemes of these two subgroups are specified in Table 5.10.

Table 5.10 Two subgroups correlation from Template 1 with different dynamic ranges

Dynamic Range	Modulation Schemes
0 to 3	BASK,4-ASK, BFSK, 4-FSK
-3 to 3	BPSK, QPSK, 8-PSK, 4-QAM, 16-QAM

Based on checking the correlation values are either single-level, or multi-level, the correlation data set with Template 1 could be re-divided. The grouping results of modulation schemes upon this attribute are shown in Table 5.11.

Table 5.11 Two subgroups of correlation from Template 1 using multi-level test

Multi/Single Level	Modulation Schemes
No	BASK, BFSK, 4-FSK, BPSK,4-QAM
Yes	4-ASK, QPSK, 8-PSK,16-QAM

By jointly grouping modulation schemes in Tables 5.10 and 5.11, four possible modulation schemes subgroups for Decision Block 1 can be determined based on two criteria listed in Table 5.12.

Table 5.12 Grouping outputs of Decision Block 1

Criterion 1: Dynamic Range	Criterion 2: Multi-Level	Modulation Schemes
0 to 3	No	BASK, BFSK, 4-FSK
0 to 3	Yes	4-ASK
-3 to 3	No	BPSK, 4-QAM
-3 to 3	Yes	QPSK, 8-PSK, 16-QAM

Based on above content, the working procedure for Decision Block 1 is summarized as the following:

- Step 1: Apply a **dynamic range test** and assign corresponding index to the normalized correlation outputs. If the data values are distributed among the range from 0 to 3, then assign the index 'a' to it. Otherwise, assign an index 'c' if the data values range from -3 to 3.
- Step 2: Then a **multi-level test** is conducted on the normalized correlation dataset in decision block and assign an index to the dataset. Assign a 's' if the data values are single-level distributed. Otherwise, assign a 'm' if the data contains multi-level values.
- Step 3: Assign subgroup index. If the dynamic range test result is index 'a' and 's' is produced by the multi-level test, then assign an output indicator of '1,' which means that the modulation scheme employed by the signal is potentially in the subgroup {BASK, BFSK, 4-FSK}.
- Step 4: Repeat Step 3 on the case of dynamic range test index is 'a' and the multi-level test index is 'm,' then the candidate modulation scheme is 4-ASK.
- Step 5: Repeat Step 3 as the case of dynamic range test result is 'c' and the multi-level test result is 's'. Now the modulation scheme used by the signal is one among the subgroup of {BPSK, 4-QAM}, designate an output index '2' to it.
- Step 6: Repeat Step 3 to the last remaining subgroup {QPSK, 8-PSK, 16-QAM}, which has attributes of the dynamic range test 'c' and the multi-level test 'm', then assign an output index '3' to it.

Step 7: If the subgroup index outputted by Decision Block 1, in Steps 3-6, is:

- a. '1,' go to the ASK and FSK Classifier Procedure
- b. '2,' go to Decision Block 2
- c. '3,' go to Decision Block 3

A procedure flowchart for Decision Block 1 is plotted in Fig. 5.4. The Decision Block 2, Decision Block 3 and the ASK & FSK classifier procedure at the bottom output level will be presented in following Section 5.2.4.

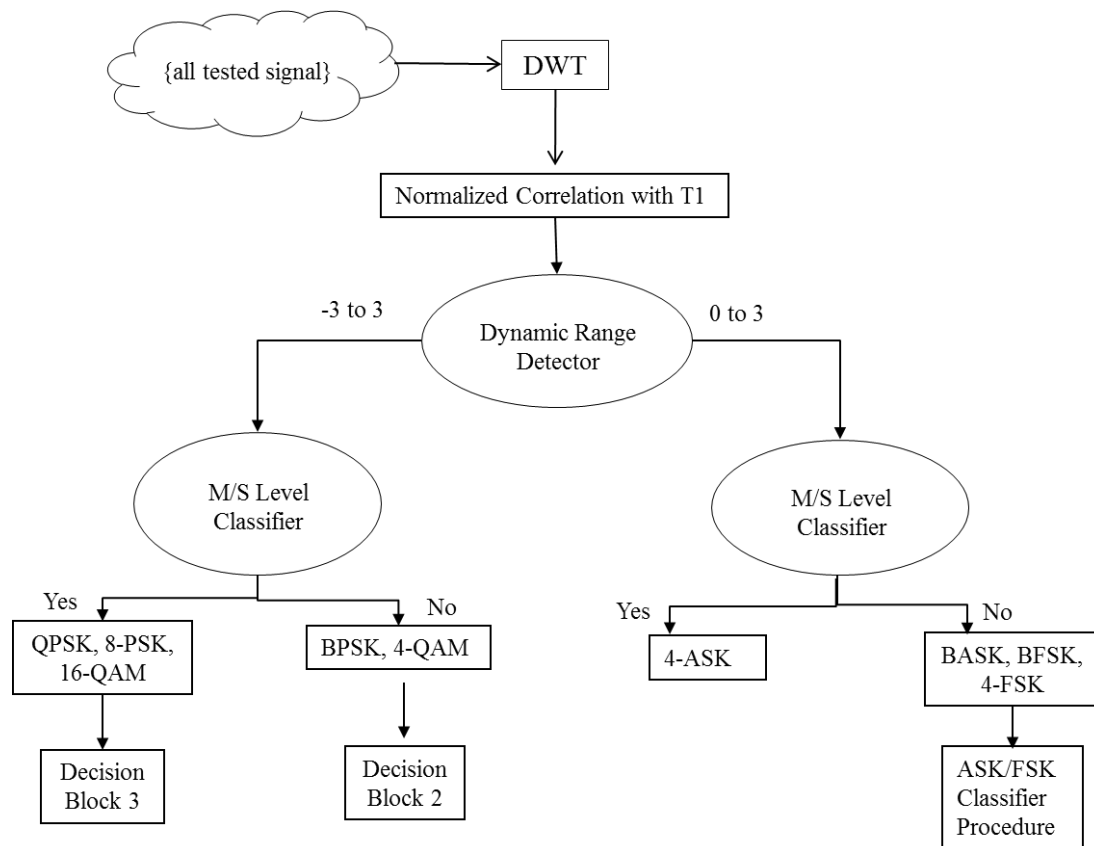


Fig. 5.4 Flowchart of the procedure for Decision Block 1

5.3.2 Procedure for Decision Block 2

If Decision Block 2 is activated by Decision Block 1, as described in Section 5.2.1. It means that the potential modulation scheme employed by the signal could be either BPSK or 4-QAM. To further identify, Decision Block 2 uses the values of the WD correlation between the signal and Template 2, and conduct a dynamic range test to the complete set of correlation values. Based on the results of the test as indicated in Table 5.11, the modulation scheme is recognized.

Table 5.13 Dynamic range test of the correlation using Template 2

Dynamic Range	Modulation Scheme
~0	BPSK
-3 to 3	4-QAM

The Decision Block 2 working flow is introduced as follows.

- Step 1: The correlation between wavelet transformed received signal and Template 2 is calculated, and then correlation values are normalized appropriately.
- Step 2: Conduct a **dynamic range test** on the resulting set of normalized correlation values from the step 1 and output indicators are assigned. If the data values range from -3 to 3, then assign the output an indicator of '0'. If the values are approximately around with zero, then the output indicator '1' is assigned.
- Step 3: If the output indicator assigned is:
- '0,' the modulation scheme is 4-QAM
 - '1,' the modulation scheme is BPSK.

The flowchart of the procedure is illustrated in Fig. 5.5.

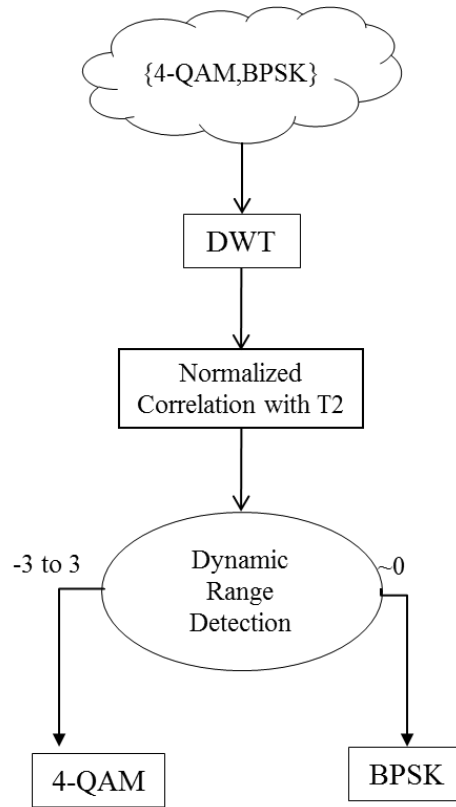


Fig.5.5 Flowchart of the procedure for Decision Block 2.

5.3.3 Procedure for Decision Block 3

Decision Block 3 is activated when the unknown received signal is identified by Decision Block 1 as among the set of {QPSK, 8-PSK, 16-QAM}. The procedure for Decision Block 3 is described below:

- Step 1: The correlation between wavelet transformed received signal and Template 3 is calculated, and then correlation values are normalized appropriately.
- Step 2: Conduct a **multi-level test** to the normalized correlation values from step 1 and output indicators are assigned. If the correlation output data is composed of

single-level values, then the output is labeled as '0' by the indicator. If the correlation values are multi-level, then the output indicator '1' is assigned.

Step 3: If the output indicator assigned is:

- a. '0,' the modulation scheme is QPSK
- b. '1,' go to the 8-PSK and 16-QAM Classifier Procedure.

The flowchart for the above procedure is provided in Fig. 5.6. The PSK and QAM classifier procedure at the bottom output level is presented in Section 5.2.4.

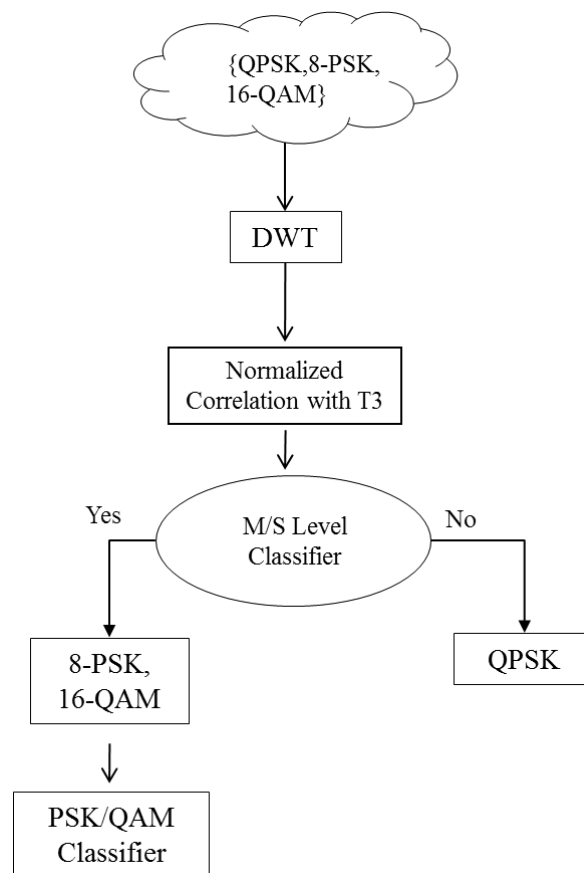


Fig. 5.6 Flowchart of the procedure for Decision Block 3.

5.3.4 Procedures for Other Decision Blocks

As mentioned in the procedures of Decision Blocks 1 and 3, there were two groups of modulation schemes that remained at the output end of these two Decision Blocks:

Group 1: {BASK, BFSK, 4-FSK} is one output of Decision Block 1

Group 2: {8-PSK, 16-QAM} is one output of Decision Block 3

Hence, these two groups signals need to be identified by two corresponding WD-based classification algorithms. In section 5.3.4.1, the ASF/FSK Classifier is invented to classify the modulation schemes in Group 1. A PSK/QAM Classifier is designed in Section 5.3.4.2 to distinguish the modulation schemes in Group 2.

5.3.4.1 ASK and FSK Classifier Procedure

The fact of multiple carrier frequencies are employed to represent different data symbols of FSK signals is revealed as the definition of ASK and FSK mentioned in Chapter 3. The FSK signal is a special case of orthogonal signal waveforms as its different data symbols carrying different frequencies which are orthogonal to each other. According to this interesting attribute, the ASK and FSK could be classified by utilizing Template 2 and 3 to distinguish these two modulation schemes from Group 1. Template 2 is completely orthogonal to the BASK. It could be viewed as one symbol of the BFSK and one symbol of the 4FSK, hence it is also orthogonal to other FSK symbols. Template 3 is introduced here because the orthogonality only exists between the Template 3 and the 4FSK, but not at all with the BFSK. To summarize, the ASK/FSK Classifier Procedure and working flows are described in following steps and diagram:

- Step 1: Calculating correlations in the WD between received signals with Template 2, and then normalize correlations appropriately.
- Step 2: Conduct the dynamic range test on the normalized correlation data and an output indicator is assigned to the dataset. In details, indicate the output as '0' if the values are zero, which indicates that the signal is BASK. If not, then label the indicator as '1', which means that the dataset numerical range from 0 to 3.
- Step 3: If the output indicator assigned is:
- a. '0,' the modulation scheme is BASK
 - b. '1,' go to Step 4.
- Step 4: Calculating correlations between the received signal with Template 3 in the WD, then normalize correlation outputs appropriately.
- Step 5: Conduct the **dynamic range test** on the normalized correlation data and an output indicator is assigned to this dataset. In particularly, labeling a '0' to correlation values signifies that whose data is concentrated around negative value '-3'. Otherwise, if the correlation values are ranging from 0 to -3, then an indicator '1' is assigned. In this case, the ratio of numbers with value "0" and value "-3" is equal to 1.
- Step 6: If the output indicator assigned is:
- a. '0,' the modulation scheme is BFSK
 - b. '1,' the modulation scheme is 4-FSK.

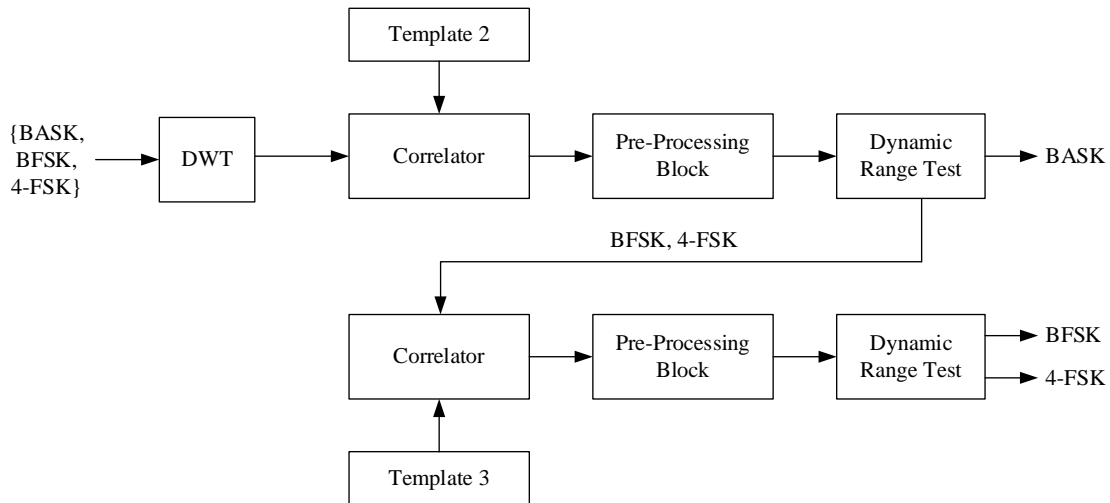


Fig. 5.7 System block diagram implementing the ASK and FSK Classifier Procedure for Group 1 signals

5.3.4.2 PSK and QAM Classifier Procedure

If Decision Block 3's output aligns with 8-PSK and 16-QAM mentioned in Section 5.2.3, then the PSK/QAM classifier is activated. This classifier uses the values of the WD correlation between the signal being processed and Template 1. Specifically, the complete set of correlation values is subjected to a dynamic range test and a zero detector. The 16-QAM signal can be claimed if its correlation with Template 1 or Template 2 carries no zero values; the 8-PSK signal can be identified if its correlation value includes a '0' value and the ratio of zero values is $\frac{1}{4}$ compared to all data. The reason for this decision rule is that, although both correlations are detected in the +3 to -3 range, a $\frac{1}{4}$ of 8-PSK symbols are orthogonal to Template 1 and 2, and orthogonality does not exist between 16-QAM and Template 1 or 2. The QAM and PSK Classifier Procedure includes:

- Step1: Correlate the received signal with Template 1 or 2 in the WD, then correlation values are normalized appropriately.
- Step2: Apply the **zero detection** to the normalized correlation data. Although both outputs show +3 to -3 range, their correlation values components are different. Assign the output carrying around 1/4 zeros with label '1' and the other dataset with no zeros is labeled as '0'.
- Step 3: If the output indicator assigned is:
- '0,' the modulation scheme is 16-QAM
 - '1,' the modulation scheme is 8-PSK.

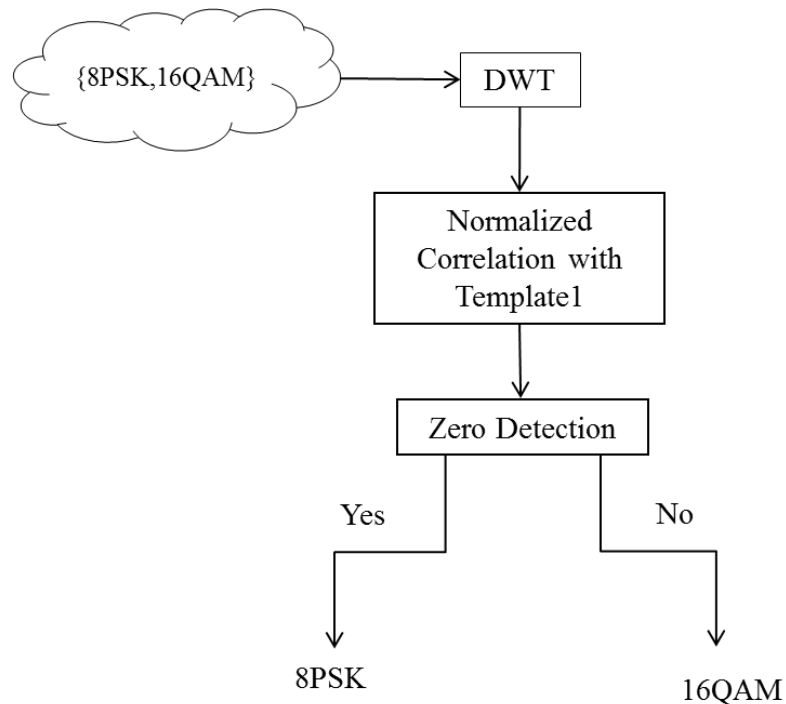


Fig. 5.8 System Block Diagram for the PSK/QAM Classifier

5.4 Simulation Experiment and Results Comparison

Similar as the test environment set up in Chapter 4. This WD AMR algorithm based on the statistical features templates developed in Section 5.2 has been implemented in MATLAB. All of the communication test signals used in the simulations have been corrupted by zero-mean AWGN having SNR values in the range from -5 dB to 10 dB. The rates of correct modulation classification have been obtained using 100,000 Monte Carlo trials. The transmitted signal used in each trial consists of 192 symbols per frame transmitted. The signal is oversampled by a factor of sixteen when compared to the Nyquist rate corresponding to the frequency of the sinusoidal carrier. The system parameters assumed to be known for the AMR process include the carrier frequency and perfect symbol timing with no timing offset.

The results of the experiments for all of the modulation schemes are given in Tables 5.11, which contain the rates of correct classification for the five different SNR values, i.e., 10 dB, 5 dB, 0 dB and -5 dB.

Several prior works on AMR that are available in the literature, which use both WT-based and non-WT based methodologies, have been surveyed in Chapter 2. In this section, the results of simulation experiments reported in these previous works are compared with the results obtained in Section 5.3. The relevant comparisons are presented in Tables 5.12-5.13.

It must be reiterated that a direct comparison of the different AMR methodologies is

Table 5.14 AMR classification rates obtained in this research work

Modulation Scheme	SNR = 10 dB	SNR = 5 dB	SNR = 0 dB	SNR = -5 dB
BPSK	100%	100%	99.1%	97.2%
QPSK	100%	99.8%	96.3%	94.6%
8-PSK	100%	97.8%	89.2%	81%
BASK	100%	100%	100%	95.8%
4-ASK	100%	99.8%	99.3%	95.9%
BFSK	100%	100%	98.2%	96.8%
4-FSK	100%	98.8%	95.3%	93.2%
4-QAM	100%	98.9%	96.8%	96.4%
16-QAM	100%	98.2%	90.6%	79.8%

impossible due to the fact that the prior works reported in the literature do not necessarily use the same general *a priori* assumptions, such as SNR values, numbers of symbols per transmission, etc.

From Table 5.14, the rates of correct classification at SNR = 10 dB and 5 dB, are almost 100% for all the communication signals considered in this work. In the case of SNR = 0 dB, majority of the rates of correct classification achieved are above or at around 97%, except in the cases of 8-PSK and 16-QAM signals for which rates of 89.2% and 90.6% were achieved, respectively. For noisy channels operating at an SNR = -5 dB, the rates of correct classification achieved are near, or above, 94% for most of the modulation schemes. The exceptions at SNR = -5 dB are 8-PSK and 16-QAM signals. The rates of correct classification at SNR = -5 dB for 8-PSK and 16-QAM are 81% and 79.8%, respectively. Upon comparison between results of this work and previous literature, the

Table 5.15 Non-wavelet transform-based AMR methods

AMR Method Devised by	SNR	Modulation Scheme	Correct Classification Rate
Azzouz, et al. [32]	15 dB	BASK	95.3%
		4-ASK	76.3%
		BPSK	100%
		QPSK	96%
		BFSK	92%
		4-FSK	100%
	20 dB	BASK	96%
		4-ASK	80.2%
		BPSK	100%
		QPSK	100%
		BFSK	92%
		4-FSK	88%
Hsue and Soliman [33]	15 dB (CNR)	BPSK	99%
		QPSK	98%
		8-PSK	100%
		BFSK	100%
		4-FSK	100%
Dobre, et al. [9]	10 dB	BPSK	100%
		QPSK	
		8-PSK	
		16-QAM	
	5 dB	BPSK	100%
		QPSK	
		8-PSK	
		16-QAM	
	0 dB	BPSK	78%
		QPSK	100%
		8-PSK	
		16-QAM	

Table 5.16 Wavelet transform-based AMR methods

AMR Method Devised by	SNR	Modulation Scheme	Correct Classification Rate
Ho, et al. [58]	13 dB (CNR)	BPSK	97%
		QPSK	97%
		8-PSK	97%
		2-FSK	100%
		4-FSK	100%
Hong and Ho [60]	20 dB (CNR)	QPSK	100%
		4-FSK	100%
		16-QAM	99.7%
	15 dB (CNR)	QPSK	99.5%
		4-FSK	100%
		16-QAM	98.7%
	10 dB (CNR)	QPSK	98.8%
		4-FSK	100%
		16-QAM	98.7%
	5 dB (CNR)	QPSK	96.6%
		4-FSK	100%
		16-QAM	100%
	13 dB	BPSK	100%
		QPSK	100%
		8-PSK	100%
		BFSK	100%
		4-FSK	100%
Jin, et al. [54]	10 dB	BPSK	100%
		QPSK	99.9%
		8-PSK	100%
		BFSK	98.1%
		4-FSK	100%
	8 dB	BPSK	100%
		QPSK	96.5%
		8-PSK	100%
		BFSK	95.3%
		4-FSK	100%

correct classification rates achieved in this work are either equal to, or better than those previous results for same SNR conditions. Even though severe noisy communication channel were not considered into simulations from most literature, it is still clear to see that majority part of the performance curve stays stable when noise increase. But the PSK/QAM classifier gets relatively more affection as noise increases.

5.5 Conclusions

In this Chapter, an effective WD AMR process and its efficacy are investigated and demonstrated through the utilization of the pattern recognition technique of correlation along with templates defined in the wavelet-domain. In this AMR process, assumed known system parameters include the carrier frequency, perfect symbol timing and no timing offset. It has been proved that, even at low values of SNR, this WD-AMR algorithm can correctly classify signals with high reliability. Rates of correct classification obtained in this work are shown in Tables 5.14, as equal to or better than those reported in the literature.

Given the reliability of the AMR process developed in this chapter, it has the potential to benefit the communications receiver design to enhance more interoperability between various communication standards. In other words, the AMR process could possibly enable the development of agile radio receivers and transceivers. Such an agile radios could be applied in many military related fields, such as threat signal analysis, spectrum management, electronic warfare, and electronics surveillance systems. In the future, more similar AMR processes could be further studied and extended to classification of more modulation schemes by using more multiple wavelet families.

Chapter 6 Development of the Wavelet Domain-Based (WD) Demodulation Technology

Two DWT-based AMR algorithms were described and validated in Chapters 4 and 5, and it is now necessary to develop the techniques for demodulation in order to complete the baseband processing system on the WD Receiver Platform. After properly classifying the unknown modulation scheme employed by a received communication signal, an appropriate demodulation process must be activated in order to recover the information-bearing signal to the baseband data.

The motivation of designing the WD-Demodulator is to achieve this WD system architecture's optimization. As shown in the system-level block diagram of Fig. 6.1, although employing a contemporary demodulation system followed by the WD-AMR could fulfill the baseband processing such as the information recovery function, this system is inefficient in its redundant algorithm and a high cost in circuit complexity.

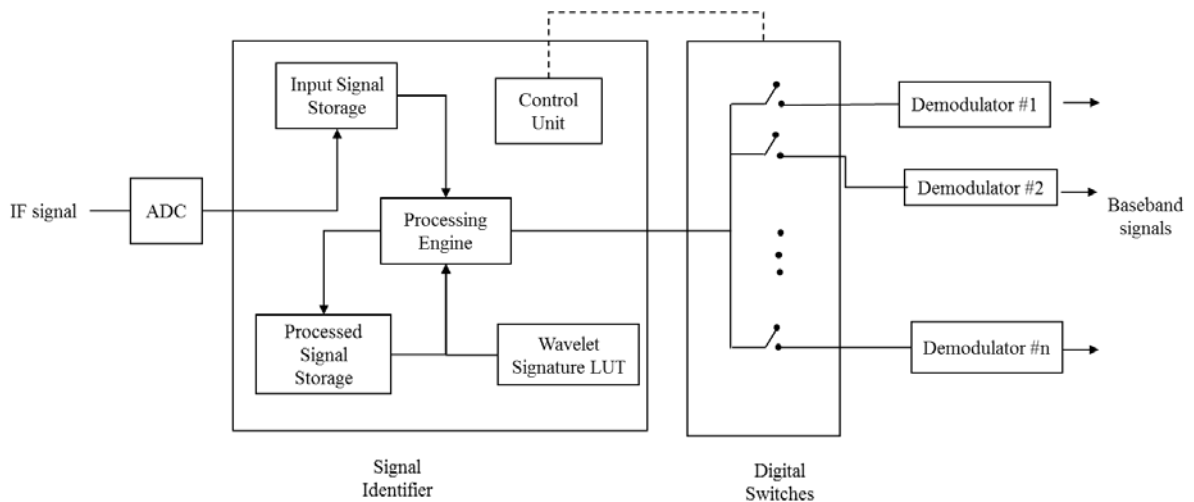


Fig. 6.1 Baseband processor using wavelet transform-based signal identification and classical demodulation

For the implementation shown in Fig. 6.1, the input signal, sampled by the ADC, is a digitally modulated signal at zero IF. The data sequence output by the ADC is accumulated in a memory location (the input signal storage). After sufficient signal samples are stored, the processing engine decomposes the digital-domain IF signal using different wavelets and the output data are stored in a second memory location (the processing signal storage). Next, the processor compares the decomposed signal with pre-existing wavelet signatures that are available in a Look-Up Table (LUT) and makes the modulation recognition decision. This decision is then released to the digital switches through the control unit. The control unit, which operates switches connected to the correct external contemporary demodulator, can be used to recover the baseband data. However, the system shown in Fig.6.1 is not reconfigurable because each modulation scheme still requires its own unique carrier signal and, correspondingly, its own specific demodulation circuit. Also, there are computational redundancies that can be refined. First, the received signal is transformed to the wavelet domain for the WD-AMR algorithm. It is then transformed in reverse back to the time domain to match with the corresponding classical demodulator. Hence, the system could be improved in two aspects: reduce the computational complexity and lower the circuit design cost. An improved system is introduced as shown in the Fig. 6.2.

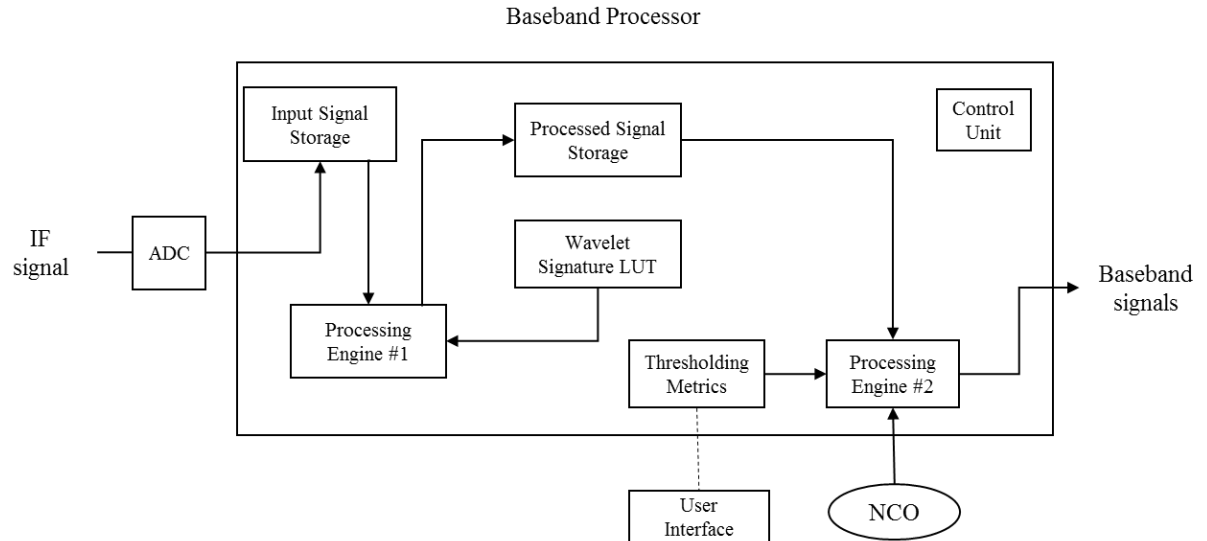


Fig. 6.2 Baseband processor using wavelet transform-based signal identification and demodulation.

The completed baseband processor for the combined processes of signal identification and demodulation is illustrated in Fig. 6.2. The main difference between the two processors is a processor implemented as a universal demodulator in the wavelet domain to detect and recover a signal. This wavelet-based demodulator can directly receive, analyze and make decisions upon the signals' wavelet domain expression without transferring back to the time domain. Besides, by employing the wavelet-based AMR and wavelet-based demodulation jointly, a reconfigurable baseband processor platform is completed and implemented.

The rest of this chapter consists of three parts. Firstly, it focuses on illustrating how this new modulator is derived from the contemporary demodulation technology. Secondly, the architecture of this WD-baseband processor and its general algorithm will be developed in Section 6.2. Lastly, the performance of the demodulation techniques is evaluated and BER curves are plotted for cases of signals corrupted with AWGN. The communications signals considered in this case are BASK, 4-ASK, BFSK, 4-FSK,

BPSK, QPSK, 8-PSK, 4-QAM (also denoted as $\pi/4$ -QPSK), 16-QAM. The corruption results in SNR values range from -5 dB to 10 dB.

6.1 Development of the WD-based Demodulation

The contemporary demodulation techniques for digitally modulated communications signals are developed based on the MAP/ML being the best decision strategy. In the classical receiver, the correlation between received signals and noise-free symbols with a known modulation type is a key part of the decision. These correlation outputs are compared and the largest value is selected. Based on the comparison result, the data bit sequence can then be demodulated. Fig. 6.3 illustrates the system block diagram for this classical correlation-based demodulation procedure. In this case, the variable η_m is usually treated as a known constant parameter.

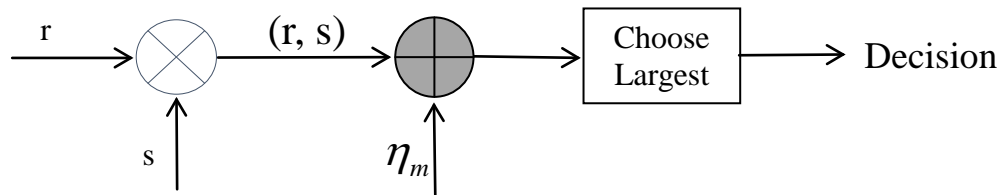


Fig. 6.3 The Contemporary Correlator based Demodulation.

In short, the best decision rule of the optimal classical demodulation is known as the maximum a posteriori (MAP/ML) probability rule [74] $\hat{m} = \arg \max_{1 \leq m \leq M} (\eta_m + (r, s_m))$. The

variable η_m consists of the signal power, the variance of the Gaussian white noise, and the signal prior probability, all of which are usually either constant values or known

variables. Hence, the correlation is the key part of the decision.

In the time domain receiver system, two inputs of the correlator are the received signal and the noise-free symbols employ the same modulation scheme as the received signals.

In a wavelet-based receiver platform, the output of the WD-based AMR is the wavelet expression of received signals with a known modulation scheme and the templates signals are also wavelet transformed. It is significant to note that the inputs in the time domain and wavelet-based receiver systems are similar, which warrant further investigation into how the WD correlation is related to the regular correlation.

To research the WD correlation, it must start from the definition of the DWT. As introduced in Chapter 3, for an arbitrary function $f(t)$, the correlation results in the decomposition of $f(t)$ into two orthogonal parts:

$$f(t) = f_j(t) + w_j(t) \quad f_j(t) \in V_j, \quad w_j(t) \in V_j^\perp, \quad f_j(t) \perp w_j(t) \quad (6.1)$$

The spaces V_j have a special structure; it is defined as a linear space of the scaled and translated replicas of a single function, called the scaling function, or the father wavelet.

Its scaled/translated replicas are defined for any integer of j, n by: $\phi_{jn}(t) = 2^{j/2} \phi(2^j t - n)$.

The functions $\phi_{jn}(t)$ are orthonormal for each fixed j , and form a basis of space

$$V_j \cdot (\phi_{jn}, \phi_{jm}) = \delta_{nm}.$$

Now the projection of an arbitrary signal $f(t) \in L^2(\mathbb{R})$ onto the subspace V_j is defined by the following expansion in the ϕ_{jn} basis:

$$f_j(t) = \sum_n c_{jn} \phi_{jn}(t) = \sum_n c_{jn} 2^{j/2} \phi(2^j t - n) \quad (6.2)$$

Another wavelet function $\psi(t)$ and its scaled and translated replicas actually span the

orthogonal complement V_j^\perp of V_j with respect to $L^2(\mathbb{R})$. Note that

$\psi_{in}(t) = 2^{i/2} \psi(2^i t - n)$, $i \geq j$, which are orthogonal to $\phi_{jn}(t)$, and are also mutually orthonormal, $(\psi_{in}, \psi_{i'n'}) = \delta_{ii'} \delta_{nn'}$, $(\phi_{jn}, \psi_{im}) = 0$, $i \geq j$.

The component $w_j(t)$ from equation (6.1) is referred to as the “detail” and incorporates the details of $f(t)$ at all the higher resolution levels $i \geq j$, or finer time scales $2^{-i} \leq 2^{-j}$.

It is spanned by the ψ -basis expansion:

$$w_j(t) = \sum_{i \geq j} \sum_n d_{in} \psi_{in}(t) = \sum_{i \geq j} \sum_n d_{in} 2^{i/2} \psi(2^i t - n) \quad (6.3)$$

Hence, taking (6.2) and (6.3) into (6.1) to complete forming the multi-resolution decomposition analysis of $f(t)$,

$$f(t) = f_j(t) + w_j(t) = \sum_n c_{jn} \phi_{jn}(t) + \sum_{i \geq j} \sum_n d_{in} \psi_{in}(t) \quad (6.4)$$

$$f(t) \xrightarrow{\text{DWT}} = \sum_n c_{jn} + \sum_{i \geq j} \sum_n d_{in}$$

The right-hand coefficients in (6.4) are:

$$c_{jk} = (f, \phi_{jk}) = \left(\sum_n c_{j+1,n} \phi_{j+1,n}, \phi_{jk} \right) = \sum_n c_{j+1,n} (\phi_{j+1,n}, \phi_{jk}) \quad (6.5)$$

$$d_{jk} = (f, \psi_{jk}) = \left(\sum_n c_{j+1,n} \phi_{j+1,n}, \psi_{jk} \right) = \sum_n c_{j+1,n} (\phi_{j+1,n}, \psi_{jk}) \quad (6.6)$$

According to the equation (6.1), in the time domain the correlation of two signals $f(t)$ and

$f'(t)$ could be re-defined as:

$$\begin{aligned} (f, f') &= (f_j + w_j, f'_j + w'_j) \\ &= (f_j, f'_j) + (f_j, w'_j) + (w_j, f'_j) + (w_j, w'_j) = (f_j, f'_j) + (w_j, w'_j) \end{aligned} \quad (6.7)$$

Because the f and w are two orthogonal parts of a signal, their correlation is 0.

Based on the discrete wavelet transform definition (6.2) and (6.3), the two components in the output of (6.7) could be reformatted in the wavelet domain in the following way. The first part of function (6.7) is re-written:

$$\begin{aligned} (f_j, f'_j) &= (\sum_n c_{jn} \phi_{jn}(t), \sum_n c'_{jn} \phi_{jn}(t)) = \sum_n c_{jn} c'_{jn} (\phi_{jn}, \phi_{jn}) = (c_{jk}, c'_{jk}) \end{aligned} \quad (6.8)$$

The scalar property of correlation and the orthonormal basis function feature are applied to the above expression equation.

Following the similar strategy, the second component of (6.7) could be expressed by wavelet coefficients.

$$\begin{aligned} (w_j, w'_j) &= (\sum_{i \geq j} \sum_n d_{in} \psi_{in}(t), \sum_{i \geq j} \sum_n d'_{in} \psi_{in}(t)) \\ &= \sum_{i \geq j} \sum_n d_{in} d'_{in} (\psi_{ik}, \psi_{ik}) = \sum_{i \geq j} (d_{ik}, d'_{ik}) = (\sum_{i \geq j} d_{in}, \sum_{i \geq j} d'_{in}) \end{aligned} \quad (6.9)$$

Now combine (6.8) and (6.9) together, then apply the scalar property of correlation and the orthogonality property of basis function, the WD correlation equation can be reformatted as:

$$\begin{aligned} (c_{jk}, c'_{jk}) + (\sum_{i \geq j} d_{in}, \sum_{i \geq j} d'_{in}) &= (c_{jk}, c'_{jk}) + 0 + 0 + (\sum_{i \geq j} d_{in}, \sum_{i \geq j} d'_{in}) \\ &= (c_{jk}, c'_{jk}) + (c_{jk}, \sum_{i \geq j} d'_{in}) + (c'_{jk}, \sum_{i \geq j} d_{in}) + (\sum_{i \geq j} d_{in}, \sum_{i \geq j} d'_{in}) \\ &= (c_{jk}, c'_{jk} + \sum_{i \geq j} d'_{in}) + (\sum_{i \geq j} d_{in}, c'_{jk} + \sum_{i \geq j} d'_{in}) = (c_{jk} + \sum_{i \geq j} d_{in}, c'_{jk} + \sum_{i \geq j} d'_{in}) \end{aligned} \quad (6.10)$$

Another direction to develop the WD correlation (6.10) is to link the wavelet coefficients to its function in the time domain with the help of (6.7),

$$\begin{aligned}
 (c_{jk}, c'_{jk}) + (\sum_{i \geq j} d_{in}, \sum_{i \geq j} d'_{in}) &= (f_j, f'_j) + (w_j, w'_j) \\
 &= (f_j + w_j, f'_j + w'_j) = (f, f')
 \end{aligned} \tag{6.11}$$

Through comparing the two expressions (6.10) and (6.11), a new equality is presented in the (6.12): The correlation of two signals in the time domain is the same as the correlation of their discrete wavelet transformed coefficients,

$$(f, f') = (c_{jk} + \sum_{i \geq j} d_{in}, c'_{jk} + \sum_{i \geq j} d'_{in}) = (DWT(f), DWT(f')) \tag{6.12}$$

6.2 The Architecture Design of the WD-Receiver System

Upon the conclusion of the last section, the correlator component can be preserved in the WD demodulation system from the contemporary receiver system. Its system block diagram is plotted in the Figure. 6.4.

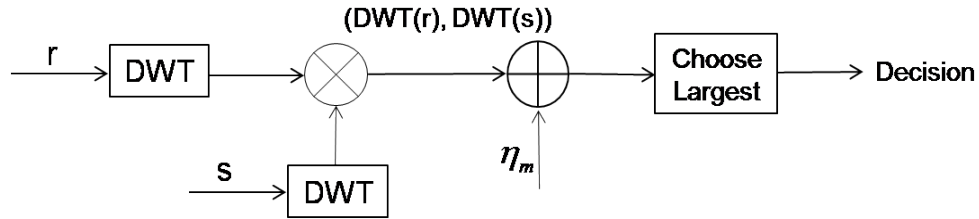


Fig. 6.4 Wavelet based-Demodulation System

As shown in Fig. 6.4, the basic construction of the WD Demodulation has not changed much from the classical demodulator system, except for two input signals that are wavelet transformed. The reason is that the correlation in the time domain generates the same correlation as it does in the wavelet domain, so the underlying decision rules for

both systems are the same as well.

Since both inputs of the correlator are wavelet-transformed signals, they are the same as the outputs of the WD-AMR. Hence, this WD-Demodulation system could be further updated to the WD-Receiver platform by combining the WD-AMR processor into the system as stated in the Fig. 6.5.

This WD-Receiver system can enable both modulation recognition and demodulation. Also, it achieves two improvements compared to the contemporary receiver:

1. Avoid transferring signals back and forth between the wavelet domain and the time domain. This WD demodulator is designed to follow after the WD-based AMR processor to complete the receiver system within the wavelet platform. The wavelet-based demodulation has proved that it is capable of directly processing the output of the WD-AMR; it can employ wavelet expressions of the received signal at its input without having to transfer the WD signals back to the time domain. Hence, the computation of this algorithm is low in redundancy.
2. This wavelet-based Receiver is a reconfigurable radio system. Signal “r” was received with unknown modulation type first, then the WD-AMR detects the modulation scheme and feeds this decision back the templates signal storage “s”. The template signal “s” will employ the same modulation technology, go through the discrete wavelet transformation, and join the following WD-Demodulation procedure. Instead of utilizing a distinct demodulation system for different modulated signals, this universal system design could fulfill the baseband process for multiple types digital transmitted signals. This feature of the WD-Receiver system highly reduces the circuit design complexity.

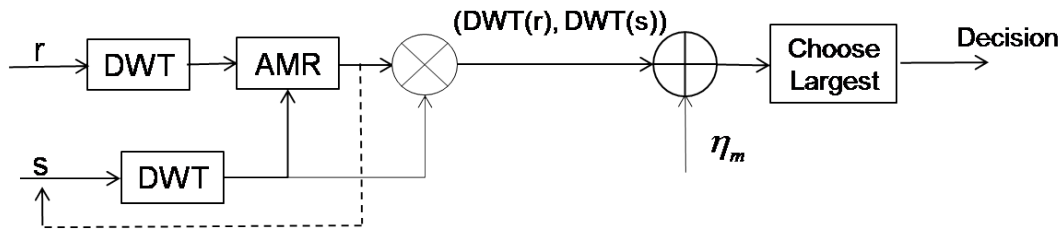


Fig. 6.5 Wavelet-based Receiver Platform

The general algorithm of this wavelet-based reconfigurable receiver system is illustrated by below:

1. After going through the channel, the received signals "r" are wavelet transformed with an unknown modulation type.
2. The template signals are wavelet transformed and stored at the "s" end.
3. As shown in Chapters 4 and 5, the wavelet expressions of "r" and "s" are analyzed.
4. After the ARM process, its outputs contain two useful pieces of information for the following WD-demodulation system:
 - a. The detected modulation scheme decision employed by the received signal. This information is transmitted to the template signal "s" end to control the modulation type for input of the correlator.
 - b. The other result of the AMR is the wavelet expression of the received signal "r" with detected modulation scheme, which will be sent to the correlator as well.
5. Two wavelet components from 4a and 4b are correlated in the WD demodulator.
6. The comparator selects the largest WD correlation and the corresponding symbol that generates the largest correlation value becomes the demodulation result.

Even if the digital communication receiver is designed in the wavelet domain, the correlator-based optimal demodulation system still preserves its main circuit structure. This is because the important features proved in (6.12) shows that the correlation of two signals in the time domain is equal to their correlation in the wavelet domain.

6.3 Simulation Experiments and Results

In this section, there are two experiments tested to verify the WD correlation and TD correlation equality. In the first experiment, the two vectors for the two signals are discrete wavelet transformed. Their wavelet coefficients correlation and also their time domain correlation are both calculated as follows:

1. We have two vectors in time domain:

$$X=[1 \ 2 \ 3 \ 4 \ 5 \ 6 \ 7 \ 8], \ Y=[6 \ 7 \ 8 \ 1 \ 2 \ 3 \ 4 \ 5]$$

2. After applying discrete wavelet transformations on X and Y through MATLAB, their WD expressions are calculated as below:

$$W_X=[12.7279 \ -1.4794 \ -4.4090 \ 2.2467 \ 0 \ 0 \ -3.7938 \ 0.9654]$$

$$W_Y=[12.7292 \ -2.9484 \ 4.8818 \ -1.5166 \ -0.1147 \ 0.2818 \ 0 \ 2.6614]$$

3. Now the correlation in the wavelet domain shows:

$$(W_X, W_Y)=143.991, (W_X, W_X)=203.997$$

And the correlation in the time domain and

$$(X, Y)=144, (X, X)=204$$

Hence, $(X, Y)=(DWT(X), DWT(Y))$

The first experiment numerically proved that the correlation values could be preserved even after being discrete wavelet transformed. This theorem can be explained

from the matrix calculation's point of view. Since the DWT is an orthogonal transformation, that is, the DWT can be written:

- a. Linear transformation $W_x = W * X$,
- b. The DWT matrix W is orthogonal,
- c. $W' * W = I$

This guarantees the preservation of the correlation value.

Previously in Chapters 4 and 5, the AMR performance was simulated and compared with existing systems from other literature. This second experiment will solely focus on the simulation of the WD-demodulation part. Also, it would be more meaningful to compare the performance of the WD demodulator with the regular demodulation system but exclude the AMR processor from the comparison. This is because when two receiver systems operate under the assumption of the same test environment, such as the same known modulation type, the same noise channel, and so on, the test results are more comparable.

In following content, the algorithm developed in this chapter shows itself using the MATLAB simulation. All of the signals involved in this study have been corrupted by zero-mean AGWN resulting in SNR values in the range of -5 dB to 10 dB. The WD Demodulator performance has been evaluated based on 10^5 Monte-Carlos trials wherein each simulation experiment consists of 192 bits per frame for ASK, FSK and PSK signals, and 1024 bits per frame for M-ary QAM signals. In order to maintain a high degree of resolution in the WD scalograms, the signal, which corresponds to the carrier frequency, is oversampled by a factor of 16 over the Nyquist rate. Here, the key parameter assumed for the demodulation process is that of perfect symbol timing with no timing offset.

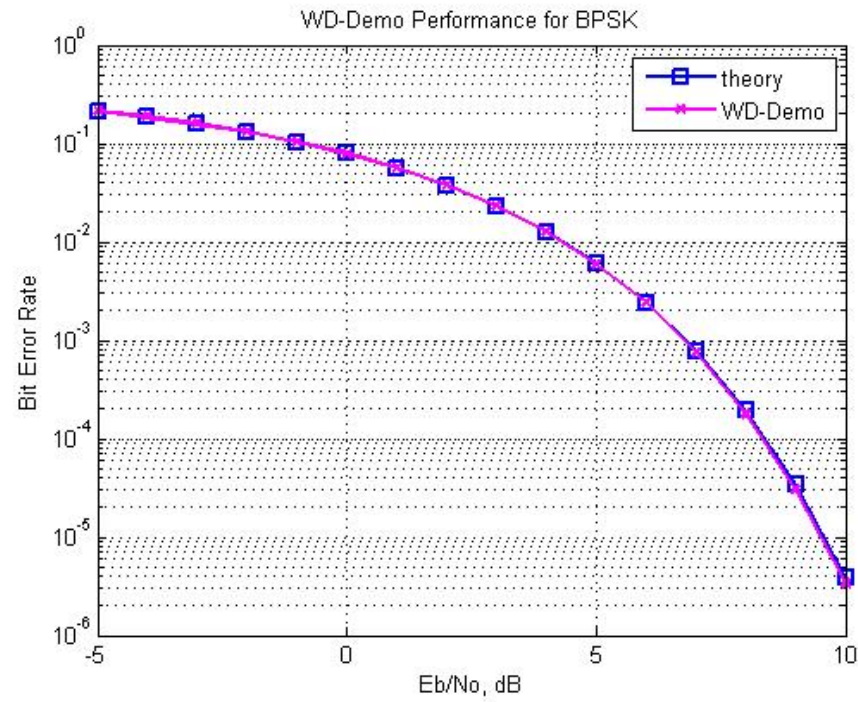


Fig. 6.6 BPSK BER Curve Comparison

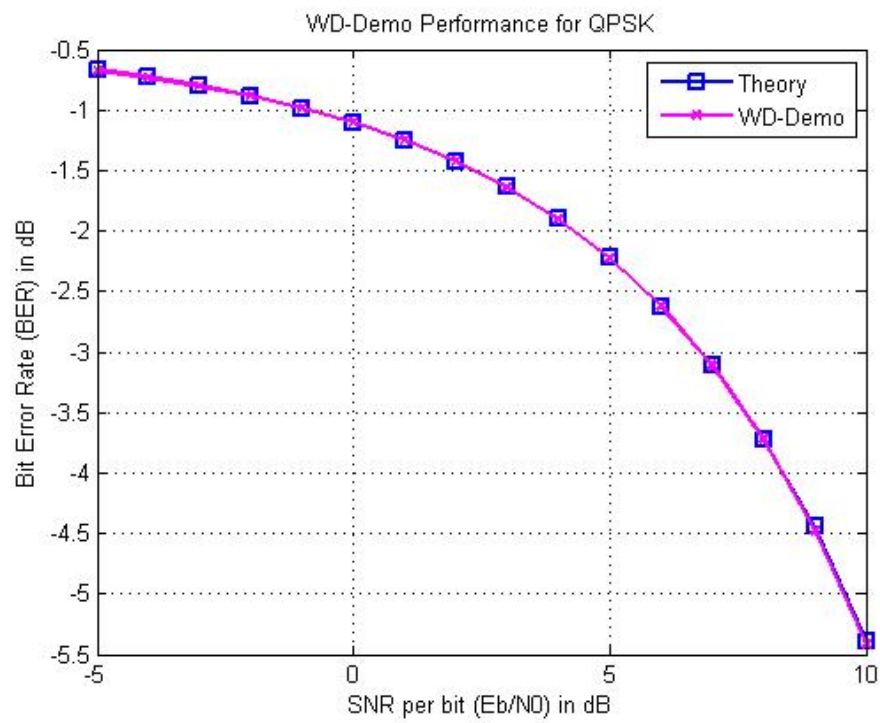


Fig. 6.7 QPSK BER Curve Comparison

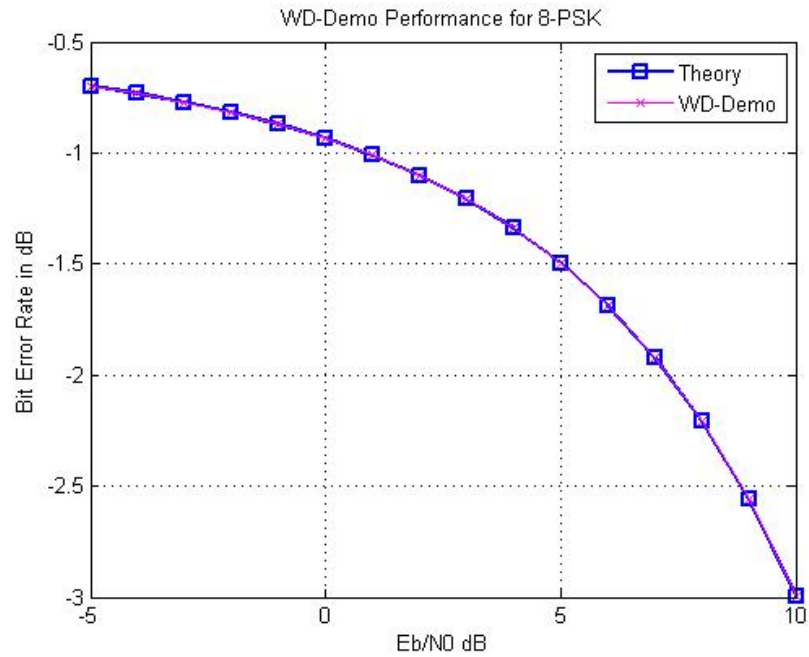


Fig. 6.8 8-PSK BER Curve Comparison

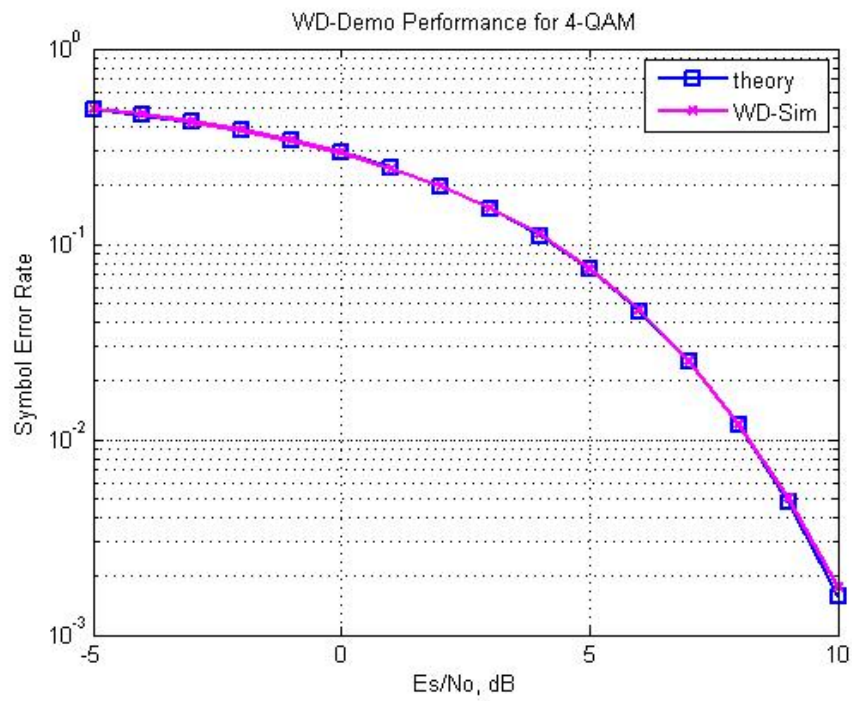


Fig. 6.9 4-QAM SER Curve Comparison

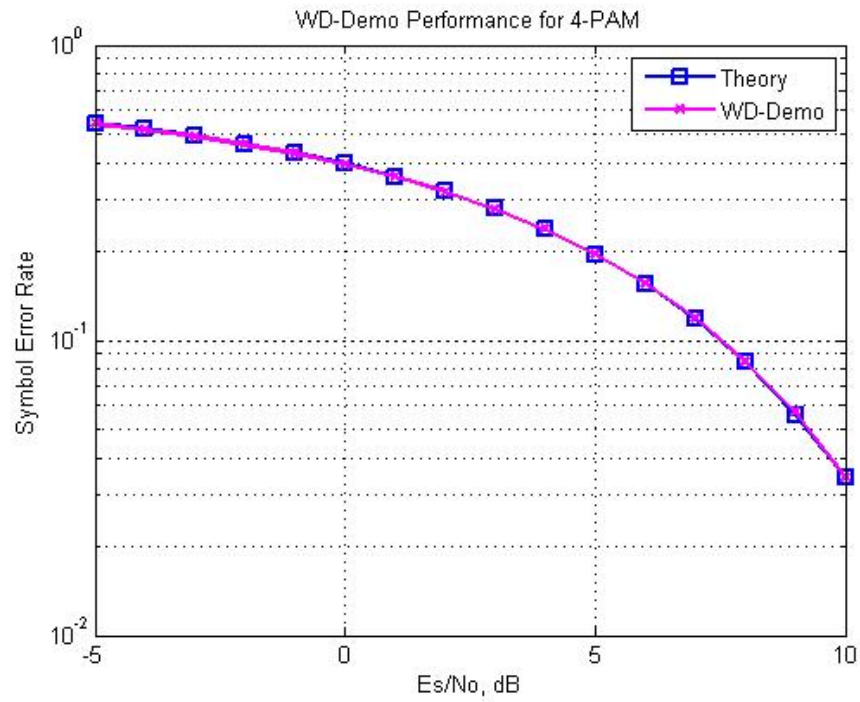


Fig. 6.10 4-PAM SER Curve Comparison

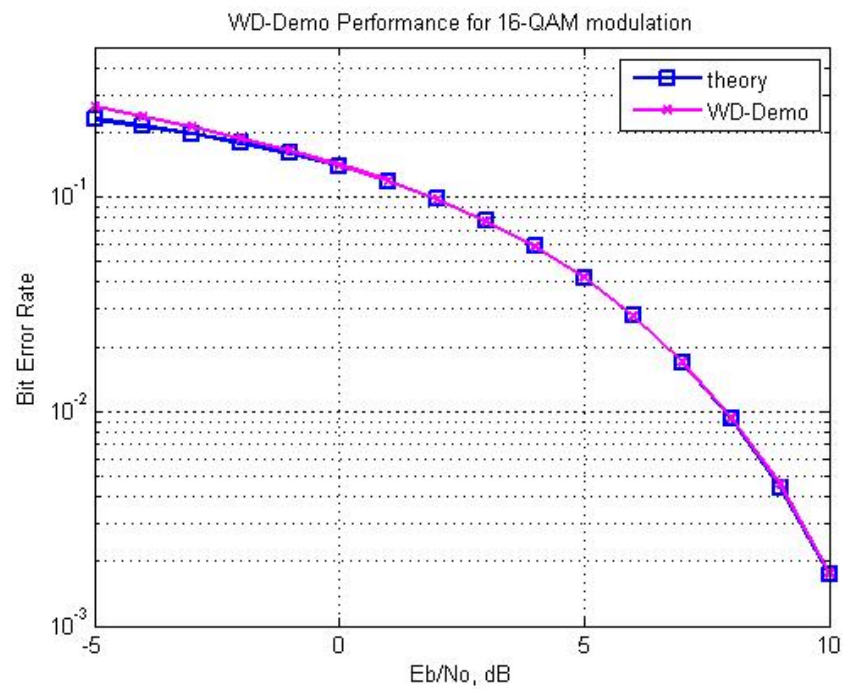


Fig. 6.11 16-QAM BER Curve Comparison

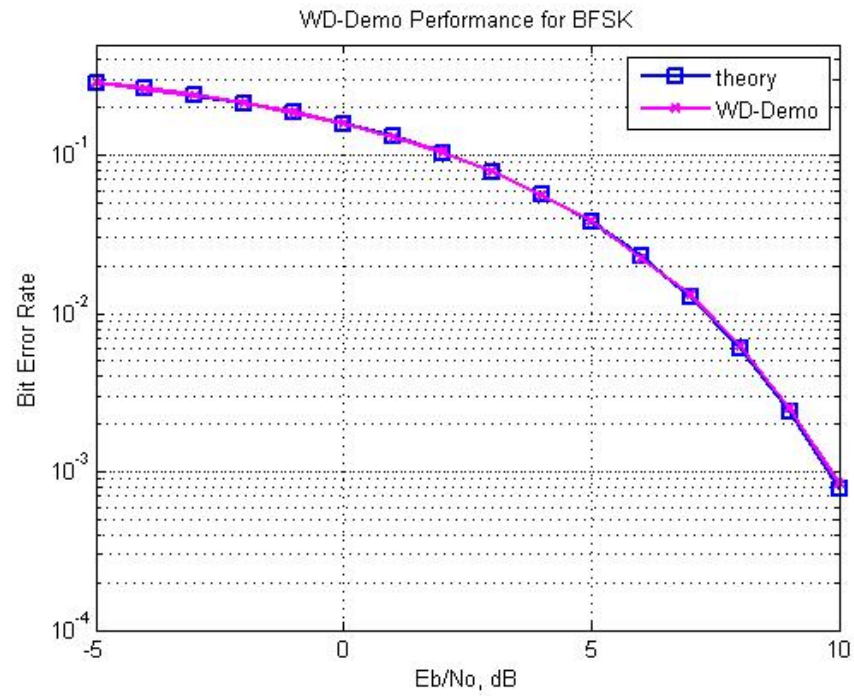


Fig. 6.12 BFSK BER Curve Comparison

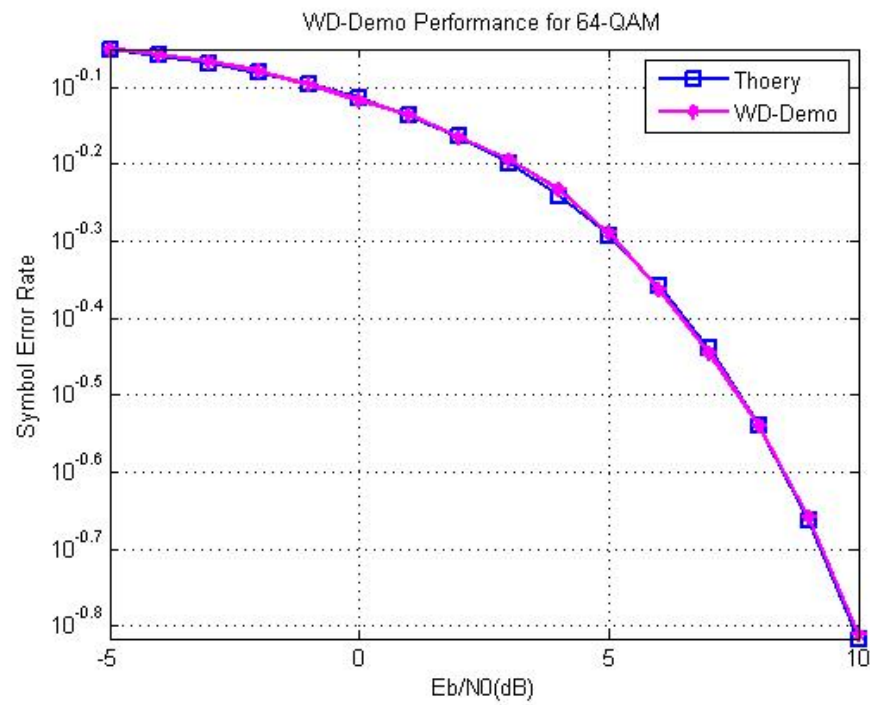


Fig. 6.13 64-QAM SER Curve Comparison

Each received, noisy signal has been demodulated using the WD demodulator. Each set of demodulator performance results presented in Figs. 6.6-6.13 contains two types of performance curves. One curve corresponds to the theoretical performance of the traditional correlation receiver demodulation. The other curve is the simulation results for the WD Demodulators developed in this dissertation. It has been observed that the probability of error is almost the same between these two systems. This result actually meets the expectation. This is because the classical correlation based demodulator is designed upon the theoretical best decision rule MAP/ML that was proven to produce the optimal detection accuracy with the AWGN channel digital signal communication system. In the WD demodulation system, although signals are wavelet transformed and processed in the wavelet domain, the communication channel and the whole environment did not change. Hence, its performance will not proceed beyond the best performance boundary given by the classical system.

Besides, the performances obtained through simulating both the WD Demodulation techniques and the TD(correlation-based) Demodulation mentioned in this chapter are also compared and showed in details in Appendix B.

In conclusion, for the test modulation signals considered in this dissertation going through the same AWGN channel system, the wavelet-based demodulation performance is, at most, as good as the contemporary optimal correlation-based demodulator.

6.4 Discussion of Results

In this chapter, the WD Demodulation methodology has been explained and described in detail. Its BER performance is also simulated and compared with the contemporary receiver. For every modulation scheme considered in this dissertation, the WD Demodulation methodology performed comparably with the traditional correlator-based demodulation system. This observation is based on comparing the BER performances obtained using both types of demodulators.

Moreover, the WD Receiver system has been devised in a manner such that automatic demodulation of a communications signal from the wavelet domain is possible after the WD AMR processor has recognized the modulation scheme. This feature, which ensures that a signal-specific demodulator can adapt and work automatically, is advantageous for the development of agile radio receivers. It allows the WD-based demodulation system to adhere to the wavelet-transformed signal perfectly from the WD-AMR. This is another advantage, which improves the computational efficiency and saves time by eliminating the transfer of signals between the time and wavelet domains. Although the final detection result is in the time domain, a complete analysis is finished in the wavelet domain. There is no domain transfer computation at all during the whole process. This improvement keeps the computational complexity as low as possible.

Chapter 7 Summary and Conclusions

7.1 Summary

In this dissertation, both WD-AMR and WD-Demodulation processes are devised based on correlation between signal and template expressions in the wavelet domain, and then jointly analyzed by the blind recognition technique.

The correlation of received, noisy digitally modulated communication signals with WD templates corresponding to a known set of modulation schemes is the basis operation of the WD-AMR algorithms design in this work. Specifically, noise-free WD templates containing distinguishing features of each modulation type are firstly constructed. Then the DWT is used to extract the WD coefficients of received signals that have been corrupted with AWGN. Based on the similarity through matching these two sets WD fractal patterns, decision metrics are developed in order to recognize the digital modulation scheme implicit in the signal.

The WD templates are represented as signature signals obtained from noise-free digitally modulated signals. Two categories of WD signatures are defined, namely the instantaneous featured templates and the statistical featured templates. The instantaneous features, introduced in the Chapter 4, contain the symbol transition characteristics of a communications signal. Each feature is unique to a particular digital modulation scheme, so that the modulation type detection could be implemented upon matching up this feature. However, for the same reason it is inappropriate for higher-order modulation schemes as more unique features templates are needed. Due to this fact, the computational effort increased. Besides, although the rates of correct classification

reported in Chapter 4 show that its results are better than those reported in the literature, this AMR algorithm has another inherent drawback. Because the instantaneous featured templates are extracted so as to capture the symbol transition characteristics, the WD AMR process might not be able to recognize the particular modulation scheme when the communications signal data sequences contain either all data “1” or data “0” symbols.

The statistical feature templates are then introduced in for higher order AMR process. These new templates represent different sinusoidal carrier characteristics present within a symbol period of a communications signal using corresponding various modulation schemes. Therefore, the new WD-AMR algorithm requires fewer numbers of templates than the one introduced in Chapter 4. For example, 256 instantaneous featured templates are needed to recognize 16-QAM signals as compared to the need for a total of 3 statistical featured templates otherwise. Statistical features of the WD-correlation between WD received signal and WD templates are extracted and jointly analyzed as parameters for the modulation scheme decision. This algorithm not only overcomes the drawback of the previous AMR methodology, but also maintain the computational complexity and circuit design cost rather low.

The WD-correlation also played an important role in the development of the WD-Demodulation system. It was shown in Chapter 7 that the DWT guaranteeing the preservation of the correlation value because it is an orthogonal transform. Hence, the BER performance of the WD Demodulation process is competitive with the traditional correlate based demodulation method. The WD Demodulation process is the first such methodology devised in the context of WTs. Besides, it could be directly connected after the WD-AMR to form a reconfigurable WD-Receiver. This system is reconfigurable in

the sense that transmitted signals at different carrier frequencies, and with different modulation schemes, can be reliably identified and appropriately demodulated by this universal receiver system. This advantage saves system design cost and complexity. The computational effort of this system is also low because the whole computational process is operated in the wavelet domain only. There is no cost for signals transformation between the time and wavelet domains.

7.2 Contributions of the Dissertation

This work contributes following key points:

1. A solution of WD signatures selection suitable for modulation recognition schemes studied in this work is invented. Two types WD signatures, named as the instantaneous featured templates and the statistical featured templates are developed and constructed.
2. Two types of DWT-based AMR algorithms, one is designed for lower order modulation recognition and the other one is more practical for higher order modulation schemes, are developed in this work by using DWT-based signatures of digitally modulated communications signals.
3. The TD-correlation of two functions is proved equal to their WD-correlation. It is the basis of development of the WD Demodulation algorithm
4. Development of the first WD Demodulation algorithms using WD-correlation of digitally modulated communications signals in the context of WTs.
5. WD-AMR and WD-Demodulation performance obtained from this work is evaluated and compared with results obtained from other literatures.

6. As DWT-based Channel Estimation and DWT-based Equalization functions were developed in previous works, they could work jointly with DWT-based AMR and DWT-based Demodulation system invented in this dissertation. Together to format an automatic, reconfigurable and reliable new WD-based transceiver.
7. This new WD-based Receiver benefit the communication system in multiple aspects. It increases the interoperability between different modulation scheme, lower the circuit design cost, and enhances the process efficiency.

7.3 Future Work

This research studied the design of DWT-based AMR and DWT-based Demodulation algorithms, which are two key processors as the basis to build a WD Receiver system. In this work, both of them have been proved for their reliable performance for the zero mean AWGN channel. In the future, more factors could be considered and included into this research to develop a more and more comprehensive WD-based communication system.

Firstly, there are more realistic parameters in the complicated real world, i.e. different channel models, non-synchronized symbol and so on, could be the introduced into the design to develop the WD-Receiver system in a more real communication environment. An assumption of synchronization is made in this work. Time offset estimation could be an essential function in the WD-receiver system just as the synchronization time estimation in the contemporary system.

Secondly, signals families studied in this work could be expanded to more communications signals using different modulation schemes, such as Gaussian Minimum Shift Keying (GMSK), (non) square M-ary QAM and other higher order signal

constellations, to improvement the WD AMR and WD Demodulation algorithms.

Furthermore, WD-based system performance assessment could be extended to other noise scenarios such as impulsive noise (of different bandwidth), band-limited noise, etc., which often existing in the real communication world. For the sake of simplicity, this research only has its majority attention focused on the zero-mean AWGN channel.

To achieve above functions, the current WD-Receiver system is demanded to add more essential processors. Two of them are investigated in the work [80], which are the WD-Equalizer and WD-Channel Estimator. One of the future works is to combine these four WD-processors as an improved WD-Receiver. The received signals are firstly discrete wavelet transformed. Then the channel impulse response function is analyzed by the WD-ChannelEstimation and the ISI is eliminated by the WD-Equalization. Following the modulation scheme and data recovery will be done by the WD-AMR and WD-Demodulation. The whole procedure is implemented in the discrete wavelet domain.

Lastly, having demonstrated the efficacy of the invented WD AMR and WD Demodulation process, another next step could be hardware implementation. For example, the Field Programmable Gate Array (FPGA) technology could be utilized for the demonstrating a WD-based radio receiver.

7.4 Conclusions

In summary, this work has shown that by using of the pattern recognition methodology of template matching, along with appropriately defined WD templates, new WD algorithms could be designed workable for both automatic modulation recognition and signal demodulation. The results in this research provide desired functionalities to implement

the new communication system that has a comparable performance with other existing approaches. It is approved that the Wavelet Platform could be a new approach for baseband signal processing, and it is particularly well-suited for reconfigurable radios.

The WD AMR process can correctly classify modulation schemes with rather high reliability even for low values of SNR. At $\text{SNR} = 10\text{dB}$ and 5dB , the correct classification rates are almost 100% for all communications signals in this work. In the case of $\text{SNR} = 0\text{dB}$, most correct detection rates are above or at around 96%, except for 8-PSK and 16-QAM signals as whose rates of 89.2% and 90.6% were obtained, respectively. Following, for noisy channels with $\text{SNR} = -5\text{ dB}$, the simulated rates of correct classification are around, or above, 94% for most modulation schemes. However, at $\text{SNR} = -5\text{ dB}$, 8-PSK and 16-QAM signals again could only achieve correct classification rate at 81% and 79.8%, respectively.

By comparing with earlier works, performances achieved in this work are either meet, or exceed those previous results reported in the literature for other AMR schemes. Furthermore, it has also been demonstrated that the WD Demodulator provides equal BER performance with the traditional correlation-based methods.

Given the reliability of both the WD AMR and WD Demodulation processes devised in this work, they can be used to advance the state-of-the-art of communications receiver design. More specifically, the development of a Wavelet Platform provides the permission of interoperability between different communications standards to subsequent automatic demodulation continually working in the wavelet domain.

Reference:

- [1] J. Mitola, "Software Radio Technology Challenges and Opportunities," SW Radio Workshop. Brussels, Belgium, May 1997.
- [2] Enrico Buracchini, "The software radio concept", IEEE Communications Magazine, September 2000
- [3] Paulraj, A. and Kailath, T., "U. S. #5345599: Increasing Capacity in Wireless Broadcast Systems Using Distributed Transmission/Directional Reception (DTDR)," September 1994.
- [4] Hong, Z., Liu, K., Heath, R. W., Jr. and Sayeed, A.M., "Spatial Multiplexing in Correlated Fading via the Virtual Channel Representation," IEEE J. Sel Area Commun., Vol. 21, No. 5, pp. 856- 866, June 2003.
- [5] Telatar, I.E., "Capacity of Multi-Antenna Gaussian Channels," European Trans. Telecommun., Vol. 10, No. 6, pp. 585-595, November/Deceber 1999.
- [6] Saltzberg, B., "Performance of an Efficient Parallel Data Transmission System," IEEE Trans. Commun., Vol. 15, No. 6, pp. 805- 811, December 1967.
- [7] Chang, R. and Gibby, R., "A Theoretical Study of Performance of an Orthogonal Multiplexing Data Transmission Scheme," IEEE Trans. Commun., Vol. 16, No. 4, pp. 529- 540, August 1968.
- [8] Chang, R.W., "Synthesis of Band-Limited Orthogonal Signals for Multi-Channel Data Transmission," Bell Syst. Tech. J., Vol. 46, pp. 1775-1796, 1966.
- [9] Vim de Beek, J.J., et al., "OFDM Channel Estimation by Singular Value Decomposition", IEEE Trans. Commun., Vol. 46, No. 7, pp. 931-939, July 1998.
- [10] Zhidkov, S.V., "Performance Analysis of Multicarrier Systems in the Presence of Smooth Nonlinearity," EURASIP Journal on Wireless Communications and Networking, Vol. 2004, No. 2, pp. 335-343, December 2004.
- [11] Banelli, P., "Theoretical Analysis and Performance of OFDM Signals in Nonlinear Fading Channels," IEEE Trans. Wireless Commun., Vol. 2, No. 2, pp. 284-293, March 2003.
- [12] Li, Y.G., Winters, J.H. and Sollenberger, N.R., "MIMO-OFDM for Wireless Communications: Signal Detection with Enhanced Channel Estimation," IEEE Trans. Commun., Vol. 50, No. 9, pp. 1471-1477, September 2002.
- [13] Jiang, M. and Hanzo, L., "Multiuser MIMO-OFDM for Next-Generation Wireless Systems," Proc. IEEE, Vol. 95, No. 7, pp. 1430-1469, July 2007.

- [14] Bolcskei, H., "MIMO-OFDM Wireless Systems: Basics, Perspectives, and Challenges," *Wireless Commun*, Vol. 13, No. 4, pp. 31-37, August 2006.
- [15] Ogawa, Y., Nishio, K., Nishimura, T. and Ohgane, T., "A MIMO-OFDM System for High-Speed Transmission," *Proc. 58th Vehicular Technology Conference*, Vol. 1, pp. 493-497, October 6-9, 2003.
- [16] Panagiotou, P., Anastasopoulos, A., and Polydoros, A.: 'Likelihood ratio tests for modulation classification'. *Proc. IEEE MILCOM*, pp. 670–674, 2000.
- [17] Sills, J.A.: 'Maximum-likelihood modulation classification for PSK/QAM'. *Proc. IEEE MILCOM*, pp. 57–61, 1999.
- [18] Wei, W., and Mendel, J.M.: 'Maximum-likelihood classification for digital amplitude-phase modulations', *IEEE Trans. Commun.*, pp. 189–193, 2000.
- [19] Sapiano, P.C., and Martin, J.D.: 'Maximum likelihood PSK classifier'. *Proc. ICASSP*, pp. 1010–1014, 1996.
- [20] A. Polydoros and K. Kim, "On the detection and classification of quadrature digital modulation in broad-band noise," in *IEEE Trans. Commun.*, vol.38, no.8, pp. 1199-1211, August, 1990.
- [21] Hong, L., and Ho. K.C.: 'Classification of BPSK and QPSK signals with unknown signal level using the Bayes technique'. *Proc. IEEE ISCAS*, IV.1–IV.4, 2003.
- [22] L. Hong and K.C. Ho, "BPSK and QPSK modulation classification with unknown signal level," in *Proc. IEEE MILCOM.*, Los Angeles, California, October, 2000.
- [23] Chugg, K.M., Long, C.S., and Polydoros, A.: 'Combined likelihood power estimation and multiple hypothesis modulation classification'. *Proc. ASILOMAR*, pp. 1137–1141, 1995.
- [24] Panagiotou, P., Anastasopoulos, A., and Polydoros, A.: 'Likelihood ratio tests for modulation classification'. *Proc. IEEE MILCOM*, pp. 670–674, 2000.
- [25] Hong, L., and Ho, K.C.: 'Modulation classification of BPSK and QPSK signals using a two element antenna array receiver'. *Proc. IEEE MILCOM*, pp. 118–122 2001.
- [26] Hong, L., and Ho, K.C.: 'An antenna array likelihood modulation classifier for BPSK and QPSK signals'. *Proc. IEEE MILCOM*, pp. 647–651 2002.
- [27] Azzouz, E.E., and Nandi, A.K. 'Automatic modulation recognition of communication signals', Kluwer Academic, 1996
- [28] Azzouz, E.E., and Nandi, A.K.: 'Procedure for automation recognition of analogue

- and digital modulations', IEE Proc., Commun., 143, pp. 259–266, 1996.
- [29] Nandi, A.K., and Azzouz, E.E.: 'Modulation recognition using artificial neural networks', Signal Process., pp. 165–175, 1997.
- [30] Wong, M.L.D., and Nandi, A.K.: 'Automatic digital modulation recognition using spectral and statistical features with multi-layer perceptrons'. Proc. Int. Symp. Signal Processing and its Applications, Kuala Lumpur, Malaysia, pp. 390–393, 2001.
- [31] Nandi, A.K., and Azzouz, E.E.: 'Algorithms for automatic recognition of communication signals', IEEE Trans. Commun., pp. 431 – 436, 1998.
- [32] Hsue, S.Z., and Soliman, S.S.: 'Automatic modulation recognition of digitally modulated signals'. Proc. IEEE MILCOM, pp. 645–649, 1989.
- [33] Hsue, S.Z., and Soliman, S.S.: 'Automatic modulation classification using zero crossing', IEE Proc. F., Radar Signal Process., 137, pp. 459–464, 1990.
- [34] Assaleh, K., Farrell, K.R., and Mammone, R.J.: 'A new method of modulation classification for digitally modulated signals'. Proc. IEEE MILCOM, pp. 712–716, 1992.
- [35] Farrell, K.R., and Mammone, R.J.: 'Modulation classification using a neural tree network'. Proc. IEEE MILCOM, pp. 1028–1032, 1993.
- [36] Dai, W., Wang, Y., and Wang, J.: 'Joint power and modulation classification using second- and higher statistics'. Proc. WCNC , pp. 155–158, 2002.
- [37] Martret, C., and Boiteau, D.M.: 'Modulation classification by means of different order statistical moments'. Proc. IEEE MILCOM, pp. 1387–1391, 1997.
- [38] Marchand, P., Lacoume, J.L., and Le Martret, C.: 'Classification of linear modulations by a combination of different orders cyclic cumulants'. Proc. Workshop on HOS , pp. 47–51, 1997.
- [39] Marchand, P., Lacoume, J.L., and Le Martret, C.: 'Multiple hypothesis classification based on cyclic cumulants of different orders'. Proc. ICASSP, pp. 2157–2160 1998.
- [40] Swami, A., and Sadler, B.M.: 'Hierarchical digital modulation classification using cumulants', IEEE Trans. Commun., pp. 416–429, 2000.
- [41] Swami, A., Barbarossa, S., and Sadler, B.: 'Blind source separation and signal classification'. Proc. ASILOMAR, pp. 1187–1191, 2000.
- [42] Hatzichristos, G., and Fargues, M.P.: 'A hierarchical approach to the classification of digital modulation types in multipath environments'. Proc. ASILOMAR, pp. 1494–

1498, 2001.

- [43] Yang, Y., and Soliman, S.S.: 'Optimum classifier for M-ary PSK signals'. Proc. ICC, pp. 1693–1697, 1991.
- [44] Yang, Y., and Liu, C.H.: 'An asymptotic optimal algorithm for modulation classification', IEEE Commun. Lett., pp. 117–119, 1998.
- [45] Yang, Y., and Soliman, S.S.: 'A suboptimal algorithm for modulation classification', IEEE Trans. Aerosp. Electron. Syst., pp. 38–45, 1997.
- [46] Yang, Y., and Soliman, S.S.: 'Statistical moments based classifier for MPSK signals'. Proc. GLOBECOM, pp. 72–76, 1991.
- [47] Soliman, S.S., and Hsue, S.Z.: 'Signal classification using statistical moments', IEEE Trans. Commun., 40, pp. 908–916, 1992.
- [48] Yang, Y., and Soliman, S.S.: 'An improved moment-based algorithm for signal classification', Signal Process., 43, pp. 231–244, 1995.
- [49] Sapiano, P.C., Martin, J., and Holbeche, R.: 'Classification of PSK signals using the DFT of phase histogram'. Proc. ICASSP, pp. 1868–1871, 1995.
- [50] Schreyogg, C., and Reichert, J.: 'Modulation classification of QAM schemes using the DFT of phase histogram combined with modulus information'. Proc. IEEE MILCOM, pp. 1372–1376 1997.
- [51] Ho, K.C., Prokopiw, W., and Chan, Y.T.: 'Modulation identification by the wavelet transform'. Proc. IEEE MILCOM, pp. 886–890, 1995.
- [52] Ho, K.C., Prokopiw, W., and Chan, Y.T.: 'Modulation identification of digital signals by the wavelet transform', IEE Proc., Radar, Sonar Navig., 47, pp. 169–176, 2000.
- [53] Hong, L., and Ho, K.C.: 'Identification of digital modulation types using the wavelet transform'. Proc. IEEE MILCOM, pp. 427–431, 1999.
- [54] Chen, J., Kuo, Y., Li, J., Fu, F., and Ma, Y., "Digital Modulation Identification by Wavelet Analysis," Proc. Sixth IEEE Int. Conf. Comput. Intell. and Multimedia Appl., pp. 29-34, Las Vegas, NV, August 16-18, 2005.
- [55] Pavlik, R., "Binary PSK/CPFSK and MSK Bandpass Modulation Identifier Based on the Complex Shannon Wavelet Transform," J. Elect. Eng., Vol. 56, No. 3-4, pp. 71-77, 2005.
- [56] Hippenstiel, R., El-Kishky, H., Frick, C., and Datasprasad, S., "Modulation

- Identification using Neural Network and Wavelet Domain Based Approaches,” Proc. 38th IEEE Asilomar Conf. Signals, Syst. and Comput., Vol. 2, pp. 2116-2120, Pacific Grove, CA, November 7-10, 2004.
- [57] Jin, J-D., Kwak, Y., Lee, K-W., Lee, K. H., and Ko, S-J., “Modulation Type Classification Method using Wavelet Transform for Adaptive Demodulator,” Proc. 2004 IEEE Int. Symp. Intell. Signal Process. and Commun. Syst., pp. 282-292, Seoul, Republic of Korea, November 18-19, 2004.
- [58] Ho, K. C., Liu, H., and Hong, L., “On Improving the Accuracy of a Wavelet Based Identifier to Classify CDMA Signal and GSM Signal,” Proc. 1999 IEEE Int. Symp. Circuits and Syst. VLSI, Vol. 4, pp. 564-567, Orlando, FL, May 30-June 2, 1999
- [59] Prakasam, P. and Madheswaran, M., “Automatic Modulation Identification of QPSK and GMSK Using Wavelet Transform for Adaptive Demodulator in SDR,” Proc. 2007 IEEE Int. Conf. Signal Process., Commun. and Networking, pp. 507-511, February 22-24, Chennai, India, 2007.
- [60] Wei, X. and Cao, Z., “Fast Identification of Amplitude Modulated Signals at Low SNR,” Proc. IEEE 2007 Int. Symp. Microwave, Antenna, Propag. and EMC Tech. Wireless Commun., Vol. 2, pp. 1119-1112, August 14-17, 2005, Hangzhou, People’s Republic of China.
- [61] Mallat, S., A Wavelet Tour of Signal Processing, Second Edition, Academic Press, San Diego, CA, 1999.
- [62] Daubechies, I., Ten Lectures on Wavelets, Eighth Printing, Society for Industrial and Applied Mathematics, Philadelphia, PA, 2004.
- [63] Beylkin, G., Coifman, R. and Rokhlin, V., “Fast Wavelet Transforms and Numerical Algorithms,” Comm. Pure Applied Math., Vol. 44, Issue 2, pp. 141-183, 1991.
- [64] Grossmann, A. and Morlet, J., “Decomposition of Hardy Functions into Square Integrable Wavelets of Constant Shape,” SIAM J. Math. Analysis, Vol. 15, Issue 4, pp. 723-736, July 1984.
- [65] Mallat, S., “Multiresolution Approximation and Wavelet Orthogonal Bases of L_2 ,” Trans. AMS, Vol. 315, No. 1, pp. 69-87, September 1989.
- [66] Sarkar, T. K., et al., “A Tutorial on Wavelets from an Electrical Engineering Perspective, Part 1: Discrete Wavelet Techniques,” IEEE Trans. Antennas Propag. Mag., Vol. 40, No. 5, pp. 49-68, October 1998.
- [67] Poularikas, A.D., Ed., The Transforms and Applications Handbook, CRC Press, Boca Raton, FL, 1996.

- [68]Benedetto, J.J. and Frazier, M. W., Wavelets: Mathematics and Applications, CRC Press, Inc., Boca Raton, FL, 1994.
- [69]Rao, R.M. and Bopadrikar, A. S., Wavelet Transforms, Addison-Wesley, Reading, MA, 1998.
- [70]Wickerhauser, M.V., Adapted Wavelet Analysis from Theory to Software, A. K. Peters, Ltd., Wellesley, MA, 1994.
- [71]Bracewell, R.N., The Fourier Transform and Its Applications, McGraw-Hill, New York, NY, 1986.
- [72]Chin-Lin, Liu, "A Tutorial of the Wavelet Transform", University of Colorado.
- [73]Mallat, S., A Wavelet Tour of Signal Processing, Second Edition, Academic Press, San Diego, CA, 1999.
- [74]Proakis, J.G., Digital Communications, Fourth Edition, McGraw-Hill, NY, NY, 2001.
- [75]Ou, X., Huang, X., Yuan, X. and Yang, W., "Qusai-Haar Wavelet and Modulation Identification of Digital Signals," Proc. 2004 IEEE Int. Conf. Commun. Circuits and Syst., Vol. 2, pp. 733-737, June 27-29, 2004, Chengdu, People's Republic of China.
- [76]Hossen, A., Al-Wadahi, F. and Jervase, J. A., "Classification of Modulation Signals Using Statistical Signal Characterization and Artificial Neural Networks," Eng. Appl. of Artificial Intell., Vol. 20, pp. 463-472, November 28, 2006.
- [77]F. F. Liedtke, "Computer Simulation of an Automatic Classification Procedure for Digitally Modulated Communication Signals with Unknown Parameters," Signal Processing, Vol. 6, Issue 4, pp. 311 - 323, August 1984.
- [78]Yang, C.-Q., Zhong, Z.-F. and Yang, J.-A., "Recognition of Digital Modulation Using Radial Basis Function Neural Networks," Proc. 2003 Int. Conf. Machine Learning and Cybernetics, Vol. 5, pp. 3012- 3015, Nov. 2003.
- [79]Effrina, Yanti, H., "Automatic Modulation Classification of Communication Signals Using Wavelet Transform," Proceedings of the International Conference on Electrical Engineering and Informatics, June 17-19, Institut Teknologi Bandung, Indonesia, 2007.
- [80]Ken Vaz, David Daut, Yao Ge, "Estimation of Communications Channel Using Discrete Wavelet Transform-Based De-convolution", IEEE Trans. Comm., May, 2013.
- [81]Yao Ge, David Daut, "Wavelet-Based Receiver Design for Reconfigurable Radios", Proposal to NSF, Feb, 2012.

- [82] Yao Ge, David Daut, "Automatic Modulation Recognition Using the Discrete Wavelet Transform", IEEE SDR- WinnComm., Jan, 2013.
- [83] Sophocles J. Orfanidis, (2010)"Introduction To Signal Processing", Pearson Education, Inc., pp.427- 451.
- [84] K.M. Ho, C. Vaz, D. G. Daut, "A wavelet-based method for classification of binary digitally modulated signals", Sarnoff Symposium, IEEE, 2009.
- [85] Lanier A. Watkins, Modulation characterization using the wavelet transform, M.S. Thesis, Clark Atlanta University, 1997.
- [86] Y. Liang, Y. Guo, C. H. Wu, Y. Gao, "Envelope Analysis Based on the Combination of Morlet Wavelet and Kurtogram", Advanced Materials Research, Vols. 490-495, pp. 305-308, 2010.
- [87] K. Hassan, I. Dayoub, W. Hamouda, "Automatic Modulation Recognition Using Wavelet Transform and Neural Networks in Wireless Systems", EURASIP Journal on Advances in Signal Processing, 2010.
- [88] Yao Ge, D. G. Daut, K.M. Ho, "Bit Error Rate Analysis of Digital Communications Signal Demodulation Using Wavelet De-noising", IEEE Sarnoff Symposium, 2011.
- [89] Yao Ge, D. G. Daut, K.M. Ho, "Automatic Modulation Recognition Using the Discrete Wavelet Transform", IEEE SDR-Winn. Comm., 2013.
- [90] Yao Ge, Z. Shu, D. G. Daut, "Feature-based AMR Design for Vehicular Network Communication", Journal of Automotive Engineering, 2014.
- [91] Yao Ge, C. Vaz, D. G. Daut, "Discrete Wavelet Transform-based Automatic Modulation Recognition Algorithm Design", in process of IEEE Trans. Comm., 2016.
- [92] Yao Ge, Z. Shu, D. G. Daut, "Wavelet-based Demodulation Algorithm Design for Vehicular Network Communication", Society of Automotive Engineers Congress, 2016.

Appendix A:

Algorithm Computational Complexity Comparison:

Comparing with the CWT, another improvement of using the DWT is reduction of the computational complexity as the different fundamental of the CWT and the DWT technologies. The overall WD-AMR method's computational complexity consists of: Generation of WD templates; Transformation of received signals into the WD; Correlation of WD-templates and WD-received signals; and Decision procedure.

If the CWT was used in the instantaneous featured template AMR process, a test signal has a length of L bits, and there are N samples for each bit. The template size is set at M samples, $M \leq N$. So the size of the CWT domain based template would be a $M \times M$ matrix and the computation cost of a CWT-template generation is $O(M^2)$. The next computation is to continuously wavelet transform received signals, whose complexity could up to $O(N^2)$. The third step is correlation of the WD template matrix with the WD received signal matrix. In the instantaneous featured template method, the size of template is usually shorter than or equal to the signal bit size. So the WD signal matrix $N \times N$ will be fragmented to $M \times M$. Hence the complexity of their correlation is $O(M^2)$. Thus, the summation this three term lead the overall complexity to $O(N^2)$.

For the CWT statistical featured template AMR process, a test signal has a length of L symbols, and there are N samples for each symbol. The template size is N samples per symbol as well. Hence, followed by similar analysis as above, the overall complexity is $O(N^2)$.

For the DWT Instantaneous featured template AMR process, by defining the same signal size as in the CWT case, a test signal has a length of L bits, and there are N samples for

each bit. The template size is set at M samples. So the size of one WD template would be a $M \times (\log_2 M)$ matrix and the computation cost of a DWT-template generation is $O(M \log_2 M)$. The next computation is to discretely wavelet transform received signals, which complexity could up to $O(N \log_2 N)$. The third step is correlation of the WD template matrix with the WD received signal matrix. In the instantaneous featured template method, the size of template is usually shorter than the signal bit size. So the WD signal matrix $N \times \log_2 N$ will be fragmented to $M \times \log_2 M$. Hence the complexity of their correlation is $O(M \log_2 M)$.

For the DWT Statistical featured template AMR process, a test signal has a length of L bits, and there are N samples for each bit. The template size is set at N samples as well. Similarly, the overall complexity is $O(N \log_2 N)$.

In CWT-based Demodulation algorithm, because it basically adheres from two CWT-AMR methodology. Hence it also contains the same complexity as the AMR.

In DWT-based Demodulation system developed in this dissertation, it has proved that the DWT-based correlation and the regular correlation deliver the same output. Hence, in the DWT-based demodulation system, the DWT-based correlator replaced the regular correlation was used in the contemporary correlation based receiver. So the overall complexity is the same as the DWT-based correlation complexity, which is $O(N \log_2 N)$.

In summary, there are two points could be pointed through the comparisons:

1. The DWT-based AMR algorithm cost less computation effort than the AMR CWT-based algorithm;
2. Although the statistical featured templates AMR algorithm costs higher computational complexity than the instantaneous featured templates AMR algorithm, the statistical

feature-based algorithm is able to process more multiple modulation signal types than the instantaneous feature based algorithm.

3. Although the instantaneous feature-based AMR algorithm remains higher efficiency, but it can only work with binary modulation signals.

Table A1. CWT-based and DWT-based Algorithm Complexity Comparison

Algorithm	Complexity
CWT Instantaneous Featured Templates AMR	$O(M^2)$
CWT Statistical Featured Templates AMR	$O(N^2)$
DWT Instantaneous Featured Templates AMR	$O(M \log_2 M)$
DWT Statistical Featured Templates AMR	$O(N \log_2 N)$
CWT-based Demodulation	$O(M^2)$ or $O(N^2)$
DWT-based Demodulation	$O(N \log_2 N)$

Appendix B:

(Supplementary to Chapter 6) WD-Demodulator and TD-Demodulator Performances Comparison

Under the same experimental environment as setup in the chapter 6, another set of comparison tests were implemented in MATALAB.

Each received, noisy signal has been demodulated using the WD demodulator, and the same each received, noisy signal has been also demodulated using the TD (correlation-based) demodulator. Correspondingly, their two performance curves of two demodulators performance results were presented in Figs. B1-B8.

One curve corresponds to the simulated performances of the TD (correlation-based) Demodulation introduced in Chapter 6. The other curve is the simulation results for the WD Demodulators developed in this dissertation.

It has been observed that the WD-Demodulation probability of error curve was always overlapped by the TD-Demodulation performance curve. This result actually meets the expectation and again, numerically proves the equality between WD-correlation and TD-correlation.

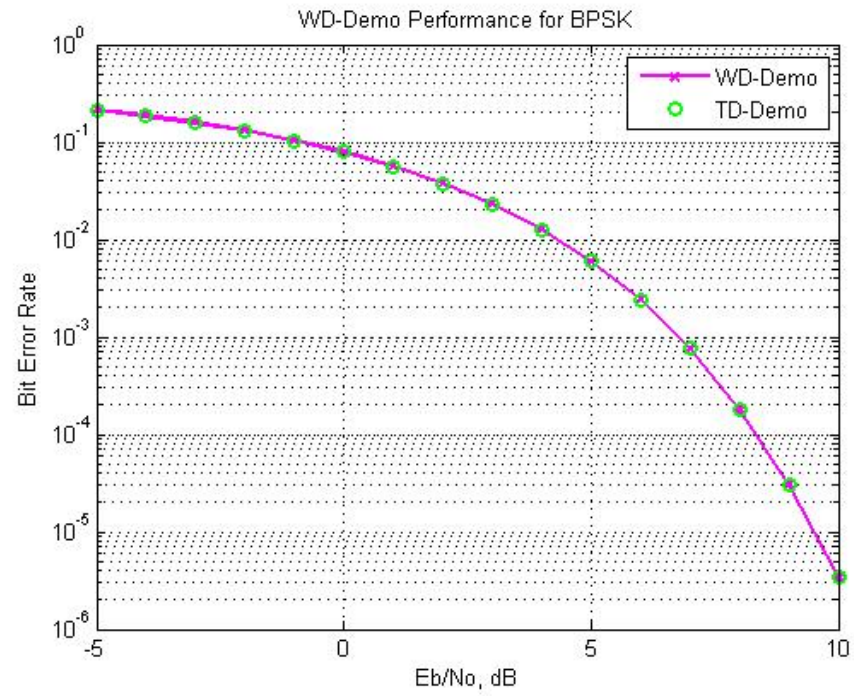


Fig. B1 BPSK BER Curve Comparison

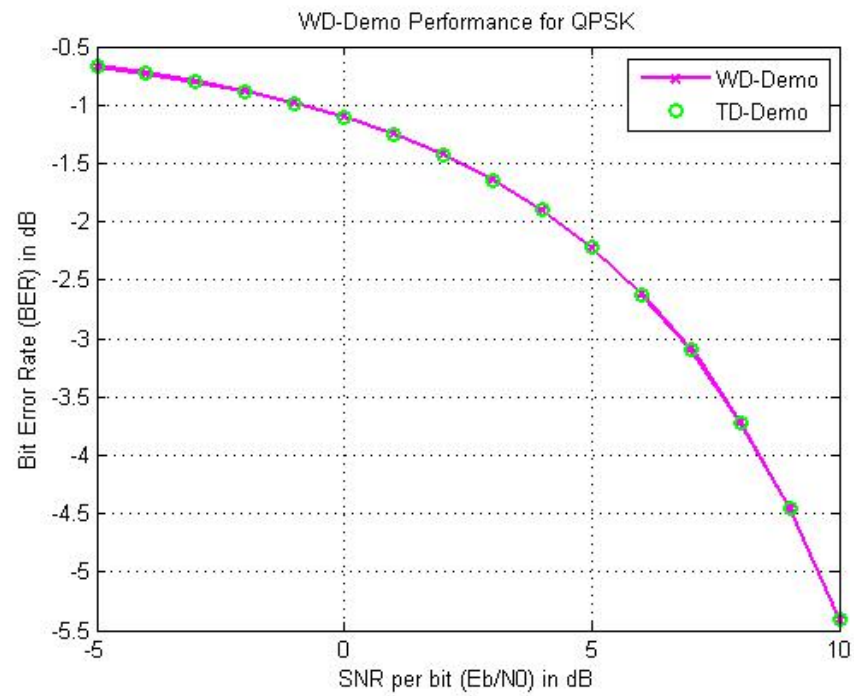


Fig. B2 QPSK BER Curve Comparison

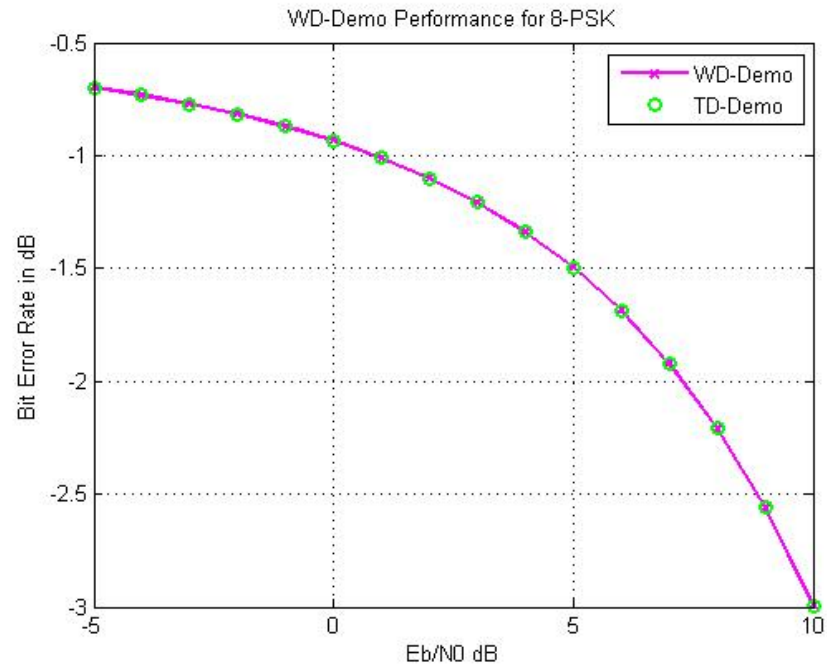


Fig. B3 8-PSK BER Curve Comparison

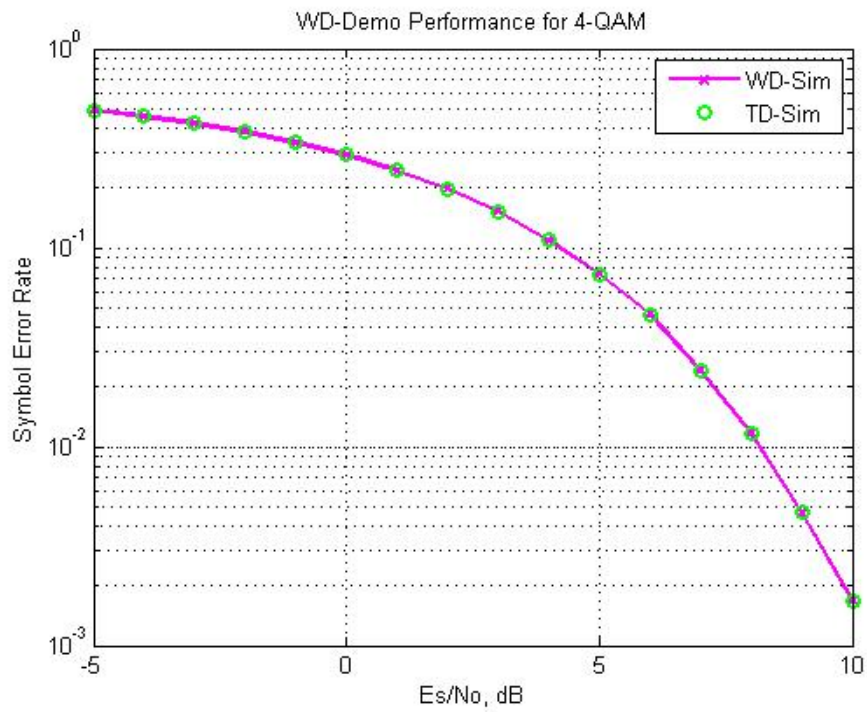


Fig. B4 4-QAM SER Curve Comparison

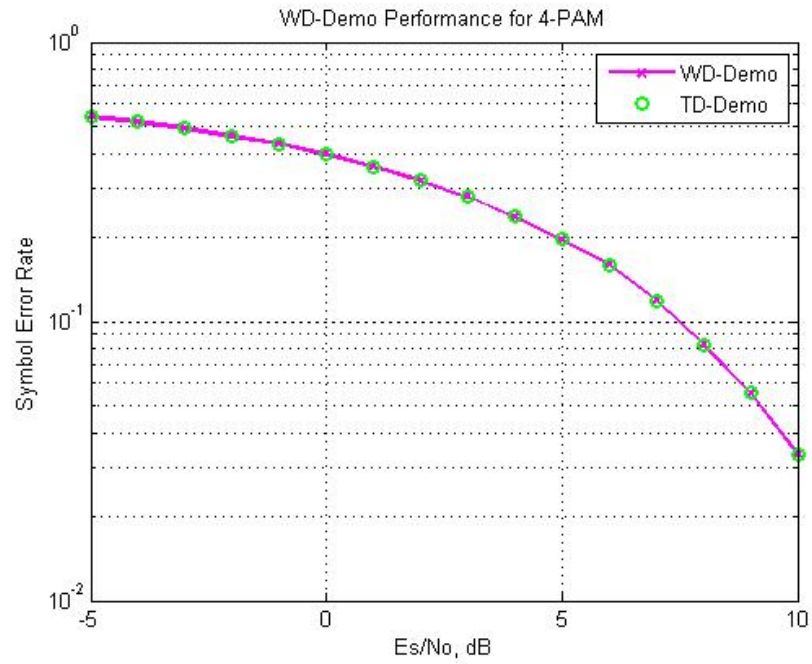


Fig. B5 4-PAM SER Curve Comparison

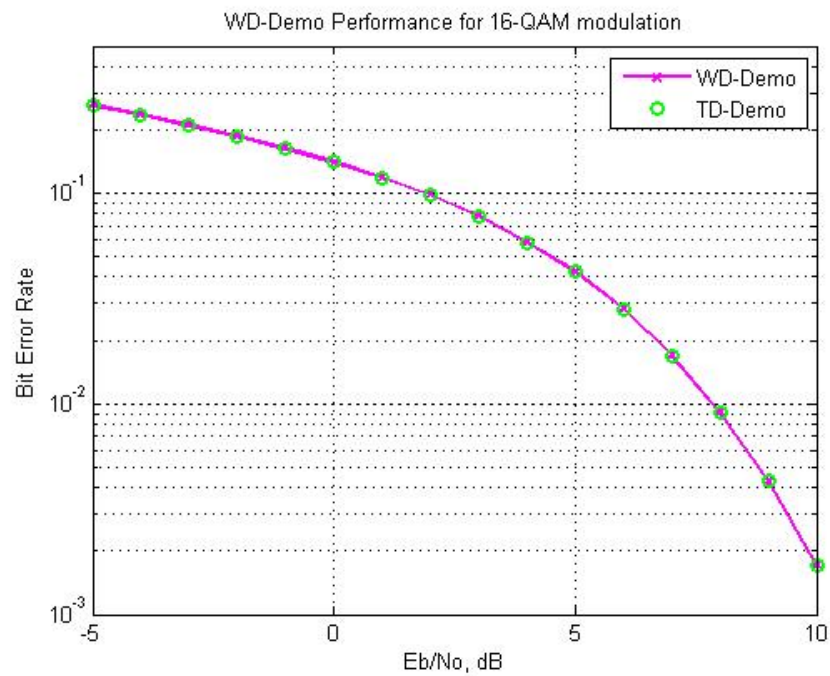


Fig. B6 16-QAM BER Curve Comparison

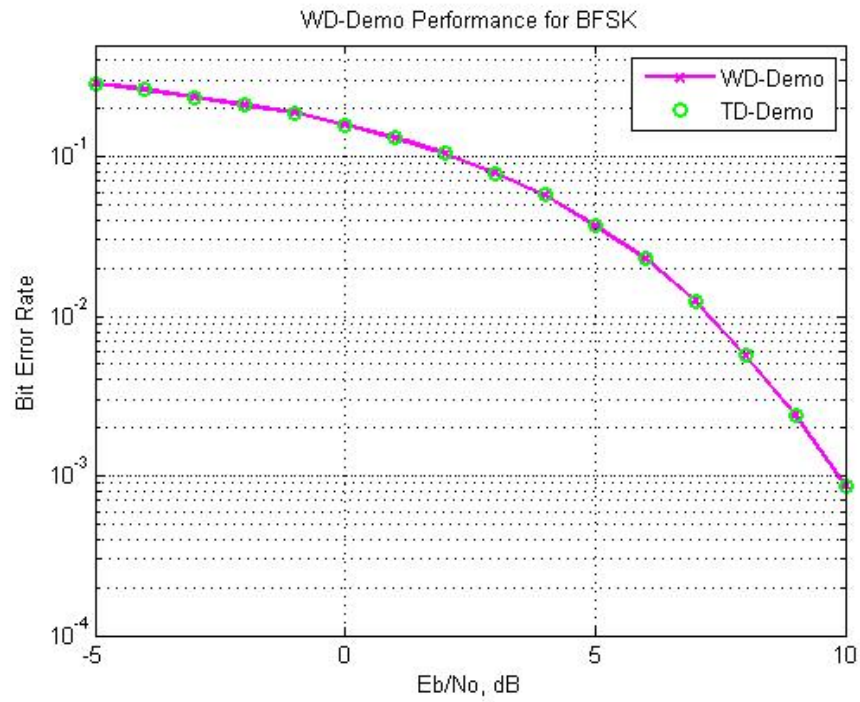


Fig. B7 BFSK BER Curve Comparison

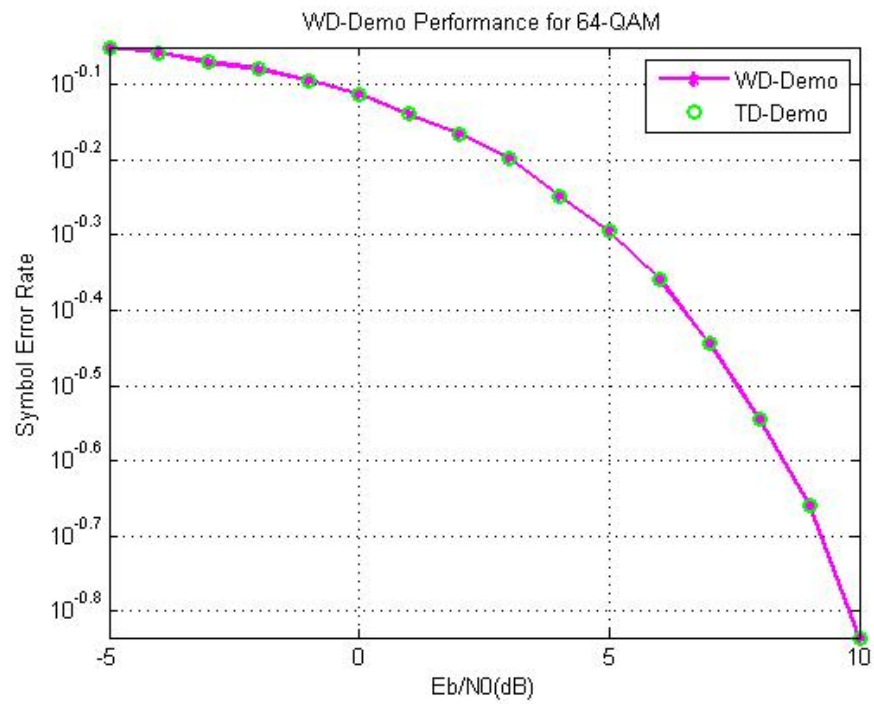


Fig. B8 64-QAM SER Curve Comparison